



VCU

Virginia Commonwealth University
VCU Scholars Compass

Theses and Dissertations

Graduate School

2012

Circuit Development in the Dorsal Lateral Geniculate Nucleus (dLGN) of the Mouse.

Tania Seabrook
Virginia Commonwealth University

Follow this and additional works at: <https://scholarscompass.vcu.edu/etd>



Part of the [Neurosciences Commons](#)

© The Author

Downloaded from

<https://scholarscompass.vcu.edu/etd/304>

This Dissertation is brought to you for free and open access by the Graduate School at VCU Scholars Compass. It has been accepted for inclusion in Theses and Dissertations by an authorized administrator of VCU Scholars Compass. For more information, please contact libcompass@vcu.edu.

© Tania A. Seabrook 2012
All Rights Reserved

Circuit Development in the Dorsal Lateral Geniculate Nucleus (dLGN) of the Mouse.

A dissertation submitted in partial fulfillment of the requirements for the degree of Doctor of Philosophy at Virginia Commonwealth University.

by

Tania A. Seabrook, B.S.
Virginia Commonwealth University, 2005

William Guido, Ph.D.
Professor
Department of Anatomy and Neurobiology

Virginia Commonwealth University
Richmond, Virginia
March, 2012

Acknowledgements

First and foremost, I would like to thank my advisor, Dr. Bill Guido. I am extremely grateful for all of his encouragement, patience, guidance, and support. I have been amazingly fortunate to have him as an advisor and his help was essential to the completion of this dissertation.

My thanks and appreciation goes to my committee members: Dr. Jason Chen, Dr. Mike Fox, Dr. Kurt Hauser, and Dr. Alexandre Medina. I would like to thank Dr. Jason Chen as well as past and present members of his lab, particularly Dr. Frank Chen, Bess Krahn, Dr. Duncan Morhardt, and Hoon Shim, for their friendship, generosity, and all of their help with Western blotting, dark rearing, and genotyping. I am grateful to Dr. Mike Fox for all of his advice and suggestions. My appreciation also goes to Dr. Fox for doing the VGlut1 staining and microarray analysis. I would like to also thank him and his lab members, Dr. Jianmin Su and Justin Brooks, for all of their help and use of equipment and reagents. I would like to thank Dr. Alexandre Medina for all of his help and use of reagents, also Weili Wang from the Medina lab for her assistance with Western blotting.

I would like to extend my thanks to the Neuroscience Graduate Program Director, Dr. John Bigbee, in addition to the Department of Anatomy and Neurobiology's administrative staff, especially Sharon Toussaint, for all of their help. I owe my deepest gratitude to the late Dr. Ary Ramoa for giving me the opportunity to work in his lab when I was an undergraduate, since this is where my interest in neuroscience and the visual system first began. In addition, many others

made this work possible including: Dr. Anthony Campagnoni (UCLA) for the *golli-τ*-GFP mice, Dr. Steve Wang (UTHMS) for the *math5*^{-/-} mice, and Dr. Rory McQuiston and Karen Bell for providing us with the ChAT-cre and GAD65-GFP mice.

My gratitude goes to all the past and current members of the Guido lab. I am especially indebted to the other two mouseketeers, Dr. Emily Dilger and Dr. Rana El-Danaf, for all of their kindness, advice, help, support, and friendship. I would also like to express my gratitude to my good friend, Dr. Thomas Krahe, for his valuable help, advice, and suggestions. I would like to thank Ania Marcinkowska and Natasha Sheybani for all of their help. I am grateful to Dr. Martha Bickford for her advice as well as help with anatomy.

Additionally, I would like to thank my boyfriend, Taka Inagaki, and my good friends: Sarah Dersch, Karl Fung, Sarah Shahmoradian, Shep Shapard, and Marion Te. And last but certainly not least, I would like to thank my family for their unending love, support, and encouragement: my mom and dad, Martha and Alex Seabrook; my brother and sister-in-law, Alex Seabrook and Rumi Takeshita-Seabrook; my grandparents, Martha Marino and the late Salvatore Marino.

Table of Contents

List of Figures	v
List of Abbreviations	vii
Abstract	viii
Introduction	1
Chapter I – Pattern of Retinal Convergence onto Interneurons in the dLGN of the Mouse	
Abstract	16
Introduction	18
Methods	23
Results	27
Discussion	49
Chapter II – Development of the Corticogeniculate Pathway in the dLGN of the Mouse	
Abstract	54
Introduction	56
Methods	59
Results	64
Discussion	88
Conclusions	96
References	111
Vita	127

List of Figures

Figure 1. Simplified schematic diagram of circuitry in the dLGN of the mouse	10
Figure 2. Summary of retinogeniculate development in dLGN	12
Figure 3. Timeline of circuit development in the dLGN of the mouse.....	14
Figure 4. Schematic showing retinogeniculate innervation of relay cells and interneurons	21
Figure 5. GFP expression in dLGN interneurons	33
Figure 6. Targeting interneurons for whole-cell recordings using GFP expression in dLGN.....	35
Figure 7. GFP expressing cells exhibit the characteristic active membrane properties of interneurons.....	37
Figure 8. GFP expressing cells possess the morphological properties of interneurons.....	39
Figure 9. The degree of retinal convergence onto interneurons was maintained across age.....	41
Figure 10. The maximum amplitude evoked by optic tract stimulation decreased with age.....	43
Figure 11. Distribution of retinal contacts on dLGN interneurons.....	45
Figure 12. Retinal contacts were widely distributed throughout the dendritic tree of an interneuron	47
Figure 13. τ -GFP expression in neocortex and dLGN of <i>golli</i> - τ -GFP mice.....	72
Figure 14. Cortical innervation of thalamus at different postnatal ages	74
Figure 15. Coordinated innervation of corticogeniculate and retinogeniculate projections in dLGN	76
Figure 16. Pattern of corticogeniculate innervation throughout dLGN at P5 and P8.....	78

Figure 17. Development of functional corticogeniculate synapses in dLGN.....	80
Figure 18. The timing of corticogeniculate innervation in dLGN relies on retinogeniculate innervation	82
Figure 19. The pattern of corticogeniculate innervation is disrupted in the absence of retinal input	84
Figure 20. Monocular enucleation only affects the timing of corticogeniculate innervation in dLGN contralateral to the enucleated eye.....	86
Figure 21. Corticogeniculate innervation in the presence and absence of retinal input	94
Figure 22. Summary of circuit development in the dLGN of the mouse	105
Figure 23. Cholinergic brainstem innervation is delayed in dLGN.....	107
Figure 24. Innervation by the thalamic reticular nucleus is delayed in dLGN	109

Abbreviations

A: anterior	IPSP: inhibitory postsynaptic potential
A: astrocyte	ISI: interstimulus interval
A: transient K ⁺ conductance	K: koniocellular
ACSF: artificial cerebral spinal fluid	L: lateral
ADAMTS: a disintegrin and metalloproteinase with thrombospondin motifs	LDT: laterodorsal tegmental nucleus
AHP: afterhyperpolarization	LH: left hemisphere
BDNF: brain-derived neurotrophic factor	LT: low threshold
BE: binocular enucleation	M: magnocellular
BNOS: brain nitric oxide synthase	M: medial
C: cortex	M: medial geniculate nucleus
cAMP: cyclic adenosine monophosphate	ME: monocular enucleation
CG: corticogeniculate	mRNA: messenger ribonucleic acid
ChAT: choline acetyltransferase	nAChR: nicotinic acetyl choline receptor
CRE: cAMP-response element	OT: optic tract
CREB: CRE binding protein	P: parvocellular
CSPGs: chondroitin sulfate proteoglycans	P: postnatal day
CTB: cholera toxin subunit B	PBG: parabigeminal nucleus
D: dorsal	PPR: paired pulse ratio
DCC: deleted in colorectal cancer	PPT: pedunculopontine tegmental nucleus
DIC: differential interference contrast	R: relay cell
dLGN: dorsal lateral geniculate nucleus	RG: retinogeniculate
E: embryonic day	RGC: retinal ganglion cell
EPSP: excitatory postsynaptic potential	RH: right hemisphere
F1/F2: flattened vesicles	RLD: round vesicles, large profile, dark mitochondria
GABA: gamma aminobutyric acid	τ-GFP: tau-enhanced green fluorescent fusion protein
GAD: glutamate decarboxylase	TRN: thalamic reticular nucleus
GFP: enhanced green fluorescent protein	TTX: tetrodotoxin
h: slow, mixed cation conductance	V: ventral
I: current	V: voltage
I: interneuron	VB: ventrobasal complex
ic: internal capsule	VGlut1: vesicular glutamate transporter 1
IGL: intergeniculate leaflet	VGlut2: vesicular glutamate transporter 2
ipRGC: intrinsically photosensitive RGC	VLG: ventral lateral geniculate nucleus

Abstract

CIRCUIT DEVELOPMENT IN THE DORSAL LATERAL GENICULATE NUCLEUS (dLGN) OF THE MOUSE.

By Tania A. Seabrook, B.S.

A dissertation submitted in partial fulfillment of the requirements for the degree of Doctor of Philosophy at Virginia Commonwealth University.

Virginia Commonwealth University, 2012

William Guido, Ph.D.
Professor
Department of Anatomy and Neurobiology

The visual system is one of the most widely used and best understood sensory systems and the dorsal lateral geniculate nucleus (dLGN) of the mouse has emerged as a model for investigating the cellular and molecular mechanisms underlying the development and activity-dependent refinement of sensory connections. Thalamic organization is highly conserved throughout species and the dLGN of the mouse possesses many features common to higher mammals, such as carnivores and primates. Two general classes of neuron are present within the dLGN, thalamocortical relay cells and interneurons, both of which receive direct retinal input. Axons of relay cells exit dLGN and convey visual information to layer IV of cortex, whereas interneurons

are involved in local circuitry. In addition, dLGN receives rich nonretinal input from numerous areas of the brain. Studies thus far have focused on the retinogeniculate pathway and the development of connections between retinal ganglion cells (RGCs) and relay cells has been well characterized. However, there are still a number of unanswered questions about circuit development in dLGN. Here we examined two aspects that are not well understood, the pattern of retinal convergence onto interneurons and the structural and functional innervation of nonretinal projections. To address the first issue we conducted *in vitro* whole-cell recordings from acute thalamic slices of GAD67-GFP mice, a transgenic strain in which dLGN interneurons express GFP. We also did 3-D reconstructions of biocytin-labeled interneurons using multi-photon laser scanning microscopy in conjunction with anterograde labeling of retinogeniculate projections to examine the distribution of retinal contacts. To begin to examine the development of nonretinal connections in dLGN we made use of a transgenic mouse (*golli- τ -GFP*) to visualize corticogeniculate projections, one of the largest sources of nonretinal input to dLGN. Using this mouse we studied the timing and patterning of corticogeniculate innervation in relation to the development of the retinogeniculate pathway. We also used binocular enucleation and genetic deafferentation to test whether the retina plays a role in regulating nonretinal innervation. We found that there is a coordination of retinal and nonretinal innervation in dLGN. Projections from the retina were the first to innervate and they entered dLGN at perinatal ages. They also made functional connections with both relay cells and interneurons at early postnatal ages. Interestingly, relay cells underwent a period of retinogeniculate refinement, whereas the degree of retinal convergence onto interneurons was maintained. This possibly reflects the different roles that these two cell types have in dLGN. Both structural and functional corticogeniculate innervation was delayed in comparison and occurred postnatally, however in the absence of

retinal input the timing of corticogeniculate innervation was accelerated. RGCs transmit the visual information encoded in the retina to dLGN so it may be necessary for these connections to be formed before those from nonretinal projections, which serve to modulate that signal on its way to cortex. Thus precise timing of retinal and nonretinal innervation may be important for the appropriate formation of connections in the visual system and the retina seems to be playing an important role in regulating this timing.

Introduction

The visual system has been used extensively for studying how precise circuits develop in the brain. Much of our present understanding of the mechanisms underlying the development of sensory connections has come from studies on the retinogeniculate pathway. Retinal ganglion cells (RGCs) send direct input to the dorsal lateral geniculate nucleus (dLGN) of the thalamus. The dLGN in turn sends projections to layer IV of cortex and is the primary relay of visual information. Recently the mouse has become one of the most widely used model organisms for studying many different aspects of visual system development. This is due to advances in genetic technology that allow for visualization and manipulation of neural elements. The mouse also makes a suitable model for studying the mammalian visual system because thalamic organization is highly conserved and has a number of features that are common to higher order mammals, such as cats, primates, and humans. The following are features of thalamic organization that the mouse has in common with other mammals: eye-specific modules; two principal cell classes; parallel organization; nonretinal circuitry; and membrane properties that regulate response mode.

Like other mammals, the dLGN receives RGC projections from both eyes. Segregation of these inputs from the two eyes into eye-specific layers is a cardinal feature of the mammalian retinogeniculate pathway. In all species of primates and carnivores studied thus far, the dLGN is partitioned into cytoarchitecturally distinct laminae that receive input from one eye or the other (Casagrande and Norton, 1991; Garey et al., 1991). Although there is no obvious lamination pattern in the dLGN of the mouse, retinogeniculate projections from the two eyes are organized

into non-overlapping territories called eye-specific domains. Eye injections of cholera toxin subunit B (CTB) conjugated to different fluorescent dyes allow for simultaneous observation of retinogeniculate projections from both eyes in a single section of dLGN and visualization of eye-specific domains (Muir-Robinson et al., 2002; Jaubert-Miazza et al., 2005).

Two principal cell classes exist in the dLGN of the mouse, thalamocortical relay cells and local-circuit interneurons. Their morphological differences have been well characterized in rodents and are similar to what has been shown for other species (Grossman et al., 1973; Rafols and Valverde, 1973; Parnavelas et al., 1977; Williams et al., 1996). Relay cells are the projection neurons and have class A morphology. These cells have large, round somata and a radial shaped dendritic tree. They have a variable number of primary dendrites and an identifiable myelinated axon that can often be traced leaving the dLGN. Interneurons exhibit class B morphology and have small, spindle-shaped somata and an overall bipolar shape. They typically have two primary dendrites that originate from opposite poles of the soma and their dendrites are long, thin, beaded, and have intricate branching patterns. It is difficult to distinguish whether an axon is present, since some dendrites exhibit an axon-like appearance.

The visual system of many mammals, such as primates and cats, consists of separate parallel pathways to process different features of the visual scene (Lennie, 1980; Stone, 1983; Nassi and Callaway, 2009). These pathways remain anatomically segregated from the retina through dLGN and into visual cortex. In dLGN, studies have revealed three classes of relay cell termed parvocellular (P), magnocellular (M), and koniocellular (K) cells in primates (Kaas et al., 1978; Irvin et al., 1986; Nassi and Callaway, 2009) and X-, Y-, and W-cells in cats (Sherman and Spear, 1982; Sherman, 1985). Each of these cell classes has unique morphological and physiological properties, receive information from analogous classes of RGCs, and exhibit

strong regional preferences within dLGN. Until recently it was unclear whether different relay cell classes exist in the mouse. Krahe and colleagues (2011) found that relay cells in mouse dLGN are morphologically distinct and closely resemble the X-, Y-, and W-cells found in the cat (Friedlander et al., 1981; Stanford et al., 1981, 1983). In addition, these different cell types exhibit regional preferences within dLGN. X-like cells have a biconical shape and are located near the ventroposterior border of dLGN in a region that corresponds to the monocular segment (Coleman et al., 2009). Y-like cells have a profile that is radially symmetric, are broadly distributed throughout a central core of dLGN, and show a strong preference for the binocular region of dLGN (Coleman et al., 2009). W-like cells have a hemispherical profile and form a ring around the perimeter of dLGN. Recent studies using a host of transgenic mice led to the identification of functionally distinct classes of RGCs that project to dLGN and connect to neurons there in a series of parallel spatially distinct territories (Huberman et al., 2008b, 2009; Kim et al., 2008; Yonehara et al., 2008; Ecker et al., 2010; Kay et al. 2011; Rivlin-Etzion et al., 2011). The morphologically distinct groups of relay cells do not seem to be positioned to serve as an exclusive retinorecipient zone for any one class of RGC. However, it could be possible that multiple RGC classes, which share a common property or are broadly tuned for one, may converge onto a specific relay cell type in dLGN. Although it is still unclear whether the X-, Y-, and W-like cells possess different functional properties these results support the notion that a system-wide parallel organization exists in rodents.

The dLGN was initially thought of as a passive relay between retina and cortex, since the receptive field properties of relay cells are quite similar to their RGC inputs (Cleland et al., 1971). However, more recently the thalamus is thought to play a more crucial role in controlling the flow of information to the cortex. One reason for this is that in addition to input from the

retina, relay cells in dLGN receive input from many other areas of the brain (Fig. 1). The synaptic architecture of mouse dLGN is highly conserved (Bickford et al., 2010) and the percentages of retinal and nonretinal terminals are similar to those found in rat, cat, and monkey (Wilson and Hendrickson, 1981; Gabbott et al., 1986; Montero, 1991; Erisir et al., 1998; Van Horn et al., 2000; Li et al., 2003). Inputs to dLGN have been separated into two categories, drivers and modulators (Sherman and Guillery, 1998). Retinal afferents to the dLGN are the drivers. They provide the primary excitatory drive to relay cells (Cleland et al., 1971; Sherman and Guillery, 1998), but make up less than 10% of synapses on these cells (Van Horn et al., 1997; Bickford et al., 2010). Retinal afferents make synapses on proximal regions of relay cell dendrites close to the cell body (Wilson et al., 1984) and activate ionotropic glutamate receptors (McCormick and von Krosigk, 1992). Retinal inputs can also indirectly activate metabotropic receptors on relay cells through interneurons (Cox et al., 1998).

The majority of synapses in dLGN are from nonretinal sources including intrinsic interneurons, thalamic reticular nucleus (TRN), brainstem, and layer VI of visual cortex (Sherman and Guillery, 2002). These modulators make up approximately 90% of all inputs, with cortex, brainstem, and GABAergic inputs each contributing around 30% (Montero, 1991; Erisir et al., 1997b; Van Horn et al., 2000). Some minor inputs (< 5%) include noradrenergic inputs from brainstem (de Lima and Singer, 1987b; Smith et al., 1988), serotonergic from the dorsal raphe nucleus (de Lima and Singer, 1987a), and histaminergic inputs from the tuberomammillary nucleus of the hypothalamus (Airaksinen and Panula, 1988; Uhlrich et al., 1993). Modulators can alter the transmission of information relayed through thalamus by changing the responsiveness, or gain, of a relay cell to retinal input (Meulders and Godfraind, 1969; Gilbert, 1977; Wrobel, 1981; Murphy et al. 1999). Unlike drivers, they can act through metabotropic receptors in

addition to ionotropic receptors (McCormick and von Krosigk, 1992). Metabotropic receptors are linked indirectly to postsynaptic ion channels through complex second messenger pathways so they produce slow, prolonged changes in membrane potential (Conn and Pin, 1997). This is ideal for modulation because these sustained changes affect the excitability of relay cells and serve to control activation of many voltage-dependent conductances.

Similar to other species, cells in the dLGN of the mouse have a variety of active membrane conductances (MacLeod et al., 1997; Jaubert-Miazza et al., 2005). These conductances vary the membrane potential of relay cells affecting their firing properties and hence alter the transmission of information through thalamus (Sherman, 2005). For example, relay cells in dLGN exhibit two different response modes to afferent input, tonic and burst firing (Crunelli et al., 1989; McCormick and Feeseer, 1990; Lo et al., 1991). The response mode of the relay cell depends on a voltage- and time-dependent low-threshold T-type Ca^{2+} current (I_T ; Deschenes et al. 1984; Crunelli et al., 1989; McCormick and Feeseer, 1990; Lo et al., 1991). If this conductance is inactive the cell will fire in tonic mode, however if the conductance is active then the cell fires in burst mode. The inactivation state of I_T can be controlled by nonretinal input and a classic example of this is input from cortex or brainstem switching the response mode of a relay cell from burst to tonic (Lu et al., 1993; Godwin et al., 1996). Tonic firing is comprised of a steady train of unitary action potentials and has a fairly linear input-output relationship (Sherman, 2001). This type of firing is important for transmitting sensory information accurately to cortex. Burst firing consists of a low-threshold (LT) spike with a burst of action potentials. Since LT spikes are all-or-none events (Zhan et al., 1999) the input-output relationship for this type of firing is nonlinear (Sherman and Guillery, 1998; Sherman, 2001). Burst firing is involved

in slow-wave sleep, but is also important for initial stimulus detection during vision (Sherman, 2001).

The dLGN has emerged as a model for studying the development of sensory connections (Guido, 2008). To date, studies have focused on two aspects of thalamic circuitry, RGC projections and connections onto relay cells and feedforward inhibitory connections between interneurons and relay cells (Fig. 2; Chen and Regehr, 2000; Lo et al., 2002; Jaubert-Miazza et al., 2005; Ziburkus and Guido, 2006; Bickford et al., 2010; Dilger et al., 2011). During early postnatal life the dLGN undergoes many changes before it resembles the pattern found in the adult (Fig. 2). As mentioned previously, the projections from the two eyes are segregated into non-overlapping domains in the dLGN of the mouse. This form of eye-specific patterning is not apparent at birth. Crossed projections begin to innervate dLGN at embryonic day (E) 15 to E16 and uncrossed projections come in later between postnatal day (P) 0 to P2 (Godement et al., 1984). Initially, projections from the two eyes are intermingled and individual relay cells in dLGN are binocularly innervated and receive numerous weak retinal inputs (Chen and Regehr, 2000; Lo et al., 2002; Jaubert-Miazza et al., 2005; Ziburkus and Guido, 2006; Dilger et al., 2011). There is a period of eye specific remodeling so that by P7 retinogeniculate projections display clear signs of segregation. Around the time of eye opening (~P12) the retinogeniculate projections are well segregated into eye-specific domains like those found in the adult. At this time dLGN relay cells are monocularly innervated and are receiving only a few strong inputs from the retina. This retinogeniculate refinement has been attributed to patterned spontaneous retinal activity (Torborg and Feller, 2005). Retinal waves are spontaneous waves of depolarization that occur in the retina and are comprised of bursts of action potentials that correlate the firing of neighboring RGCs (Meister et al., 1991; Demas et al., 2003). High

frequency correlated bursting of neighboring RGCs has been found to be essential for eye-specific segregation (Torborg et al., 2005). Spontaneous retinal activity and the early phases of visually evoked activity have also been shown to be vital for the strengthening and pruning of retinal synapses on relay cells (Hooks and Chen, 2006). Around the time that waves subside and visually evoked activity emerges functional connections between interneurons and relay cells form.

Around the second postnatal week, disynaptic feedforward inhibition mediated by intrinsic interneurons begins to emerge in dLGN (Bickford et al., 2010). Functional retinal connections with relay cells are present at very early postnatal ages (Mooney et al., 1996; Chen and Regehr, 2000; Ziburkus et al., 2003; Jaubert-Miazza et al., 2005; Bickford et al., 2010) and during the first postnatal week, synaptic responses evoked in relay cells with optic tract stimulation are primarily excitatory (Bickford et al., 2010). This suggests that synapses between interneurons and relay cells have not yet developed (Ziburkus et al., 2003). In the mature rodent, synaptic responses evoked in relay cells consist of an EPSP followed by inhibitory postsynaptic potential (IPSP) activity (Crunelli et al., 1988; Ziburkus et al., 2003; Blitz and Regehr, 2005; Jaubert-Miazza et al., 2005). These inhibitory responses often contain two distinct hyperpolarizing components including an early, short-duration GABA_A-mediated IPSP and a slower, long-duration GABA_B-mediated IPSP. This full complement of IPSP activity does not emerge until after eye opening (Bickford et al., 2010).

Based on Figure 3, it is clear that there are a number of unanswered questions concerning the development of thalamic circuits. How the connections between RGCs and interneurons, the other major cell type in dLGN, develop is not well understood. There is also a great deal that we do not know about the development of nonretinal connections in dLGN.

In dLGN, intrinsic interneurons play a key role in thalamic function by regulating retinogeniculate transmission through feedforward inhibition. Interneurons are thought to play a role in contrast gain control, shaping the receptive fields of relay cells, altering the temporal precision of retinogeniculate inputs, and synchronizing thalamic oscillations (Sillito and Kemp, 1983; Crunelli et al., 1988; Norton et al., 1989; Norton and Godwin, 1992; Steriade et al., 1993; Govindaiah and Cox, 2004; Sherman, 2004; Blitz and Regehr, 2005). Retinal inputs drive feedforward inhibition in dLGN, but nearly nothing is known about the pattern of retinal convergence onto these interneurons during postnatal development. To examine this we conducted *in vitro* whole-cell recordings using acute thalamic slices from a transgenic mouse strain (GAD67-GFP; Chattopadhyaya et al., 2004), in which the interneurons in dLGN express enhanced green fluorescent protein (GFP). We used GFP to identify and target interneurons for recordings. To study retinal convergence we utilized a slice preparation (Chen and Regehr, 2000; Bickford et al., 2010; Dilger et al., 2011) that allowed us to evoke synaptic activity in interneurons by placing stimulating electrodes in optic tract. Electrical stimulation of optic tract was gradually increased and the amplitude of the resulting EPSPs were plotted against stimulus intensity to estimate the number of retinal inputs onto interneurons (Lo et al., 2002; Jaubert-Miazza et al., 2005; Ziburkus and Guido, 2006; Dilger et al., 2011). We also examined the distribution of the retinal contacts on interneurons by filling them with biocytin during whole-cell recordings, allowing us to do 3-D reconstructions of individual cells (Krahe et al., 2011), in combination with anterograde labeling of retinal projections with CTB.

The bulk of synapses in dLGN are formed by nonretinal projections (Sherman and Guillery, 2002; Bickford et al., 2010). One of the major sources of nonretinal input to dLGN comes from layer VI of primary visual cortex (Erisir et al., 1997a,b). Corticogeniculate input to

dLGN has been shown to be important for sharpening receptive field properties of relay cells and influencing the gain of their output (Sherman and Guillery, 2002; Briggs and Usrey, 2008).

Despite the enormity of this projection and its extensive influence on thalamic signal transmission virtually nothing is known about how and when the corticogeniculate pathway develops. In other species corticogeniculate innervation of dLGN is delayed (Shatz and Rakic, 1981; Clasca et al., 1995) and a recent study by Jacobs and colleagues (2007) suggests a similar progression in mouse. We examined this further by doing a detailed study of corticogeniculate innervation in relation to retinogeniculate development using the *golli- τ -GFP* mouse (Jacobs et al., 2007) to visualize the projections from cortical layer VI to dLGN. In order to do this we did eye injections of CTB in *golli- τ -GFP* mice to visualize both retinogeniculate and corticogeniculate projections within the same animal. In addition, we examined the development of functional corticogeniculate synapses with both immunohistochemical staining for functional synaptic machinery and *in vitro* whole-cell recordings. Corticogeniculate innervation was also studied in the absence of retinal input by adopting a loss of function approach either by removing retinal input prior to arrival of corticogeniculate projections through enucleation or genetic deafferentation using a mouse lacking nearly all RGCs (*math5*-null; Wang et al., 2001).

Figure 1

Simplified schematic diagram of circuitry in the dLGN of the mouse.

Both relay cells and interneurons in dLGN receive direct input from the retina. Relay cells project to layer IV of visual cortex whereas interneurons form local connections within dLGN. In addition to retinal input, relay cells are receiving modulatory input from various nonretinal sources including intrinsic interneurons, TRN, layer VI of visual cortex, and brainstem. dLGN, dorsal lateral geniculate nucleus; R, relay cell; I, interneuron; TRN, thalamic reticular nucleus.

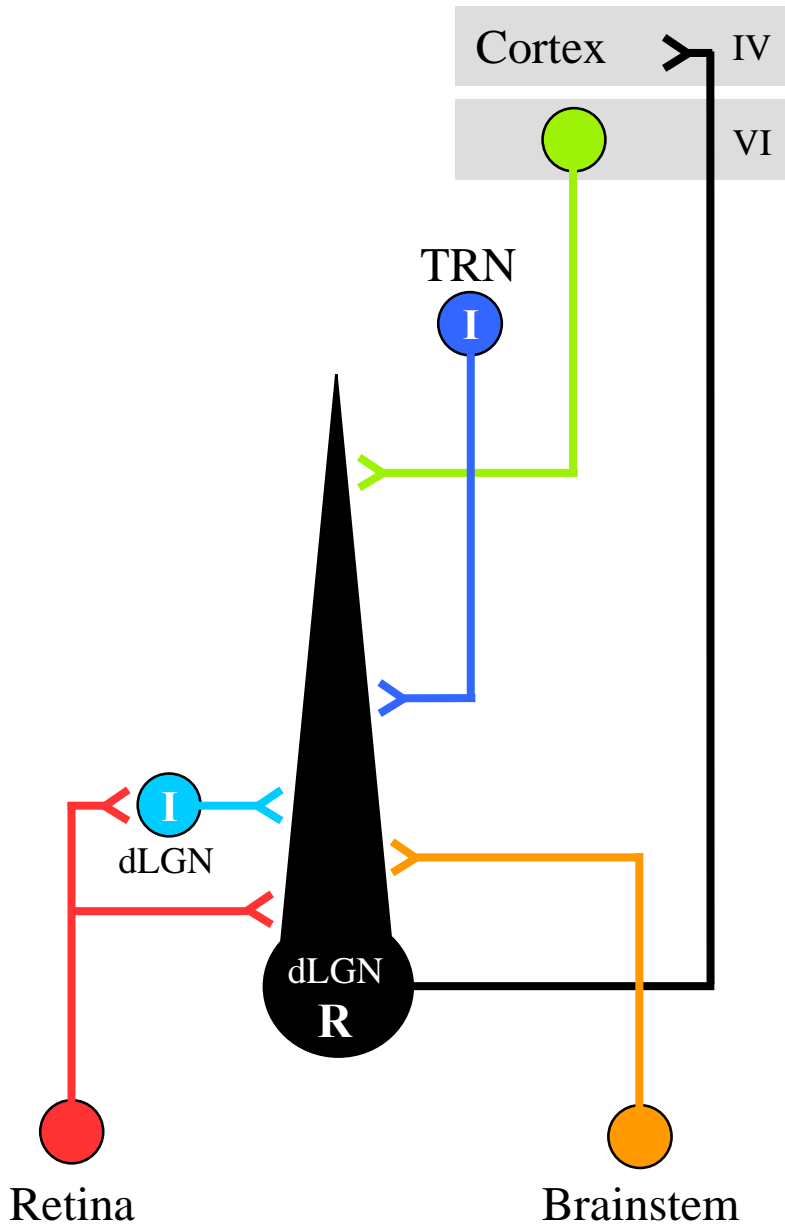
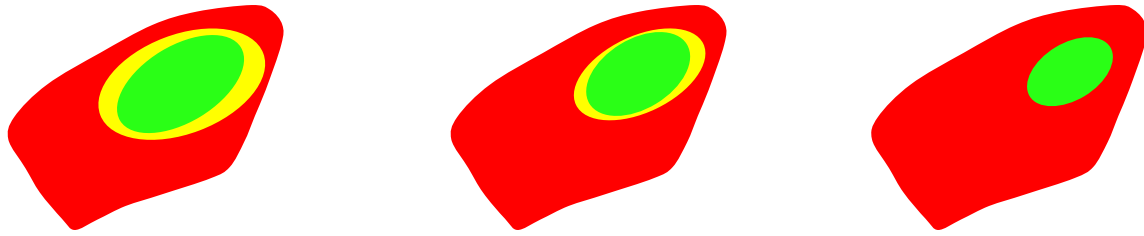


Figure 2

Summary of retinogeniculate development in dLGN.

Eye-specific segregation of retinogeniculate projections is shown in the top panel. Crossed retinogeniculate projections from the contralateral eye are shown in red and uncrossed retinogeniculate projections coming from the ipsilateral eye are green. The dLGN in the mouse receives projections from the two and at first these projections overlap (yellow). During early postnatal development there is a retraction uncrossed terminal arbors. Around the time of eye opening, projections from the two eyes are well segregated and resemble the pattern found in the adult. Bottom panel shows that a single relay cell initially receives numerous weak, binocular inputs from the retina. After the first postnatal week retinal convergence onto relay cells decreases so that by the third postnatal week only a few strong, monocular retinal inputs remain. It is not known when functional retinal connections with interneurons form, but during the second postnatal week feedforward inhibition involving interneurons appears. R, relay cell; I, interneuron. Adapted from Guido, 2008.

Eye-specific Segregation



Synaptic Connectivity and Refinement

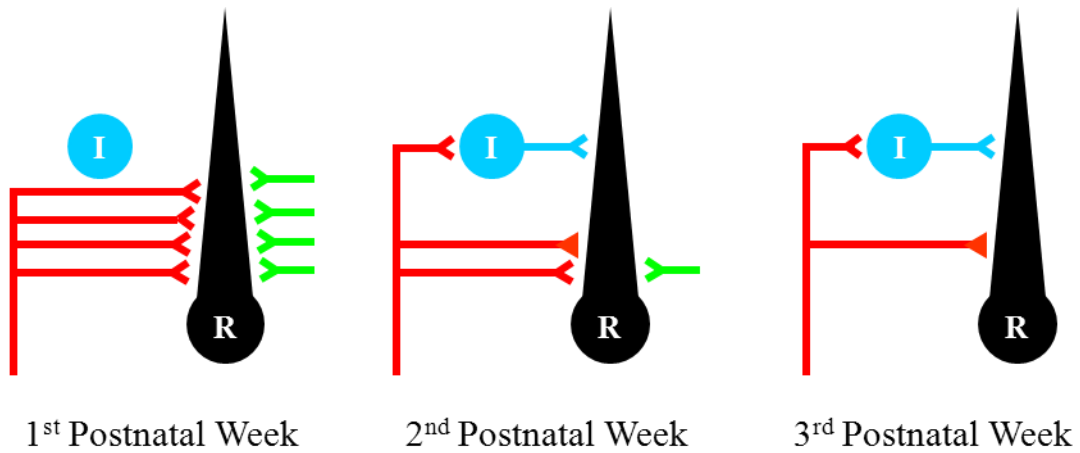
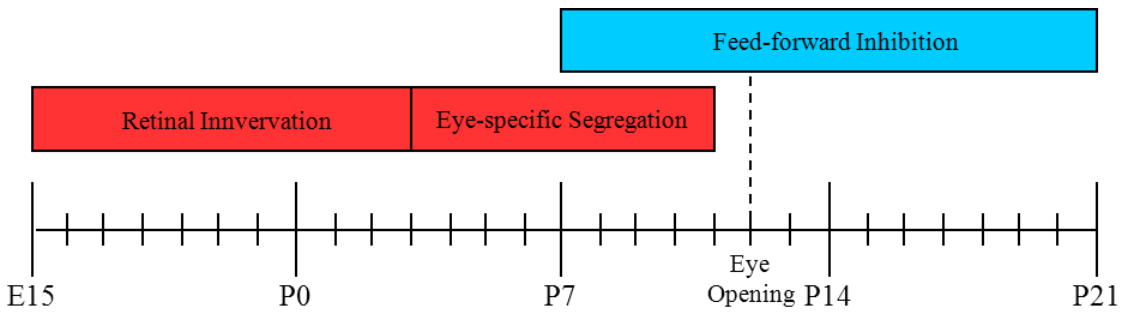
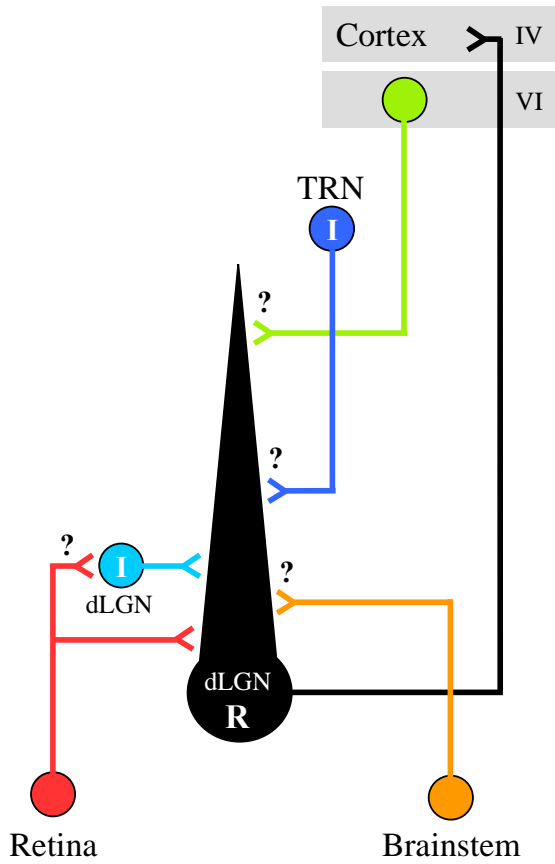


Figure 3

Timeline of circuit development in the dLGN of the mouse.

Top shows a schematic diagram of circuitry in the dLGN of the mouse. Question marks indicate which connections are not well understood. dLGN, dorsal lateral geniculate nucleus; R, relay cell; I, interneuron; TRN, thalamic reticular nucleus. Below is a timeline showing the sequence of events occurring during circuit development in the dLGN of the mouse. Retinal innervation of dLGN occurs at perinatal ages. A period of eye-specific segregation of retinogeniculate projections begins during the first postnatal week and is complete by eye opening. Disynaptic feedforward inhibition involving intrinsic interneurons begins to appear around P7-P9.



Chapter I

Pattern of Retinal Convergence onto Interneurons in the dLGN of the Mouse

Abstract

Two general classes of neuron are present within the dorsal lateral geniculate nucleus (dLGN), relay cells and interneurons. While both receive direct input from the retina, studies on the development of the retinogeniculate pathway have focused largely on the connections between retinal ganglion cells (RGCs) and relay cells. Little is known about the pattern of retinal convergence onto interneurons and whether they, like relay cells, undergo a period of pruning during early postnatal life. To address this we conducted *in vitro* whole-cell recordings from acute thalamic slices of GAD67-GFP mice, in which GFP is expressed in dLGN interneurons. Since interneurons comprise a small fraction of neurons in dLGN, GFP expression allowed us to readily identify and target them during *in vitro* recordings. To estimate the degree of retinal convergence onto interneurons, we prepared a slice, in which the retinal connections and intrinsic circuitry of dLGN were maintained. Electrical stimulation of optic tract was used to evoke excitatory postsynaptic potentials (EPSPs) in interneurons. Across all ages tested a progressive increase in stimulus intensity led to a graded increase in EPSP amplitude. Estimates of retinal convergence derived from EPSP by stimulus intensity plots revealed that interneurons received on average about 8 retinal inputs. Even at late postnatal ages interneurons received as

many as 10-13 inputs. Biocytin-labeled interneurons filled during recordings were imaged using multi-photon laser scanning microscopy to obtain 3-D reconstructions of their dendritic processes. Retinal terminals from both eyes were labeled with cholera toxin subunit B (CTB) conjugated to Alexa dyes in order to visualize retinal contacts on interneurons. The dendrites of interneurons were quite long, spanned large regions of dLGN, and readily crossed eye-specific borders. Retinal contacts were widely distributed on the soma and both proximal and distal regions of dendrites. Thus unlike relay cells, interneurons appear to receive input from several retinal ganglion cells with contacts scattered throughout their dendritic trees. Since high rates of convergence were apparent even at late postnatal ages it seems that interneurons are perhaps immune to the influence of early spontaneous retinal activity, an event that figures prominently in the segregation of eye-specific modules and pruning of RGC axons.

Introduction

The dLGN consists of two principal cell types, which both receive direct input from the retina (Hamos et al., 1985; Humphrey and Weller, 1988). Relay cells have a thick unbranched axon, large round somata, and multipolar dendritic arbors typical of class A morphology (Grossman et al., 1973; Rafols and Valverde, 1973; Parnavelas et al., 1977) and serve as the primary relay of retinal information to neurons in layer IV of visual cortex. Interneurons are local-circuit neurons involved in feedforward inhibition onto relay cells within dLGN and have class B morphology, which consists of small somata, bipolar shape, and long, thin dendrites that often run for large distances (Grossman et al., 1973; Rafols and Valverde, 1973; Parnavelas et al., 1977).

To date, studies on the development of the retinogeniculate pathway have focused primarily on the connections between retinal ganglion cells (RGCs) and relay cells. The dLGN of the mouse receives input from both eyes and in the adult these projections are organized into non-overlapping eye-specific domains (Guido, 2008). During early postnatal development terminal arbors from the two eyes are intermingled. However, these overlapping terminal fields recede so that by the second postnatal week projections from the two eyes are well segregated and form eye-specific domains (Jaubert-Miazza et al., 2005). *In vitro* intracellular recordings in mouse and rat show that retinal convergence onto relay cells in dLGN declines with age (Chen and Regehr, 2000; Lo et al., 2002; Jaubert-Miazza et al., 2005; Ziburkus and Guido, 2006; Dilger et al., 2011). Initially, a single relay cell receives numerous RGC inputs from both eyes, but

during early postnatal development there is a pruning of retinal axons so that by the third postnatal week only 1-3 monocular inputs remain (Fig. 4). Relay cells have well-defined concentric center-surround receptive fields that are dominated by input from a few RGCs of the same center type (Hubel and Wiesel, 1961; Cleland et al., 1971; Mastronarde, 1987; Usrey et al., 1999; Grubb and Thompson, 2003).

We know that feedforward inhibition involving interneurons in dLGN does not appear until the second postnatal week (Bickford et al., 2010) yet, little is known about the pattern of retinal convergence onto these interneurons throughout development and whether they, like relay cells, undergo a period of pruning (Fig. 4). Similar to relay cells, interneurons have circular receptive fields comprised of a concentric center and surround, which have opposite preferences for luminance (Dubin and Cleland, 1977; Wang et al., 2011a). It has been suggested that the receptive fields of interneurons may be larger than those of relay cells, since they are fewer in number and have very large dendritic processes (Wang et al., 2011a; Wang et al., 2011b). Moreover, retinal inputs make up the majority of contacts onto interneurons. For example in cats, only 7% of all terminals onto relay cells are of retinal origin, whereas almost 50% of the terminals onto interneurons originate from retina (Van Horn et al., 2000). Taken together this would suggest that there is a high degree of retinal convergence onto interneurons even at adult ages (Acuna-Goycolea et al., 2008). However, age-related patterns of retinal convergence have not been fully explored especially at early postnatal ages when retinogeniculate projections are remodeling.

To address this we conducted *in vitro* whole-cell recordings using acute thalamic slices from GAD67-GFP mice. In this transgenic mouse the GAD1 promoter was used to target enhanced green fluorescent protein (GFP) in the parvalbumin subset of GABAergic interneurons

(Chattopadhyaya et al., 2004) and as a result the interneurons intrinsic to dLGN express GFP. Since interneurons make up only a small portion (5-10%) of the total cell population in the dLGN of rodents (Gabbott et al., 1986; Arcelli et al., 1997; Jaubert-Miazza et al., 2005) it has been difficult to target them for whole-cell recordings. Using the GAD67-GFP mouse we can take advantage of GFP expression in dLGN to easily identify and target interneurons for recordings. To study retinal convergence we utilized a slice preparation that preserves optic tract and its connections with dLGN as well as the intrinsic circuitry of dLGN (Chen and Regehr, 2000; Bickford et al., 2010; Dilger et al., 2011). To evoke synaptic activity in interneurons stimulating electrodes were placed in optic tract. Electrical stimulation of optic tract was gradually increased and the resulting excitatory postsynaptic potentials (EPSPs) were examined. Plots of EPSP amplitude by stimulus intensity were used to estimate the number of retinal inputs onto interneurons (Lo et al., 2002; Jaubert-Miazza et al., 2005; Ziburkus and Guido, 2006; Dilger et al., 2011).

Retinal contacts on relay cells are restricted primarily to proximal regions of dendrites (Wilson et al., 1984), but whether there is a regional preference for retinal contacts on interneurons is not known. To assess this we did 3-D reconstructions of individual cells (Krahe et al., 2011) by filling interneurons with biocytin during whole-cell recordings. When done in conjunction with anterograde labeling of retinal projections using cholera subunit B (CTB) this allowed us to examine the distribution of retinal contacts onto interneurons.

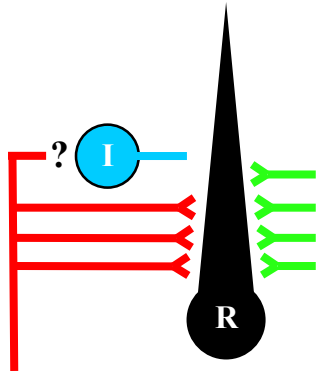
Figure 4

Schematic showing retinogeniculate innervation of relay cells and interneurons.

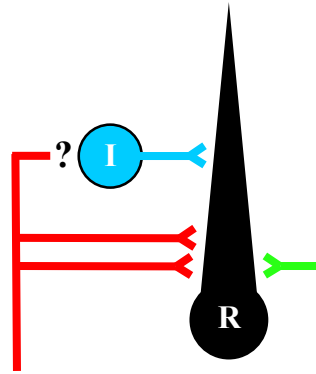
Retinogeniculate innervation begins at perinatal ages. Initially a single relay cell receives binocular input from many RGCs. After the first postnatal week retinal convergence onto relay cells decreases so that by the third postnatal week only a 1-3 monocular retinal inputs remain.

Both relay cells and interneurons are receiving direct retinal input, but the pattern of convergence onto interneurons is unknown. Note that during the second postnatal week feedforward inhibition involving interneurons intrinsic to dLGN appears. R, relay cell; I, interneuron.

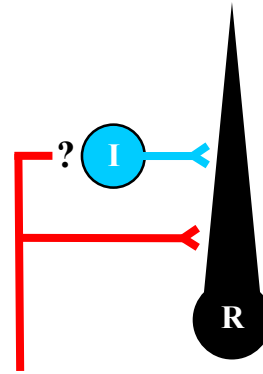
1st Postnatal Week



2nd Postnatal Week



3rd Postnatal Week



Methods

Subjects. Experiments were performed on C57BL/6 mice (Taconic Farms) and GAD67-GFP (The Jackson Laboratory, stock number 007677) mice ranging in age from postnatal day (P) 7 to 34. For GAD67-GFP mice, founder line was on a pigmented background (C57BL/6 x CB6F1/J). To visualize dLGN interneurons, GAD67-GFP mice were used (Chattopadhyaya et al., 2004). Pups were bred in a resident colony from breeders that were obtained from commercial vendors. For all surgical procedures, animals were deeply anesthetized with isoflurane vapors. All experiments were conducted under the guidelines of the Institutional Animal Care and Use Committee at Virginia Commonwealth University.

Intravitreal eye injections. Eye injections were carried out as reported previously (Jaubert-Miazza et al., 2005). Prior to natural eye opening, fused eyelids were separated or cut to expose the temporal region of the eye. The sclera was pierced with a sharp-tipped glass pipette and excess vitreous was drained. Another pipette, filled with a 1% solution of cholera toxin subunit B (CTB; Invitrogen) conjugated to either Alexa Fluor 594 or 555 dissolved in distilled water, was inserted into the hole made by the first pipette. The pipette containing the CTB was attached to a picospritzer and a prescribed volume (1-4 μ l at P0–P10 and 5-8 μ l for ages >P10) of solution was injected into the eye. After a 24-48 h survival period, animals were transcardially perfused with phosphate buffered saline followed by 4% paraformaldehyde in 0.1 M phosphate buffer for anatomical studies. The brains were postfixed overnight and sectioned at 70 μ m in the coronal plane using a vibratome (Leica, VT100S). Sections were mounted in ProLong Gold

antifade reagent with DAPI (Invitrogen) and imaged with epifluorescence microscopy. Images of dLGN were acquired with a Photometrix Coolsnap camera attached to a Nikon Eclipse fluorescence microscope using a 20x objective. Fluorescent images of labeled sections were acquired and digitized separately (1300×1030 pixels/frame) using the following filter settings: Alexa 488: Exciter 465–495, DM 505, BA 515–555; Alexa 594: Exciter 528–553, DM 565, BA 600–660.

Cell count and density measurements. A grid consisting of $50 \mu\text{m}$ by $50 \mu\text{m}$ boxes was overlaid onto dLGN by utilizing ImageJ software (NIH). The number of interneurons contained within each box was recorded. To calculate the overall cell density, the total number of cells was divided by the total number of boxes. To determine whether interneurons had a preference for the regions of dLGN where either contralateral or ipsilateral retinogeniculate projections reside or monocular or binocular segments, the total number of cells in those regions were divided by the total number of boxes the regions occupied.

In vivo slice physiology, intracellular filling, and tissue preparation. To visualize optic tract and dLGN in the thalamic slice as well as retinal contacts onto interneurons, we first performed CTB injections as described above. After a 24–48 h survival period, mice were prepared for acute *in vitro* thalamic slice recordings. To examine the synaptic responses evoked by optic tract stimulation we used a thalamic slice preparation in which retinal connections and intrinsic circuitry in dLGN were maintained (Chen and Regehr, 2000; Bickford et al., 2010; Dilger et al., 2011; see Fig. 6).

Individual ($300 \mu\text{m}$ thick) slices containing dLGN were placed into a recording chamber and maintained at 32°C and perfused continuously at a rate of 2.0 ml/min with oxygenated ACSF (in mM): 124 NaCl, 2.5 KCl, 1.25 NaH_2PO_4 , 2.0 MgSO_4 , 26 NaHCO_3 , 10 glucose, and 2

CaCl₂ (saturated with 95% O₂/5% CO₂), pH 7.4. *In vitro* recordings were done in the whole-cell current-clamp configuration with the aid of differential interference contrast (DIC) and fluorescence optics on a fixed stage, visualized recording apparatus (Olympus EX51WI). Patch electrodes (3-7 MΩ) made of borosilicate glass were filled with either a solution containing (in mM): 140 K gluconate, 10 HEPES, 0.3 NaCl, 2 ATP-Mg, 0.1 GTP-Na, pH 7.25 or a 5% biocytin solution containing (in mM): 130 K-gluconate, 10 HEPES, 8 NaCl, 2 ATP-Mg, 0.1 GTP-Na, pH 7.25. Once whole-cell recording was established, some neurons were filled with biocytin by passing alternating positive and negative current pulses (± 0.5 nA, 200 ms) through the recording electrode. For some cells, membrane properties and firing characteristics were examined by recording the voltage responses to intracellular injections of square-wave current pulses.

To evoke synaptic activity in dLGN, square-wave pulses (0.1-0.3 ms, 0.1-1 mA) were delivered at a rate of 0.2-1.0 Hz through a pair of thin-gauge tungsten wires (0.5 MΩ) positioned in the optic tract. Neuronal activity was digitized (10-20 KHz) through an interface unit (National Instruments, Baltimore, MD), acquired and stored directly on the computer, and analyzed by using commercial software (Strathclyde, Glasgow, Scotland; Electrophysiology Software, Whole Cell Analysis Program V3.8.2.). The amplitude of EPSPs evoked by progressive increases in stimulus intensity applied to the optic tract was measured and estimates of retinal convergence were based on EPSP amplitude by stimulus intensity plots. Once the single fiber response was determined, current intensity was increased in small increments (0.5 to 1.0 μ A) until a response of maximal amplitude was consistently reached. A change in amplitude that was equal to or exceeded a value that corresponded to the single fiber response was used to distinguish one input from another.

After recording, slices were fixed overnight with 4% paraformaldehyde in 0.1 M PBS, pH 7.2, and then incubated for 24 h in a 0.1% solution of Alexa Fluor 647 conjugated to streptavidin (Invitrogen) dissolved in PBS with 0.1% Triton X-100. Slices were washed with PBS and then mounted with ProLong Gold (Invitrogen), cured overnight at room temperature, and stored in a freezer at -20°C . Sections were initially visualized and photographed with an upright epifluorescence microscope (Nikon E6000) to select labeled cells that were suitable for multi-photon laser scanning microscopy.

Cellular imaging and reconstruction. Reconstructions were done as reported previously (Krahe et al., 2011) using a multi-photon laser scanning microscope (Carl Zeiss LSM510 NLO Meta). Fluorescence from labeled dLGN neurons was excited using a 633 nm helium–neon laser and emission was detected over a range of 651–694 nm. Fluorescence from retinal terminals was excited using a 561 nm diode-pumped solid-state laser and emission was detected over a range of 575–615 nm. Targeted neurons were imaged with a C-Apochromat 40x (1.2 NA) water-immersion objective at a scan resolution of 2048×2048 pixels. 3-D datasets, collected through a depth of 20–50 μm , were compiled from a sequential series of optical slices with a step size through the z-axis of 0.48 μm (40x, 1.2 NA). Z-stack datasets were rendered using Volocity software (Improvision, version 6.0.1). Image stacks were collected in a plane that was parallel to the surface of the slice and were then deconvolved using an iterative restoration technique to reduce signal noise generated from outside the focal plane of interest. Threshold values were set according to signal intensity and background noise. A colocalization protocol based on minimum pixel intensity (bit depth = 8) and volume ($0.08 \mu\text{m}^3$) was employed to locate and measure retinal contacts on interneurons. ImageJ software (NIH) was used to quantify the amount of colocalization for the P20 interneuron.

Results

In order to study interneurons in the dLGN we made use of a transgenic GAD67-GFP mouse, in which the Gad1 promoter was used to selectively express enhanced green fluorescent protein (GFP) in parvalbumin-containing interneurons (Chattopadhyaya et al., 2004). The distribution of interneurons in a coronal section of thalamus from a P7 GAD67-GFP mouse is shown in Figure 5A. The highest density of interneurons in thalamus was found in dLGN and the lateral portion or retinorecipient zone of the ventral lateral geniculate nucleus (VLG). As expected, only a few interneurons were seen in the neighboring ventrobasal complex (VB; Ottersen and Storm-Mathisen, 1984; Arcelli et al., 1997). Figure 5B shows interneurons expressing GFP in coronal sections of dLGN in P7 (*left*) and P26 (*right*) GAD67-GFP mice. One eye was injected with cholera toxin subunit B (CTB) conjugated to Alexa 594 in these mice and uncrossed retinogeniculate projections are shown in red. The presence of a small ipsilateral patch located in the anteromedial region of dLGN served as a landmark for estimating the monocular and binocular segments as well as eye-specific domains of dLGN (Coleman et al., 2009). A grid consisting of 50 μm by 50 μm boxes was placed over the dLGN and cell count and density measurements were obtained from three sections corresponding to the middle of dLGN. At both ages the GFP expressing interneurons were evenly distributed throughout dLGN (one-way ANOVA, $F = 2.98$, Bonferroni's *post hoc* test, $p = 1$). Figure 5B shows that at P7 (*left*) and P26 (*right*) there was no difference in cell density between the monocular and binocular regions of dLGN. There was also no preference for the areas that were occupied by either contralateral or

ipsilateral retinogeniculate projections (one-way ANOVA, $F = 2.98$, Bonferroni's *post hoc* test, $p = 1$). Finally, there was no significant difference in cell density with age (one-way ANOVA, $F = 2.98$, Bonferroni's *post hoc* test, $p > 0.30$) with the average density of interneurons in dLGN at P7 and P26 being between 1-2 cells per $2500 \mu\text{m}^2$.

We did *in vitro* whole-cell recordings in order to study the electrophysiological properties and synaptic responses of interneurons by making use of a parasagittal slice preparation, in which retinal connections and circuitry in dLGN were maintained (Fig. 6A; Chen and Regehr, 2000; Bickford et al., 2010; Dilger et al., 2011). GFP expression in interneurons allowed us to readily identify and target them during *in vitro* recordings (Fig. 6B). A bipolar electrode was placed in optic tract and used to stimulate retinal fibers in order to evoke excitatory postsynaptic potentials (EPSPs) during whole cell recordings of interneurons.

Targeted recordings at different postnatal ages confirmed that GFP expressing cells possessed the functional and morphological properties of interneurons. The active membrane properties of GFP expressing cells were examined and Figure 7A,B shows representative examples of voltage responses to current injection in cells recorded at P10 (A) and P18 (B). At all ages tested the active membrane properties resembled those typically observed for interneurons ($n = 10$, P10-P20; Pape et al., 1994; Pape and McCormick, 1995; Williams et al., 1996; Zhu et al., 1999a; Zhu et al., 1999b). Membrane hyperpolarization evoked a slow, mixed cation conductance (h), which produced a large, depolarizing sag (Fig. 7A,B, *bottom*) and a strong inward rectification that can be seen in the current-voltage plots (Fig. 7C,D). Termination of the hyperpolarizing current sometimes led to the activation of a T-type low threshold Ca^{2+} conductance (LT) which takes the form of a small rebound triangular depolarization with a single action potential riding its peak (Fig. 7A,B, *bottom*). Figure 7A,B (*middle*) shows that moderate

depolarization produced an outward rectification that reflects the activation of a transient K^+ conductance (A), an event that delays the firing of action potentials. Strong depolarization evoked to a train of action potentials that showed little or no spike frequency accommodation (Fig. 7A,B, top).

During whole-cell recordings neurons can be filled with biocytin by passing alternating positive and negative current pulses through the recording electrode. Post-fixed slices can then be histologically reacted for biocytin in order to examine cell morphology. We used this to further confirm that our recordings were from interneurons since they can be readily distinguished from relay cells by their different morphological characteristics (Williams et al., 1996; Krahe et al., 2011). Examples of biocytin-labeled interneurons at different postnatal ages are shown in Figure 8. At all ages, labeled cells had type B morphology (Grossman et al., 1973; Rafols and Valverde, 1973; Parnavelas et al., 1977) and tended to have primary dendrites that originated from opposite poles of a small, spindle-shaped soma. There were around 2-4 primary dendrites with a branching pattern that spanned large sectors of dLGN, sometimes even crossing eye-specific domains (Fig. 8, upper left panel).

To estimate the degree of retinal convergence onto interneurons, we measured the amplitude of EPSPs evoked by progressive increases in stimulus intensity applied to optic tract fibers (Lo et al., 2002; Jaubert-Miazza et al., 2005; Ziburkus and Guido, 2006; Dilger et al., 2011). EPSP amplitude by stimulus intensity plots were constructed by first determining the minimum stimulus intensity needed to evoke a postsynaptic response, this was the single fiber response. Once the single fiber response was determined, current intensity was increased in small increments (0.5 to 1.0 μ A) until a response of maximal amplitude was consistently reached. Plots of EPSP amplitude as a function of stimulus intensity for P7, P16, P21, and P27 interneurons are

provided in Figure 9A. The insets are the corresponding EPSPs evoked at increasing levels of optic tract stimulation for the different ages. The plots were used to estimate the number of retinal inputs a cell received. At all ages, increasing the intensity of optic tract stimulation resulted in a graded increase in EPSP amplitude. Such functions are believed to reflect a high degree of retinal convergence (Chen and Regehr, 2000; Lo et al., 2002; Ziburkus et al., 2003). Indeed we estimated that these cells received between 7-9 retinal inputs even at late postnatal ages. A summary plot comparing the number of retinal inputs throughout age for interneurons (P7-P33) is shown in Figure 9B. Initially interneurons received as many as 6-18 retinal inputs and at older ages interneurons continued to receive an average of 8 inputs. This is in stark contrast to what has been reported for relay cells (Chen and Regehr, 2000; Lo et al., 2002; Jaubert-Miazza et al., 2005; Ziburkus and Guido, 2006; Dilger et al., 2011). For example, relay cells originally receive as many as a dozen retinal inputs, but at older ages only 1-3 inputs remain. These differences are best illustrated by comparing the convergence ratio (total number of inputs at a particular age/total number of cells at that age) for a group of relay cells (Dilger et al., submitted) and our present data for interneurons. This summary plot is shown in Figure 9C. While the degree of retinal convergence onto relay cells decreased with age the degree of retinal convergence onto interneurons remained relatively stable and high throughout postnatal development and had a distribution that was significantly different from that of relay cells (Kolmogorov-Smirnov, $Z = 2.391$, $p = 0$)

From the EPSP amplitude by stimulus intensity plots we were also able to estimate single fiber response (minimum) and maximum amplitudes across different postnatal ages. Figure 10A shows examples of synaptic responses evoked at increasing levels of optic tract stimulation for interneurons recorded at P7, P14, P20, and P33. Figure 10B shows a summary plot comparing

the minimum amplitude of EPSPs evoked with optic tract stimulation throughout the first 5 postnatal weeks. The minimum amplitudes were relatively small (0.8-1.3 mV) and did not vary with age (one-way ANOVA, $F = 1.56$, Bonferroni's *post hoc* test, $p > 0.183$). A summary plot comparing the maximum amplitude for postnatal weeks 1-5 is shown in Figure 10C. Maximum responses were typically several-fold greater in amplitude (11-24 mV) compared to the minimum responses. In addition, we found that the maximum amplitude decreased with age. The maximum amplitude at week 1 was significantly higher than at weeks 2, 4, and 5 (one-way ANOVA, $F = 8.56$, Bonferroni's *post hoc* test, $p < 0.03$).

In addition to studying how retinal convergence onto interneurons changes during development we also wanted to examine how retinal contacts are distributed on the dendrites of interneurons. To accomplish this we injected CTB conjugated to Alexa 555 in both eyes of GAD67-GFP mice and filled interneurons with biocytin during *in vitro* whole-cell recordings. These biocytin-labeled interneurons were then reconstructed using multi-photon laser scanning microscopy. Maximum intensity projection images of reconstructed biocytin-labeled interneurons are shown in Figure 11A,B for two cells at P8 (*left*) and P20 (*right*). Based on synaptic responses to optic tract stimulation the interneurons shown were estimated to receive 10-13 retinal inputs. The interneuron (green) and retinal terminals labeled with CTB (red) can be seen in Figure 11A. To determine where retinal inputs contact dendrites of these interneurons we examined the regions of colocalization between CTB and biocytin. In Figure 11B the sites of colocalization for contacts located on interneurons are shown in purple. To better illustrate all sites of retinal contact, the interneurons were removed from the images (Fig. 11C). There were a large number of retinal contacts on the interneurons that were distributed on the soma as well as proximal and distal regions of dendrites. For the entire P20 interneuron (see Fig. 11, *right*), the

total surface area of retinal contacts was calculated and expressed as a percentage of the total surface area of the cell. Figure 12 (*inset*) shows that around 25% of the total surface area of this interneuron contained retinal contacts. A plot of the location of these retinal contacts with respect to the soma revealed that they were widely distributed throughout the entire dendritic tree of the P20 interneuron and did not show any proximal or distal gradient (Fig. 12). Around 21% of the total surface area of retinal contacts was found on the soma. Each region of the dendritic tree contained between 11-22% of the total surface area of retinal contacts.

Figure 5

GFP expression in dLGN interneurons.

A, Coronal section of dLGN from a P7 GAD67-GFP mouse showing the distribution of GFP expressing interneurons. The highest density of interneurons in dorsal thalamus was found in dLGN. Also note the high density of interneurons in the lateral portion of VLG, which is the retinorecipient region of this nucleus. dLGN, dorsal lateral geniculate nucleus; VLG, ventral lateral geniculate nucleus; VB, ventrobasal complex. Scale bar, 100 μm . **B**, Coronal sections of dLGN from P7 (*left*) and P26 (*right*) GAD67-GFP mice that had one eye injected with CTB conjugated to Alexa Fluor 594. Interneurons in dLGN express GFP (green) and uncrossed retinogeniculate projections from the ipsilateral eye were anterogradely labeled with CTB (red). Dashed lines separate the monocular and binocular segments of dLGN. Scale bar, 100 μm . **C**, Summary plots showing the cell density in dLGN overall (total), the monocular region of dLGN (monocular), and the binocular region of dLGN (binocular). At P7 (*left*) and P26 (*right*) the GFP expressing interneurons were evenly distributed throughout dLGN. For both ages the density of interneurons was around 1-2 cells/2500 μm^2 . Error bars represent SEM.

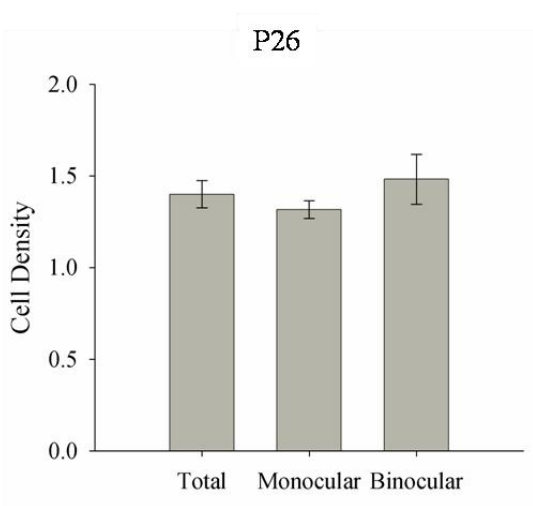
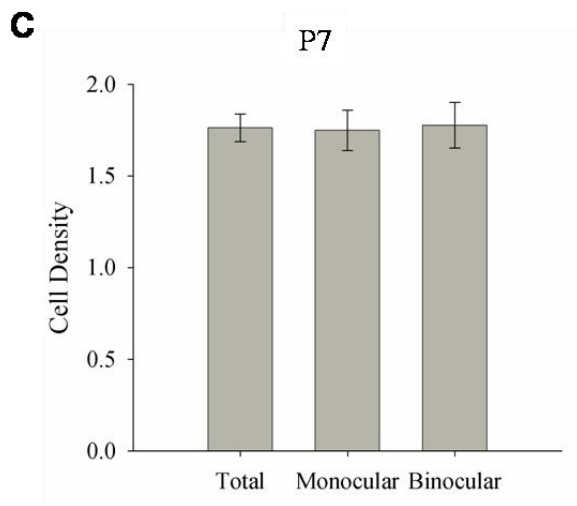
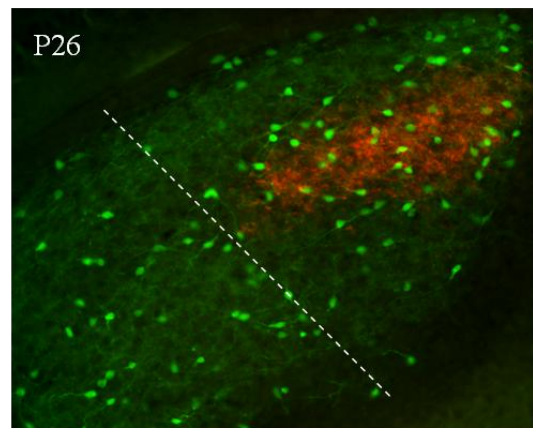
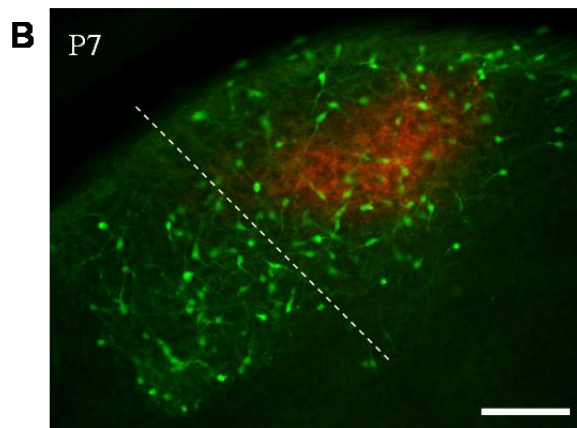
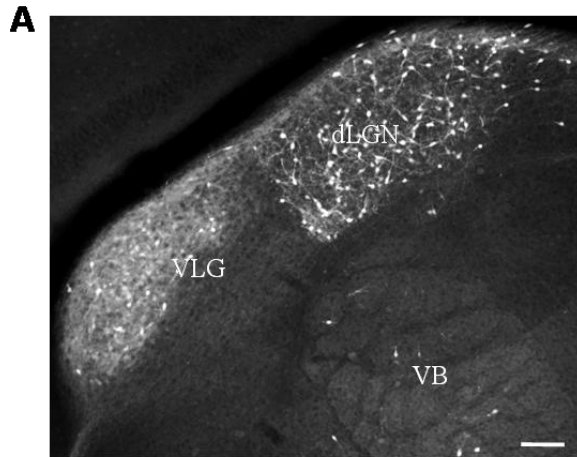


Figure 6

Targeting interneurons for whole-cell recordings using GFP expression in dLGN.

A, Schematic of thalamic slice preparation used for *in vitro* whole-cell recordings. Retinal connections and intrinsic circuitry in dLGN were maintained in this slice. dLGN, dorsal lateral geniculate nucleus; VLG, ventral lateral geniculate nucleus; OT, optic tract; D, dorsal; A, anterior. Recording electrode (white) in dLGN and bipolar stimulating electrode (black) placed in OT are also shown. Slice preparation adopted from Chen and Regehr, 2000. **B**, GFP expression was used to identify and target interneurons for recording. Interneuron expressing GFP in a 300 μm thick parasagittal slice as seen with fluorescence optics during *in vitro* recording is shown.

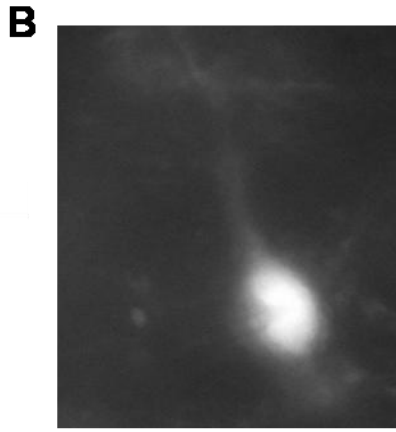
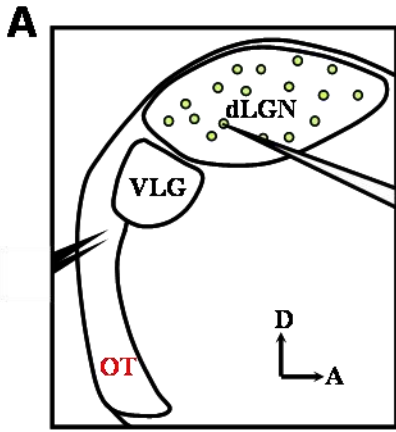
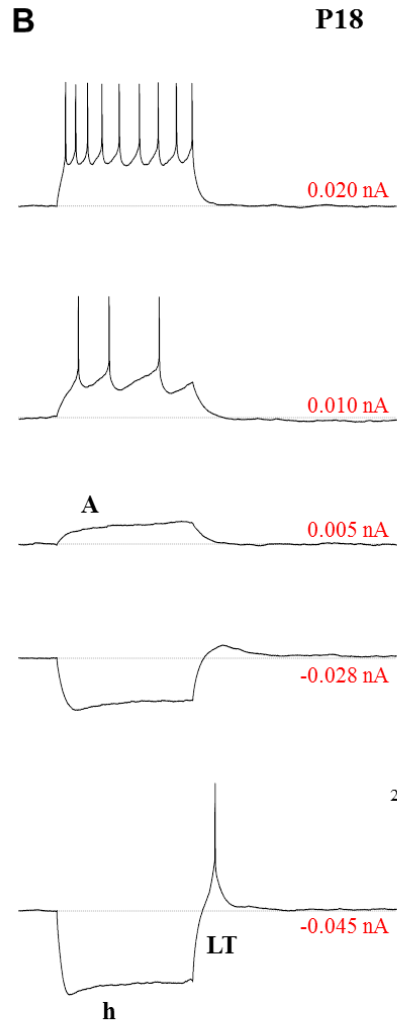
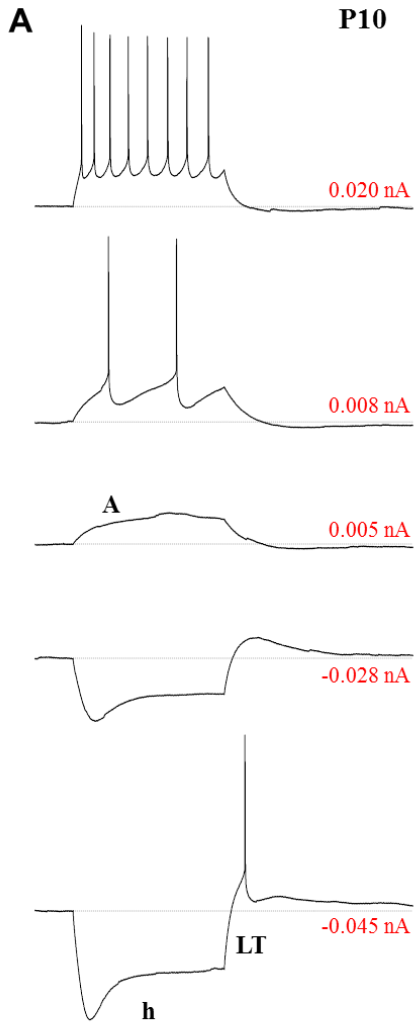


Figure 7

GFP expressing cells exhibit the characteristic active membrane properties of interneurons.

A-B, Examples of voltage responses to varying current injection in P10 (**A**) and P18 (**B**) interneurons. Sustained depolarization resulted in a train of action potentials showing little or no frequency accommodation as shown in the top two sets of responses. The middle set of responses shows a transient outward conductance (**A**). The bottom two sets of responses show that hyperpolarization elicited a large depolarizing sag mediated by a mixed cation conductance (**h**). In the same set of responses, termination of the hyperpolarizing current triggers a low-threshold Ca^{2+} (LT) spike. Interneurons did not produce the typical LT spike that triggers a burst of action potentials but instead tended to generate a single spike. The amount of current injected is shown in red. **C-D**, Current–voltage (I-V) plots for the P10 (**C**) and P18 (**D**) interneurons. Note the inward and outward rectification during hyperpolarization and depolarization, which correspond to **h** and **A**, respectively. The resting membrane potential and input resistance for the P10 interneuron was -62 mV and 1445.6 M Ω . The resting membrane potential and input resistance for the P18 interneuron was -65 mV and 1449.4 M Ω .



20 mV
250 ms

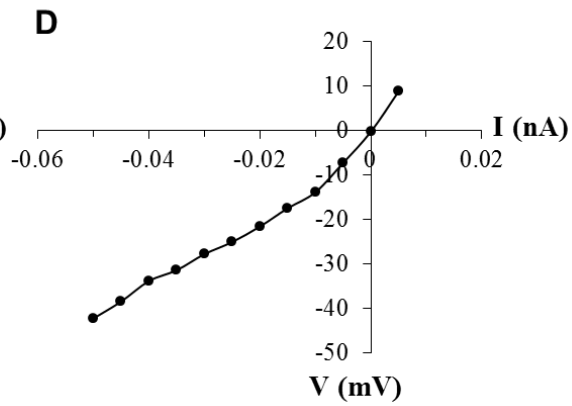
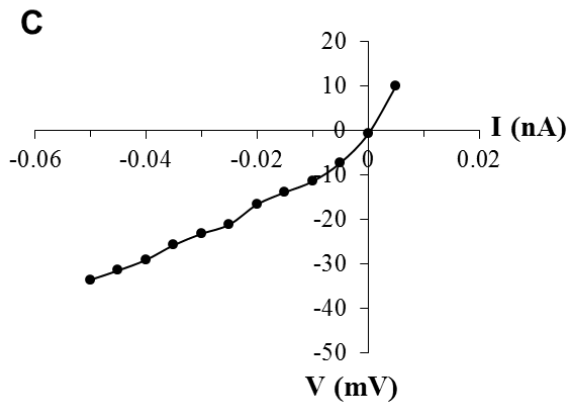


Figure 8

GFP expressing cells possess the morphological properties of interneurons.

Parasagittal sections of dLGN with biocytin-labeled cells at different postnatal ages. In the upper left panel, crossed retinogeniculate projections were labeled with CTB (red). At all ages biocytin-labeled cells exhibited the type B morphology characteristic of interneurons. Labeled cells typically had small, fusiform somata and primary dendrites, which originated from either end of the soma. There were 2-4 primary dendrites with a branching pattern that spanned large sectors of dLGN, often crossing eye-specific domains. Scale bar, 100 μm .

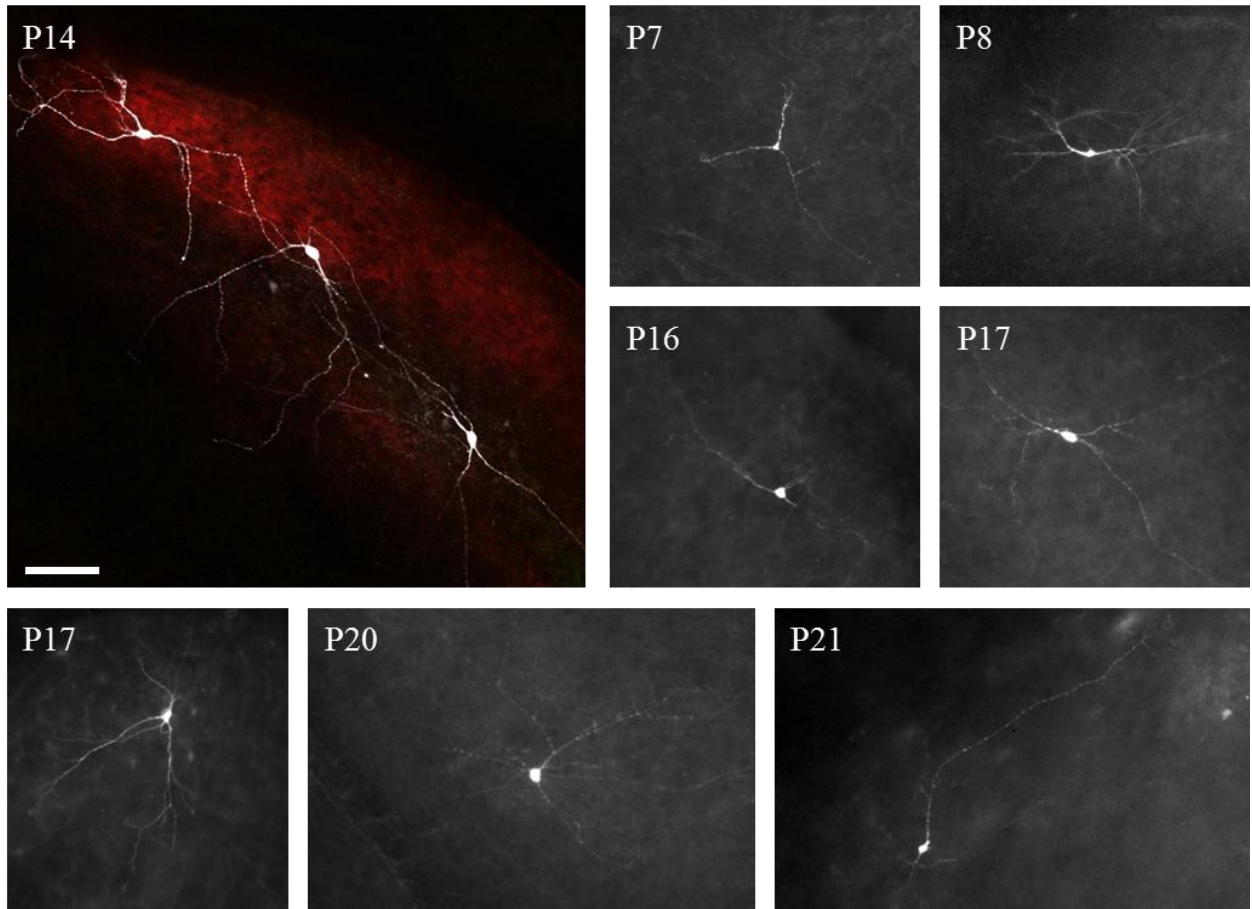


Figure 9

The degree of retinal convergence onto interneurons was maintained across age.

A, Shown are examples of stimulus by EPSP amplitude plots for P7, P16, P21, and P27 interneurons. These plots were used to estimate the number of retinal inputs a cell received (number of inputs are shown on the right side). Horizontal lines delineate separate retinal inputs. Insets depict corresponding responses evoked by increasing levels of optic tract stimulation. At all ages, increasing the intensity of optic tract stimulation resulted in a graded increase in EPSP amplitude, suggesting a high degree of retinal convergence. **B**, Scatter plot showing the number of inputs for interneurons at different postnatal ages. Each circle represents one cell. **C**, Summary plot of the convergence ratio (total number of inputs at a particular age/total number of cells at that age) for relay cells (black) and interneurons (gray). As opposed to that of relay cells the degree of retinal convergence onto interneurons remained relatively stable during development.

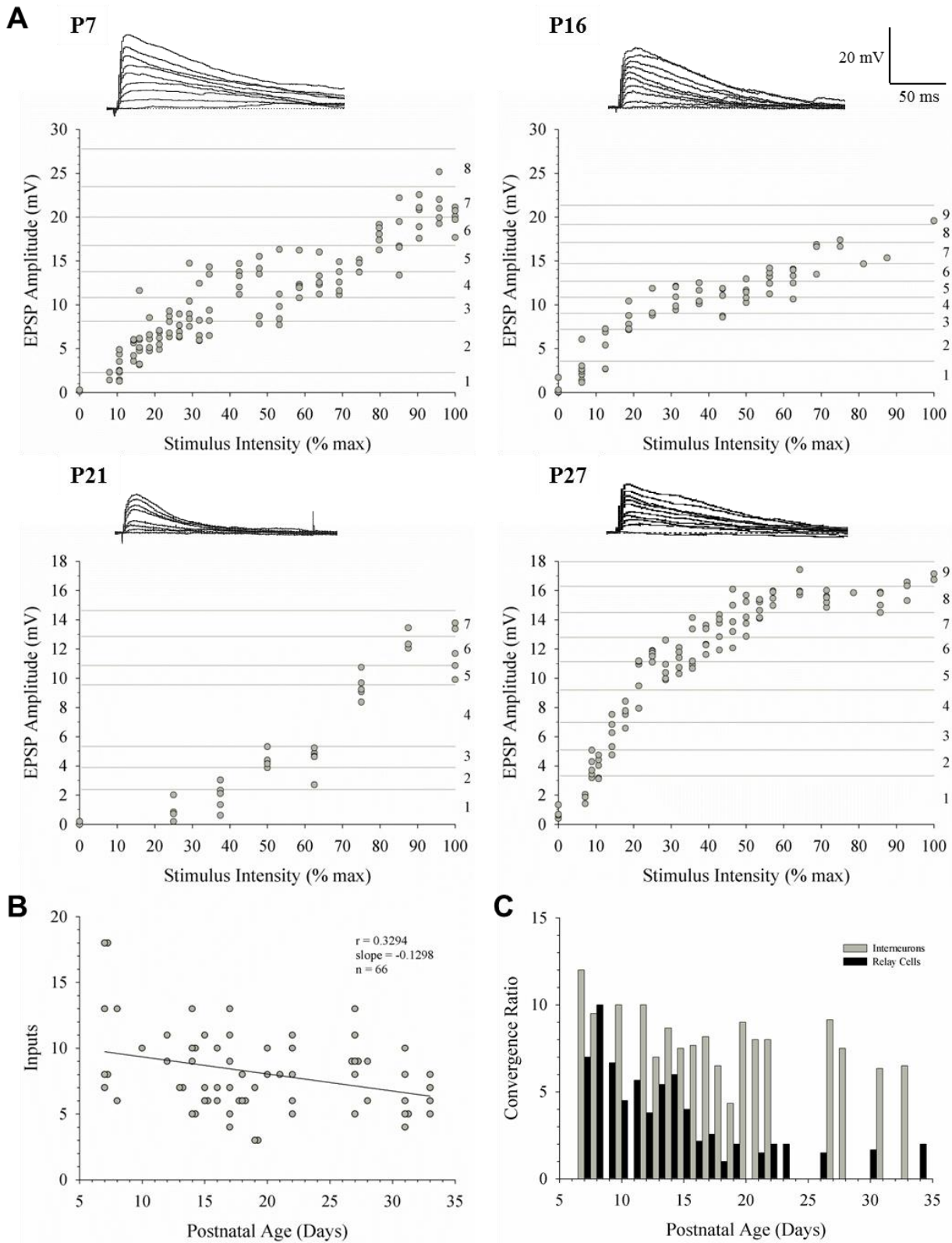


Figure 10

The maximum amplitude evoked by optic tract stimulation decreased with age.

A, Examples of excitatory postsynaptic potentials (EPSPs) evoked at increasing levels of optic tract stimulation for interneurons recorded at P7, P14, P20, and P33. At all ages, an increase in stimulus intensity led to a progressive (graded) increase in EPSP amplitude. **B-C**, Summary plots showing the mean minimum amplitude of EPSPs (**B**) or the mean maximum amplitude of EPSPs (**C**) from postnatal weeks 1 through 5. The minimum amplitude did not vary significantly with age however the maximum amplitude decreased with age (* $p < 0.05$). Week 1, $n = 6$; Week 2, $n = 13$; Week 3, $n = 23$; Week 4, $n = 14$; Week 5, $n = 10$. Error bars represent SEM.

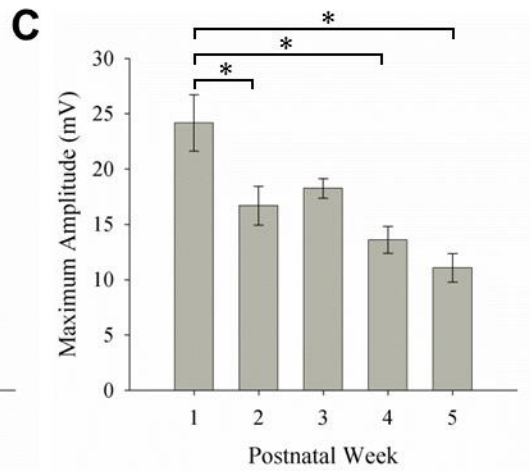
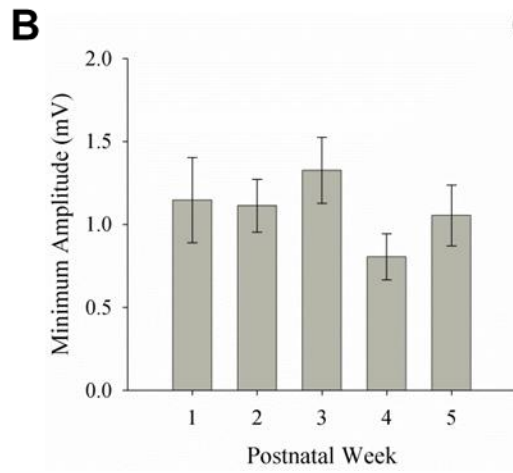
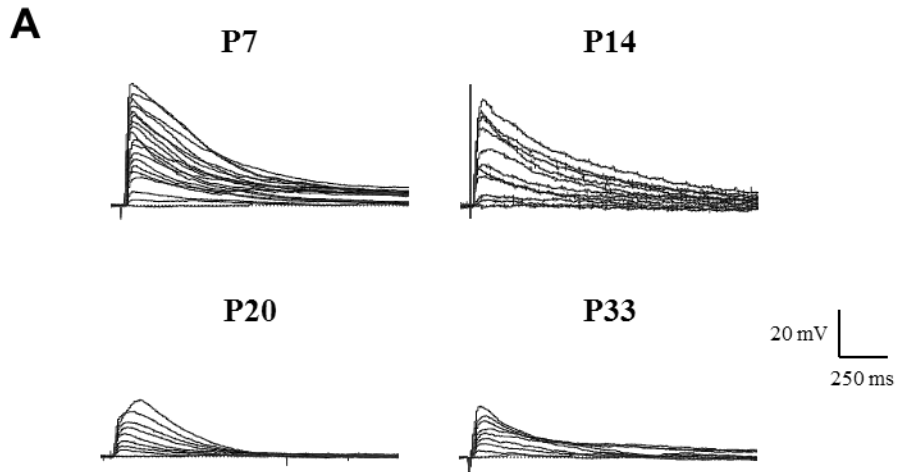


Figure 11

Distribution of retinal contacts on dLGN interneurons.

A, Maximum intensity projection images of reconstructed biocytin-labeled P8 (*left*) and P20 (*right*) interneurons (green) in thalamic slices of dLGN in which the retinal terminals from both eyes were labeled with CTB (red). Insets are lower magnification projection images showing the entire dendritic tree of each interneuron (asterisks mark reference points). Inset scale bar, 100 μm . **B**, The sites of colocalization between CTB and biocytin are shown in purple. **C**, The interneuron was removed in order to better visualize all sites of retinal contact. Unlike relay cells, interneurons displayed multiple sites of contact that were found on the soma as well as proximal and distal regions of dendrites. Scale bar, 41 μm .

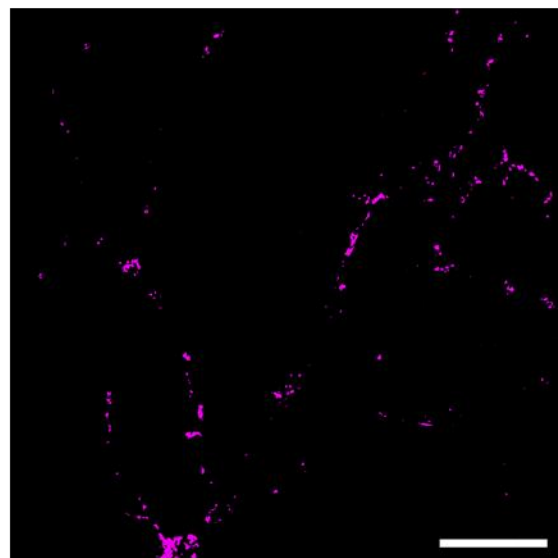
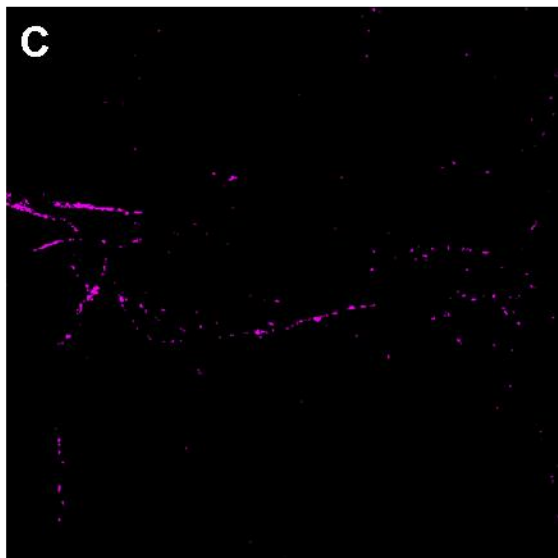
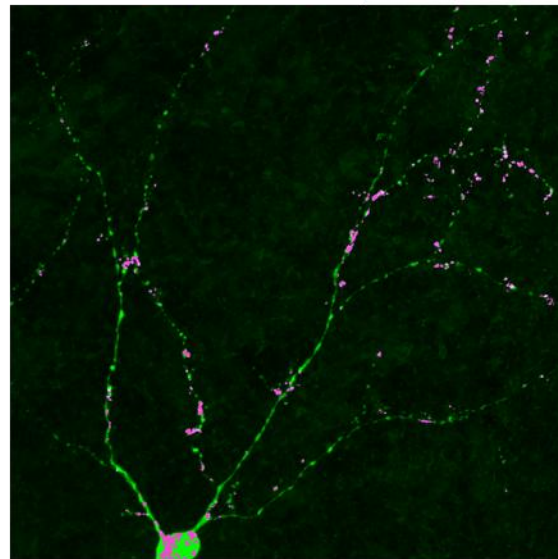
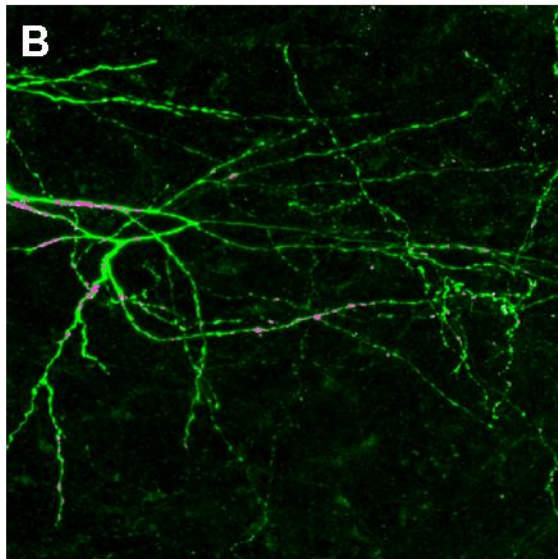
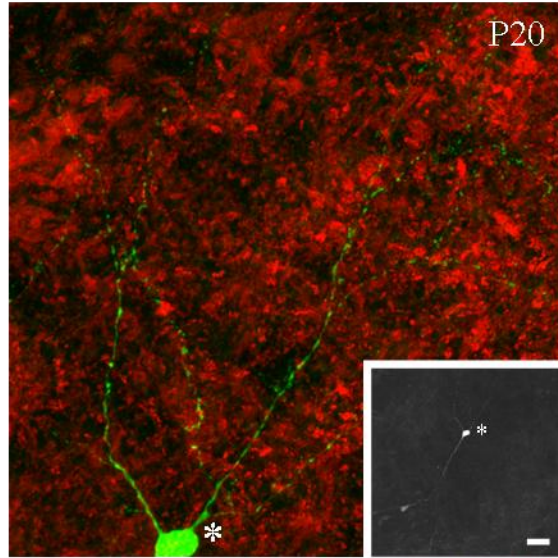
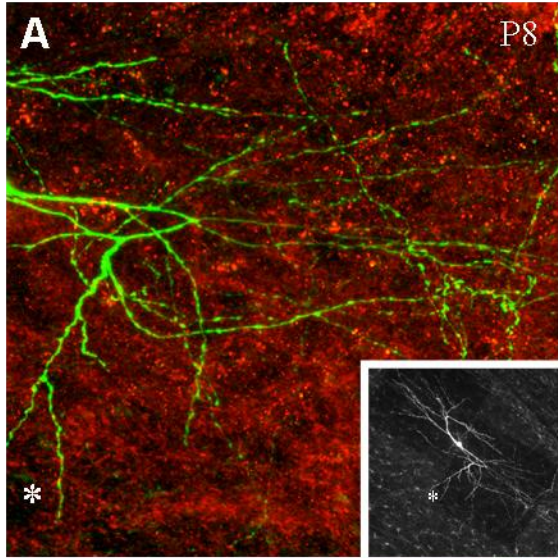
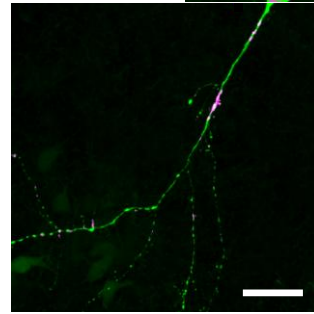
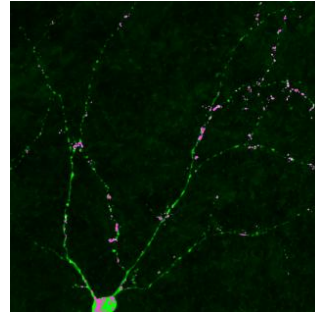
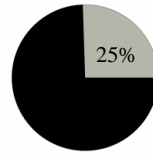
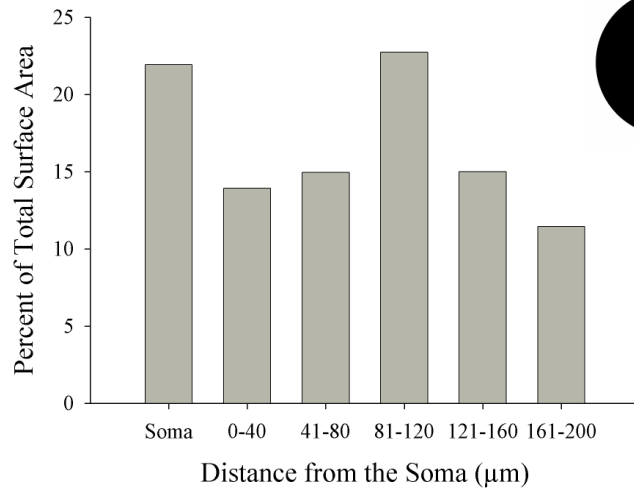


Figure 12

Retinal contacts were widely distributed throughout the dendritic tree of an interneuron.

Summary plot showing the distribution of retinal contacts on the soma and dendritic tree of a P20 interneuron. The first bar shows the surface area of retinal contacts on the soma as a percentage of the total surface area of retinal contacts. The following bars show the surface area of retinal contacts on dendritic regions at different distances from the soma as a percentage of the total surface area of retinal contacts. Inset is a pie graph showing that retinal contacts take up 25% of the total surface area of this interneuron. Far right shows the sites of retinal contacts (purple) on the maximum intensity projection image of the reconstructed biocytin-labeled P20 interneuron (green). Scale bar, 41 μm . Retinal contacts were roughly evenly distributed throughout the entire dendritic tree of this interneuron.

Retinal Contacts



Discussion

To study the pattern of retinal convergence onto interneurons we made use of a GAD67-GFP mouse (Chattopadhyaya et al., 2004). Another GAD67-GFP mouse strain (Tamamaki et al., 2003) has typically been used to examine interneurons in thalamus (Acuna-Goycolea et al., 2008; Antal et al., 2010; Augustinaite et al., 2011). However, this is a knock-in mouse, so there is targeted insertion of GFP into a specific locus. Therefore, in addition to interneurons intrinsic to dLGN, the GABAergic cells in the thalamic reticular nucleus (TRN), which send projections to dLGN, also express GFP. (Tamamaki et al., 2003; Augustinaite et al., 2011). Due to random insertion, GFP in the transgenic strain that we used is expressed in dLGN interneurons but not the cells in TRN. This is advantageous for studies that require labeling of only the inhibitory cells intrinsic to dLGN.

We confirmed that GFP expressing cells in the dLGN of GAD67-GFP mice were indeed interneurons through examination of their physiological and morphological properties. We found that the active membrane properties of GFP expressing cells were consistent with those previously characterized for interneurons (Pape et al., 1994; Pape and McCormick, 1995; Williams et al., 1996; Zhu et al., 1999a; Zhu et al., 1999b). Membrane hyperpolarization evoked a slow, mixed cation conductance (h), which produced a strong inward rectification, and termination of the hyperpolarizing current led to generation of a LT spike. Moderate depolarization activated a transient K^+ conductance (A) that created an outward rectification. Strong depolarization evoked a train of action potentials that showed little or no spike frequency

accommodation. Moreover, the morphological characteristics that we observed for cells expressing GFP were in accord with what has been shown for interneurons in rodents. They exhibited class B morphology, which consisted of primary dendrites that originated from opposite poles of a small soma and a branching pattern that spanned large sectors of dLGN (Grossman et al., 1973; Rafols and Valverde, 1973; Parnavelas et al., 1977).

Our results revealed that the pattern of retinal convergence onto interneurons in dLGN is maintained throughout age. Furthermore, we found that at all ages tested there was a high degree of retinal convergence onto interneurons, so that interneurons received between 6-18 retinal inputs before eye opening and continued to receive as many as 13 inputs even at late postnatal ages. This convergence of retinal input was also reflected in the distribution of retinal contacts on interneurons. There were numerous retinal contacts found on soma as well as proximal and distal regions of dendrites. A quantitative analysis of one cell at P20 revealed that retinal contacts did not exhibit any regional preferences on dendrites of interneurons.

Overall these results are in stark contrast to the pattern of retinal convergence observed for relay cells. Retinal convergence onto relay cells in dLGN is reduced with age (Chen and Regehr, 2000; Lo et al., 2002; Jaubert-Miazza et al., 2005; Ziburkus and Guido, 2006; Dilger et al., 2011). Initially, relay cells receive as many as a dozen weak, binocular inputs from different RGCs. However, in the mature mouse there is little convergence since relay cells are receiving only 1-3 strong, monocular inputs. Conversely, we found that there is a high degree of retinal convergence onto interneurons in dLGN that remains relatively stable throughout age. Single fiber responses in relay cells have been shown to become larger after eye opening (Chen and Regehr, 2000), however we observed that the amplitude of single fiber responses in interneurons were small and did not vary with age. For interneurons we also observed a change in the

maximum amplitude of EPSPs, which actually got smaller with age and is perhaps related to low pass filtering or dendritic attenuation (Bloomfield et al., 1987). In rat, the dendrites of interneurons expand during early postnatal development so that dendritic length as well as branching increases with age (Perreault et al., 2003). If this is occurring in mouse then the increased dendritic length and branching at older ages could be causing more attenuation of EPSPs traveling from distal dendrites to the soma.

The synaptic refinement of retinal inputs on relay cells correlates well with the maturation of their receptive field properties. At first, receptive fields of relay cells are large, irregularly shaped, and lack distinct on- and off-subregions. Mature receptive fields of relay cells are smaller, have well-defined concentric center-surround organization, and are quite similar to those of RGCs (Cleland et al., 1971; Tootle and Friedlander, 1986; Mastronarde, 1987; Usrey et al., 1999; Tavazoie and Reid, 2000; Grubb and Thompson, 2003). The high rate of convergence onto interneurons is consistent with their receptive field structure, morphology, and ultrastructure. They also have a concentric center-surround structure but may be larger than those of relay cells (Wang et al., 2011a; Wang et al., 2011b) due to the fact that interneurons make up only 5-10% of the total cell population in dLGN (Jaubert-Miazza et al., 2005) and receive many more retinal synapses than relay cells (Montero, 1991; Van Horn et al., 2000).

By design interneurons in dLGN must receive a large number of retinal inputs that are distributed throughout their soma and dendritic trees. dLGN interneurons have both conventional axonal (F1 terminals) as well as dendritic (F2 terminals) synaptic outputs (Guillery, 1969; Ralston, 1971; Famiglietti and Peters, 1972; Wilson et al., 1984; Hamos et al., 1985) allowing for multiple forms of inhibition. In contrast to relay cells, whose axons exit dLGN and project to primary visual cortex, the axon of an interneuron does not leave the dLGN but instead arborizes

within the dendritic tree of the interneuron (Perreault et al., 2003; Sherman, 2004). The axonal outputs of interneurons are controlled by retinal input on their soma and proximal dendrites. F1 terminals form simple contacts onto proximal dendrites of relay cells (Wilson et al., 1984; Hamos et al., 1987). F2 terminals are typically found on distal dendrites of interneurons and are usually involved in complex synaptic arrangements or triads (Sherman, 2004) that are located within glomeruli, which are tightly packed groups of presynaptic and postsynaptic profiles enclosed in a glial sheath (Szentagothai, 1963). In a synaptic triad, a single retinal terminal contacts both an F2 terminal of an interneuron and a dendritic appendage of a relay cell (Rafols and Valverde, 1973; Sherman, 2004). The same F2 terminal in turn contacts the same relay cell dendritic appendage. Both anatomical and physiological evidence suggests that inhibitory dendrodendritic synapses formed by F2 terminals are preferentially localized on proximal dendrites of relay cells (Guillery, 1969; Montero, 1986; Ralston, 1971; Famiglietti and Peters, 1972; Crandall and Cox, 2012).

F1 terminals appear to have a more global inhibitory influence in dLGN. For example, sodium action potentials have been shown to result in widespread calcium elevations in interneurons that evoke GABA release throughout the dendrites and axons of interneurons (Acuna-Goycolea et al., 2008; Casale and McCormick et al., 2011). The dendrites of interneurons span large areas of dLGN hence widespread inhibitory output could affect large regions of the visual field (Eysel et al., 1986; Zhu and Heggelund, 2001, Perreault et al., 2003). F2 terminals may provide focal inhibitory influences to dLGN and therefore act like independent, local processors (Ralston, 1971; Hamos et al., 1985; Govindaiah and Cox, 2004; Govindaiah and Cox, 2006; Crandall and Cox, 2012). The tight coupling within synaptic triads provides the ideal machinery for very localized and independent information processing and

would allow interneurons to function like multiplexors or a single neuron containing numerous independently operating input-output devices (Bloomfield and Sherman, 1989; Cox et al., 1998; Crandall and Cox, 2012). Both widespread and local forms of inhibition would require a high degree of retinal convergence onto interneurons.

What is the cellular mechanism that can account for pruning in one class of dLGN neuron but not the other? The refinement of retinal connections onto relay cells in dLGN has been attributed to early spontaneous retinal activity in the form of waves that occur before eye opening (Torborg and Feller, 2005). Waves are likely to drive postsynaptic activity in both relay cells and interneurons. However, in relay cells such activity is also likely to evoke plateau potentials that are mediated by high-threshold L-type Ca^{2+} channels (Lo et al., 2002; Jaubert-Miazza et al., 2005; Dilger et al., 2011). Activation of these channels has been shown to be important for the induction of long-term changes in synaptic strength in dLGN relay cells (Ziburkus et al., 2009). Ca^{2+} influx through L-type Ca^{2+} channels has also been linked to the activation of transcription factors that lead to the expression of genes associated with synaptic plasticity and remodeling, such as the cAMP-response element (CRE)/CREB transcriptional pathway (Mermelstein et al., 2000; Dolmetsch et al., 2001; Lonze and Ginty, 2002). Moreover, when L-type plateau activity is greatly attenuated by the use of a mouse lacking the β_3 subunit of the L-type Ca^{2+} channel (Dilger et al., submitted) or when CREB expression is reduced using α,Δ -CREB hypomorphic mice (Pham et al., 2001) eye specific segregation and/or pruning fails to occur. While interneurons are reported to have L-type activity (Acuna-Goycolea et al., 2008), we never observed it in the form of retinally evoked plateau potentials. Thus, it is intriguing to speculate that the propensity to prune in an activity dependent manner is linked to L-type activity and CREB, and that interneurons may lack such machinery.

Chapter II

Development of the Corticogeniculate Pathway in the dLGN of the Mouse

Abstract

Neurons in layer VI of visual cortex are one of the largest sources of nonretinal input to the dorsal lateral geniculate nucleus (dLGN), but little is known about how and when these nonretinal projections arrive and make connections. Here we make use of a transgenic mouse to visualize corticogeniculate projections in order to examine the timing and patterning of corticogeniculate innervation in dLGN. We found that corticogeniculate innervation occurred postnatally and was delayed in comparison to retinogeniculate innervation. Corticogeniculate fibers appeared to wait to invade dLGN until around P3-P4, a time when retinogeniculate innervation is complete, and did not fully innervate dLGN until eye opening, well after eye-specific segregation was finished. Slice recordings revealed that axons coming from cortex formed functional connections with dLGN relay cells during the early phase of corticogeniculate innervation, but these synapses did not become fully mature until after the first postnatal week. Finally, we found that retinal input regulates the timing of corticogeniculate innervation in dLGN. Corticogeniculate innervation was accelerated after eye removal but inter-areal targeting of these projections seemed to be unaffected. Our results indicate that innervation of dLGN by retinogeniculate and corticogeniculate projections occurs in a coordinated manner. Furthermore,

we showed that retinal input to dLGN is important for regulating the timing of corticogeniculate innervation.

Introduction

In the mouse dorsal lateral geniculate nucleus (dLGN), retinal projections provide the primary excitatory drive for relay cells. However, these inputs account for less than 10% of all synapses in dLGN (Bickford et al., 2010). The majority of synapses are formed by nonretinal projections that arise from thalamic reticular nucleus (TRN), brainstem, and layer VI of cortex (Sherman and Guillery, 2002; Bickford et al., 2010). Neurons in cortical layer VI are one of the largest sources of nonretinal input to dLGN (Erisir et al., 1997a,b) and have a major impact on thalamic signal transmission, sharpening receptive field properties of relay cells and influencing the gain of their output (Sherman and Guillery, 2002; Briggs and Usrey, 2008).

Despite the enormity of this projection and its extensive influence on thalamic signal transmission, virtually nothing is known about how and when the corticogeniculate pathway develops. Moreover, how it might be coordinated with the development and remodeling of retinal projections to dLGN. Visualizing corticogeniculate projections and isolating them for experimental manipulation has been a major challenge. For example it is difficult to label large regions of visual cortex while at the same time restricting the tracers to layer VI. In addition, corticogeniculate axons and terminals are very small making them difficult to resolve with bulk labeling techniques. To overcome these limitations, neurons can be selectively labeled through the use of transgenic methods (Young and Feng, 2004). In a recent study, a transgenic mouse was used to examine corticothalamic projections by utilizing a 1.3 kb *golli* promoter element of the myelin basic protein gene (Jacobs et al., 2007), which was previously shown to target

expression to neurons in deep cortical layers (Landry et al., 1998; Xie et al., 2002). This promoter drives the expression of a tau-enhanced green fluorescent fusion protein (τ -GFP) in the cell bodies and processes of layer VI cortical neurons. The use of the *golli*- τ -GFP mouse revealed that corticothalamic projections innervate thalamus in a ventrolateral to dorsomedial fashion and first target nuclei involved in motor and somatosensory processing. The medial geniculate nucleus and dLGN were not innervated until late postnatal ages.

What is lacking is a more detailed study of the progression of corticogeniculate innervation in dLGN and how it relates to the timing and remodeling of retinal projections. Retinogeniculate projections innervate dLGN perinatally (Godement et al., 1984) and form functional synapses at very early postnatal ages (Mooney et al., 1996; Chen and Regehr, 2000; Ziburkus et al., 2003; Jaubert-Miazza et al., 2005; Bickford et al., 2010). During early postnatal development retinogeniculate remodeling occurs so that projections from the two eyes are segregated into non-overlapping eye-specific domains in dLGN (Guido, 2008). To examine corticogeniculate innervation in relation to retinogeniculate development we did eye injections of cholera toxin subunit B (CTB) in *golli*- τ -GFP mice in order to visualize both retinogeniculate and corticogeniculate projections within the same animal. It is also important to know when these projections make functional connections in dLGN. Corticogeniculate synaptic responses have only been examined at later ages (Turner and Salt, 1998; Granseth et al., 2002; Granseth and Lindstrom, 2003; Alexander and Godwin, 2005; Kielland et al., 2006), therefore not much is known about the development of these synapses. We addressed this with both immunohistochemical staining for functional synaptic machinery and *in vitro* whole-cell recordings.

If retinogeniculate and corticogeniculate innervation is coordinated it may also imply that the retina could be playing a role in regulating corticogeniculate innervation in dLGN. In tree shrew, eye removal disrupts targeting within dLGN so that corticogeniculate fibers are no longer restricted to the koniocellular layers but instead now innervate retinorecipient layers (Brunso-Bechtold et al., 1983). However, in anophthalmic mice the topographic organization of corticogeniculate projections was indistinguishable from control animals (Rhoades et al., 1985). Whether the timing of corticogeniculate innervation is affected by the loss of retinal input remains to be tested. To study corticogeniculate innervation in the absence of retinal input we removed retinal input prior to the arrival of corticogeniculate projections. This was accomplished by enucleation at birth and genetic deafferentation. For genetic deafferentation, we crossed the *golli-τ*-GFP mouse with a *math5*-null (-/-) mouse (Wang et al., 2001). The transcription factor *math5* is required for retinal progenitor cells to differentiate into retinal ganglion cells (RGCs) (Brown et al., 1998). In the absence of *math5* there is a greater than 98% reduction in RGCs (Brown et al., 2001; Wang et al., 2001; Moshiri et al., 2008) and the remaining ones fail to form an optic nerve resulting in a dLGN devoid of retinal input (Brown et al., 2001; Wee et al., 2002; Brzezinski et al., 2005; El-Danaf et al., 2011). We used genetic deafferentation in addition to binocular enucleation for several reasons. The first is that retinal innervation begins at late embryonic ages (Godement et al., 1984), so there is some retinal input in dLGN prior to enucleation. Also with mechanical deafferentation the animals must undergo surgery and there is a process of retinal axon degeneration, which could make it challenging to resolve the underlying mechanisms regulating corticogeniculate innervation.

Methods

Subjects. Experiments were performed on C57BL/6 mice (Taconic Farms) and two different transgenic strains, *golli-τ-GFP* (Jacobs et al., 2007) and *math5*-null (-/-; Wang et al., 2001) mice, ranging in age from postnatal day (P) 0 to 45. For transgenic strains, founder lines were on a pigmented background (i.e., CB6F1/J, B6;129SV, or C57BL/6). *golli-τ-GFP* mice were used to visualize corticogeniculate projections. In order to visualize corticogeniculate innervation in the absence of retinal input, the offspring of *golli-τ-GFP* mice crossed with *math5*-/- mice were used to produce *golli-τ-GFP/math5*-/- mice. For all surgical procedures, animals were deeply anesthetized with isoflurane vapors. All experiments were conducted under the guidelines of the Institutional Animal Care and Use Committee at Virginia Commonwealth University.

Intravitreal eye injections. Eye injections were carried out as reported previously (Jaubert-Miazza et al., 2005). Prior to natural eye opening, fused eyelids were separated or cut to expose the temporal region of the eye. The sclera was pierced with a sharp-tipped glass pipette and excess vitreous was drained. Another pipette, filled with a 1% solution of cholera toxin subunit B (CTB; Invitrogen) conjugated to either Alexa Fluor 594 (red), 555 (red), or 488 (green) dissolved in distilled water, was inserted into the hole made by the first pipette. The pipette containing the CTB was attached to a picospritzer and a prescribed volume (1-4 μ l at P0–P10 and 5-8 μ l for ages >P10) of solution was injected into the eye. After a 24-48 h survival period, animals were transcardially perfused with phosphate buffered saline followed by 4%

paraformaldehyde in 0.1 M phosphate buffer for anatomical studies. The brains were postfixed overnight and sectioned at 70 μm in the coronal plane using a vibratome (Leica, VT100S). Sections were mounted in either ProLong Gold antifade reagent (Invitrogen) or ProLong Gold antifade reagent with DAPI (Invitrogen) and imaged with epifluorescence microscopy.

Enucleation. Monocular and binocular enucleations were done on *golli- τ -GFP* mice within 18 h after birth. Under deep anesthesia by inhalation of isoflurane (Phoenix Pharmaceuticals), the palpebral fissure was opened and the eyeball was isolated using a pair of curved forceps. The optic nerve and the ophthalmic artery were then cut and the eye was carefully removed. The orbit was filled with Gelfoam (Upjohn) to avoid hemorrhage. For monocular enucleation, the spared eye was injected with CTB conjugated to Alexa Fluor 594 (Invitrogen). The animals were allowed to recover on a heated pad and then were returned to their home cage.

Image Analysis. Images of dLGN were acquired with a Photometrix Coolsnap camera attached to a Nikon Eclipse epifluorescence microscope using a 10x objective. Fluorescent images of labeled sections were acquired and digitized separately (1300 \times 1030 pixels/frame) using the following filter settings: Alexa 488: Exciter 465–495, DM 505, BA 515–555; Alexa 594: Exciter 528–553, DM 565, BA 600–660; DAPI: Exciter 330–380, DM 400, BA 435–485. To determine the spatial extent of retinogeniculate and corticogeniculate projections in the dLGN, threshold imaging protocols were used (Jaubert-Miazza et al., 2005). Briefly, background fluorescence was subtracted and grayscale images were normalized (0–255) using MetaMorph software (Molecular Devices). In Photoshop (Adobe) the boundaries of dLGN were delineated so as not to include label from the optic tract, intergeniculate leaflet, and ventral lateral geniculate nucleus. The Threshold command was used to convert grayscale images into high-

contrast black and white images. A threshold value was chosen that corresponded to a location within the grayscale histogram where there was a clear distinction between signal and residual background fluorescence. The total number of pixels in the defined area of dLGN representing either green or red fluorescence was measured. The spatial extent of retinogeniculate and corticogeniculate projections was estimated by summing the area across 2-5 successive sections through the middle of dLGN and then expressed as a percentage of the total area of dLGN.

For some animals we examined the pattern of corticogeniculate innervation through a rostral-caudal series by generating 3-D mesh plots in SigmaPlot (Systat Software). In MetaMorph the images in the series were individually aligned from the most dorsomedial point of dLGN and a user-defined stack was built. CTB-labeled retinogeniculate projections were used to define the borders of dLGN and a uniform grid with a specific dimension was overlaid onto each stack by utilizing ImageJ software (NIH). The segmented line tool was used to delineate the ventral and dorsal borders of dLGN and the dorsal border of corticogeniculate innervation. The coordinates of the points along the segmented lines were used to calculate the dorsal-ventral extent of the corticogeniculate projections in dLGN ($[(\text{dorsal } \tau\text{-GFP border} - \text{ventral CTB border}) / (\text{dorsal CTB border} - \text{ventral CTB border})]$).

Immunohistochemistry. Animals were sacrificed and perfused as described above. Brains were postfixed overnight and sectioned at 20 μm in the coronal plane using a cryostat. Sections were preincubated for 1 h in blocking solution (5% NGS, 2.5% BSA, 0.1% triton in PBS). The sections were then treated with the primary antibodies (mouse anti-VGlu1, 1:100, NeuroMab; rabbit anti-GFP, 1:250, Invitrogen) diluted in blocking solution and incubated overnight at 4°C. The following day the tissue was washed with PBS and incubated at room temperature for 2 h in blocking solution containing the secondary antibodies (Alexa Fluor 594 goat anti-mouse IgG1

(highly cross absorbed), 1:1000, Invitrogen; Alexa Fluor 488 goat anti-rabbit (highly cross absorbed), 1:1000, Invitrogen). The tissue was washed with PBS and then coverslipped.

Slice Physiology. To assess when functional corticogeniculate synapses develop in dLGN a thalamic slice preparation that allows for separate activation of optic tract and corticothalamic fibers was used (Turner and Salt, 1998; see Fig. 17B). Individual (300 μm thick) slices containing dLGN were placed into a recording chamber and maintained at 32°C and perfused continuously at a rate of 2.0 ml/min with oxygenated ACSF (in mM): 124 NaCl, 2.5 KCl, 1.25 NaH_2PO_4 , 2.0 MgSO_4 , 26 NaHCO_3 , 10 glucose, and 2 CaCl_2 (saturated with 95% O_2 /5% CO_2), pH 7.4. *In vitro* recordings were done in the whole-cell current-clamp configuration with the aid of differential interference contrast (DIC) and fluorescence optics on a fixed stage, visualized recording apparatus (Olympus EX51WI). Patch electrodes (3-5 $\text{M}\Omega$) made of borosilicate glass were filled with a solution containing (in mM): 140 K gluconate, 10 HEPES, 0.3 NaCl, 2 ATP-Mg, 0.1 GTP-Na, pH 7.25. Pipette capacitance, series resistance, and whole cell capacitance were carefully monitored and compensated electronically during the recording. To evoke synaptic activity in dLGN, square-wave pulses (0.1-0.3 ms, 0.1-1 mA) were delivered at a rate of 0.2-1.0 Hz through a pair of thin-gauge tungsten wires (0.5 $\text{M}\Omega$) positioned in the thalamic reticular nucleus region. Pairs of electrical stimuli were delivered with interstimulus intervals (ISIs) of 100-1000 msec. The degree of facilitation was determined by calculating the paired pulse ratio (PPR), which is the amplitude of the second stimulus EPSP response (EPSP_2) divided by the amplitude of the first stimulus EPSP response (EPSP_1). GABA antagonists, bicuculline (25 μM ; Tocris, Ellisville, MO) and CGP (10 μM , Tocris), were bath-applied to block GABA_A - and GABA_B -mediated activity, respectively. Neuronal activity was digitized (10-20 KHz) through an interface unit (National Instruments, Baltimore, MD), acquired and stored

directly on the computer, and analyzed by using commercial software (Strathclyde, Glasgow, Scotland; Electrophysiology Software, Whole Cell Analysis Program V3.8.2.).

Results

In order to visualize corticogeniculate projections we made use of the *golli- τ -GFP* mouse, in which τ -GFP is restricted to neurons in layer VI of cortex (Jacobs et al., 2007). Figure 13A shows the τ -GFP expression in layer VI neurons in a coronal section of neocortex from a P14 *golli- τ -GFP* mouse. Most notable is the high density of τ -GFP expressing neurons restricted to layer VI. Apical dendrites of pyramidal neurons can also be seen projecting to more superficial layers of cortex. In the same mouse, the descending axonal arbors and terminals of layer VI neurons were evident in dLGN (Fig. 13B). At P14, robust τ -GFP labeling was seen throughout dLGN. The small areas devoid of τ -GFP depict the location of dLGN somata, which are better illustrated in the corresponding DAPI stain. Corticothalamic τ -GFP expression was also seen throughout other adjacent first order sensory nuclei, such as the ventrobasal complex (VB, see also Fig. 14). However, the ventral lateral geniculate (VLG) nucleus was devoid of τ -GFP expressing terminals, since it receives input from layer V of cortex (Consenza and Moore, 1984; Bourassa and Deschenes, 1995).

Figure 14 shows the developmental progression of cortical layer VI innervation of thalamus at P1, P8, and P14. Descending projections can be seen coursing through the internal capsule and innervating thalamus in a ventrolateral to dorsomedial direction (see also Jacobs et al., 2007). For example, at P1 projections were readily apparent in VB whereas dLGN was

lacking corticothalamic innervation. At P8 cortical innervation of dLGN was well underway and by P14 corticothalamic projections occupied all of dLGN.

To further characterize the progression of corticogeniculate projections into dLGN we examined corticogeniculate innervation in relation to the development of the retinogeniculate pathway. To accomplish this we injected one or both eyes of *golli- τ -GFP* mice with cholera toxin subunit B (CTB) conjugated to Alexa Fluor dyes to anterogradely label retinogeniculate projections. In Figure 15, are examples of coronal sections from different postnatal ages showing corticogeniculate projections visualized with τ -GFP and retinogeniculate projections labeled with CTB (Fig. 15A,B). By injecting CTB into both eyes or just one, we were able to visualize both crossed and uncrossed projections (Fig. 15A) or simply uncrossed projections (Fig. 15B). To better illustrate the gradual progression and increase in density of corticogeniculate projections, pseudocolor images of τ -GFP are also shown (Fig. 15C). At P1-P2 corticogeniculate projections were seen along the ventral edge of dLGN. In contrast, retinogeniculate projections have already innervated dLGN with the bulk of projections arising from the contralateral eye (i.e. crossed projections). Uncrossed projections were seen innervating the dorsal region of dLGN. Corticogeniculate projections appeared to pause along the ventral border of dLGN for a few days before entering and did not begin to innervate dLGN until P4, a time when retinogeniculate projections completely innervate dLGN. Initially, uncrossed projections terminated diffusely in the anteromedial region of dLGN. As uncrossed retinogeniculate projections began to recede to form an eye-specific patch in the anteromedial region of dLGN, corticogeniculate projections continued to innervate in a ventral to dorsal manner to fully innervate dLGN by eye opening (P12).

To quantify these results we then estimated the spatial extent of corticogeniculate and retinogeniculate projections in dLGN at different ages during early postnatal development (Fig. 15D). In the summary graph, we plotted the percent area in dLGN occupied by both crossed and uncrossed retinogeniculate projections (red, filled circles), uncrossed retinogeniculate projections (red, open circles) and corticogeniculate projections (green, filled circles) as a function of age. Measurements of uncrossed retinogeniculate projections were taken from both C57BL/6 and *golli- τ -GFP* mice and there was no difference in the spatial extent of ipsilateral retinogeniculate projections between these two strains (univariate ANOVA, $F = 2.68$, $p = 0.111$). At P1 about 63% of the total area of dLGN was occupied by retinogeniculate projections. By P2-P3 retinogeniculate innervation was complete and the spatial extent of these projections in dLGN peaked to occupy as much as 85-95% of dLGN. Uncrossed retinogeniculate projections began to innervate dLGN at later ages than crossed projections (Godement et al., 1984) and we observed that between P1 to P3 the spatial extent of uncrossed projections increased from 17% to 54%. Around P4, uncrossed projections began to recede so that by the second postnatal week they occupied around 12-15% of the total area of dLGN. Once retinogeniculate innervation was complete, corticogeniculate projections started to innervate dLGN and at P4 the spatial extent was around 15%. There was a gradual progression of corticogeniculate projections into dLGN so that after eye-specific segregation is complete they only occupied approximately 50% of the total area. By eye opening and well after the period of eye-specific segregation, corticogeniculate innervation was finished and these projections occupied around 92-94% of the total area of dLGN.

We next examined the pattern of corticogeniculate innervation in dLGN (Fig. 16A,B) by generating 3-D mesh plots from a rostral-caudal series of coronal sections taken from a P5

mouse (Fig. 16A), a time when corticogeniculate projections occupy about 25% of dLGN, and a P8 mouse (Fig. 16B), when corticogeniculate is more advanced and projections occupy around 60% of dLGN. These mesh plots were used to determine if any medial to lateral or rostral to caudal preferences appeared in corticogeniculate innervation. Accompanying the mesh plots are pseudocolor images of representative rostral, middle, and caudal sections illustrating the degree and intensity of corticogeniculate innervation. Initially, corticogeniculate projections entered dLGN along the entire ventral aspect and began to innervate along a dorsal axis towards optic tract. However, at P5 a higher degree of innervation was present more medially in the caudal portion of dLGN (Fig. 16A). At P8, innervation was more advanced in rostral sections of dLGN but the projections climbed along all of the outer edges of dLGN (Fig. 16B), with the inner core of dLGN showing the least amount of corticogeniculate innervation.

To examine when during the period of corticogeniculate innervation functional corticogeniculate synapses appear, we first stained for vesicular glutamate transporter 1 (VGlut1), a vesicle-associated transporter and known marker for corticogeniculate terminals within dLGN (Ni et al., 1995; Yoshida et al., 2009). VGlut1 is involved in the transport of glutamate into excitatory synaptic vesicles, making it important for neurotransmission (Bellocchio et al., 2000; Takamori et al., 2000; Wojcik et al., 2004). Thus, its presence can be used as a potential indicator of when functional synapses emerge. Figure 17A shows VGlut1 staining and pseudocolor images to indicate the density of label in coronal sections of dLGN at P7, P9, and P14. At P7, when around 50% of dLGN is innervated by corticogeniculate projections, little or no VGlut1 staining was apparent. More VGlut1 was expressed at P9 and finally by P14 robust staining could be seen throughout dLGN. To further examine whether functional corticogeniculate synapses are present during the period of corticogeniculate

innervation we did *in vitro* whole-cell recordings of relay cells using a slice preparation that preserves corticothalamic axons and their connections to dLGN cells (Fig. 17B). To generate excitatory postsynaptic potentials (EPSPs) of corticothalamic origin, a bipolar stimulating electrode was placed adjacent to dLGN in the thalamic reticular nucleus, a region where the bulk of corticothalamic axons pass before entering dLGN. We delivered paired electrical pulses at different postnatal ages to corticothalamic fibers to evoke EPSPs in dLGN relay cells. Such protocols have been used to study paired pulse facilitation, a hallmark feature of corticothalamic synapses (Turner and Salt, 1998; Granseth et al., 2002; Alexander and Godwin, 2005). We studied paired pulse facilitation in 35 cells at P7, P15-P16, P21-P22, P40, and P45. Figure 17C shows examples of EPSPs from the different age groups and the corresponding plots of the paired pulse ratio ($PPR = EPSP_2/EPSP_1$) at different interstimulus intervals (ISI). We found that corticogeniculate responses were apparent as early as P7 and that EPSPs could be readily evoked in areas of dLGN with dense τ -GFP expression. At this age relatively weak facilitation was seen at an ISI of 100 msec, but as the time between stimuli increased the paired pulse ratio became 1 indicating that there was no longer facilitation. Overall more paired pulse facilitation is seen after P7 and by P15 it resembled the adult profile with ratios reaching a value of 3 or more (Granseth et al., 2002). At all ages the largest degree of facilitation was observed with an ISI of 100 msec consistent with results from others showing that shorter intervals between pulses of electrical stimulation increase the degree of paired pulse facilitation (Turner and Salt, 1998; Alexander and Godwin, 2005). The summary plot in Figure 17D shows the peak magnitude of paired pulse facilitation at an ISI of 100 msec, during the first few postnatal weeks. The paired pulse ratio was significantly higher at the second and third postnatal weeks compared to the first (one-way ANOVA, $F = 21.59$, Bonferroni's *post hoc* test, $p < 0.01$). Taken together, this suggests that

functional corticogeniculate synapses are present during the early phase of innervation, but do not fully mature until sometime after the first postnatal week.

The coordination of cortical and retinal projections in dLGN suggests that corticogeniculate innervation may rely on the retinogeniculate pathway. To begin to assess this possibility we examined the timing and patterning of corticogeniculate innervation in the absence of retinal input to dLGN. We used both binocular enucleation (BE) at birth and a form of genetic deafferentation by making use of a *math5*-null (-/-) mouse (Wang et al., 2001). Since *math5* is essential for the differentiation of retinal ganglion cells, there is a near complete loss of these cells in this mutant mouse, which results in a dLGN absent of retinal input. Crossing the *math5*-/- mouse with the *golli*- τ -GFP mouse allowed us to visualize descending corticothalamic projections in a dLGN devoid of retinal innervation. In Figure 18A are coronal sections from control, BE, and *math5*-/- (genetic deafferentation) mice showing corticogeniculate projections visualized with τ -GFP along with corresponding pseudocolor images to demonstrate the spatial extent of corticogeniculate projections. At P3 (Fig. 18A, *top*) and P7 (Fig. 18A, *bottom*) cortical projections extended further into dLGN after BE as well as in *math5*-/- mice compared to controls.

A summary plot compares the spatial extent of corticogeniculate projections in control, BE, and *math5*-/- mice in Figure 18B. The fact that all three groups showed little or no innervation at P2 (5-10%) suggests that corticogeniculate innervation does not necessarily occur earlier but rather is greatly accelerated after the onset of innervation by the removal of retinal input. Between P3-P9, corticogeniculate projections occupied a significantly larger percent area of dLGN in BE and *math5*-/- mice compared to controls (univariate ANOVA, $F = 13.81$, Bonferroni's *post hoc* test, $p < 0.001$). During this time there was a 2- to 5-fold increase in the

amount of corticogeniculate innervation in BE and *math5*^{-/-} mice. There was no significant difference in corticogeniculate innervation between BE and *math5*^{-/-} mice (univariate ANOVA, $F = 13.81$, Bonferroni's *post hoc* test, $p = 1$). By P10, the rate of innervation plateaued and there was no difference in the percent area of dLGN occupied by corticogeniculate projections between groups (univariate ANOVA, $F = 2.345$, Tamhane's *post hoc* test, $p > 0.097$). While the rate of innervation was affected, inter-areal targeting did not seem to be disrupted after the loss of retinal input, since τ -GFP expressing fibers continued to avoid the VLG (Fig. 18A). However, the pattern of innervation within dLGN appeared to be disrupted by the lack of retinal input as shown in the 3-D mesh plot of Figure 19 taken from a P5 *math5*^{-/-} mouse. Corticogeniculate projections continued to innervate in a ventral to dorsal manner. However, the medial to lateral and rostral to caudal biases noted in controls (Fig. 16A) were no longer apparent. Instead corticogeniculate fibers seemed to innervate dLGN in a uniform fashion.

Corticogeniculate innervation occurs around the period of eye-specific segregation and interactions between projections from the two eyes are critical in the formation of eye-specific domains with dLGN. It has been shown that when one eye is removed at birth the retinogeniculate projections from the remaining eye spread throughout the entire dLGN (Lund et al., 1973; So et al., 1978; Manford et al., 1984). To see how the loss of one eye affects corticogeniculate innervation we carried out monocular enucleation experiments. Coronal sections of dLGN from both hemispheres in P3 and P7 *golli*- τ -GFP mice are shown in Figure 20A. On the day of birth one eye was removed and the spared eye was injected with CTB. CTB labels the projections from the spared eye (Fig. 20A, *top panel*) and τ -GFP is used to visualize corticogeniculate projections (Fig. 20A, *middle panel*). Corresponding pseudocolor images of τ -GFP are shown to better illustrate the differences in breadth and intensity of corticogeniculate

innervation between the two hemispheres (Fig. 20A, *bottom panel*). Figure 20B shows a summary plot comparing the percent area of dLGN occupied by corticogeniculate projections in control, BE, and both hemispheres of ME mice at P3, P4, P5, and P7. At all ages we found that there was a significant increase in the amount of corticogeniculate innervation in dLGN contralateral to the enucleated eye compared to control (univariate ANOVA, $F = 22.99$, Tamhane's *post hoc* test, $p < 0.001$). The spatial extent of corticogeniculate projections in this hemisphere was comparable to values seen after BE (univariate ANOVA, $F = 22.99$, Tamhane's *post hoc* test, $p = 0.992$). In this hemisphere, crossed retinal projections, which occupy the bulk of terminal space in dLGN, have been eliminated; what remains are the uncrossed retinal projections that originate from the spared eye. Spared uncrossed retinogeniculate projections are known to expand in dLGN after monocular enucleation (Lund et al., 1973; So et al., 1978; Manford et al., 1984), so we determined the spatial extent of uncrossed retinogeniculate projections and found that in ME mice these projections occupied an average of 46% of dLGN from P3-P7, similar to that of controls (42%). The spatial extent of corticogeniculate projections occupying dLGN in the hemisphere ipsilateral to the enucleated eye was not significantly different from control (one-way ANOVA, for P3, $F = 40.788$, Bonferroni's *post hoc* test, $p = 1$; for P4, $F = 26.50$, Tamhane's *post hoc* test, $p = 0.787$; for P5, $F = 64.18$, Bonferroni's *post hoc* test, $p = 0.216$; for P7, $F = 25.19$, Bonferroni's *post hoc* test, $p = 1$). In this hemisphere, only uncrossed retinal projections have been eliminated and the projections coming from the spared eye, which make up the majority of retinal input to dLGN have been maintained. Thus, an accelerated rate of corticogeniculate innervation was limited to the hemisphere contralateral to the enucleated eye, the side where the bulk of retinogeniculate projections were eliminated.

Figure 13

τ -GFP expression in neocortex and dLGN of *golli*- τ -GFP mice.

A, Left panel shows the distribution of neurons expressing τ -GFP (green) in a coronal section of neocortex at P14, just rostral of visual cortex. Inset on the far left is DAPI stain of the same section and used to illustrate the boundaries of cortical layers. τ -GFP labeled neurons are restricted to layer VI. Note the apical dendrites of pyramidal cells that radiate throughout superficial layers. Right panel is a higher power image of τ -GFP expressing neurons for the outlined area in the left panel. Scale bars, 100 μ m **B**, Coronal section of dLGN in the same P14 mouse showing corticogeniculate axon arbors and terminals expressing τ -GFP. DAPI is shown for the same section to delineate the boundaries of dLGN from other adjacent nuclei. Note the lack of τ -GFP fluorescence in VLG. dLGN, dorsal lateral geniculate nucleus; VLG, ventral lateral geniculate nucleus. Scale bar, 100 μ m. On the far right, is a high power confocal image of τ -GFP expression in dLGN. The large areas lacking label are the locations of dLGN cell bodies. Scale bar, 20 μ m.

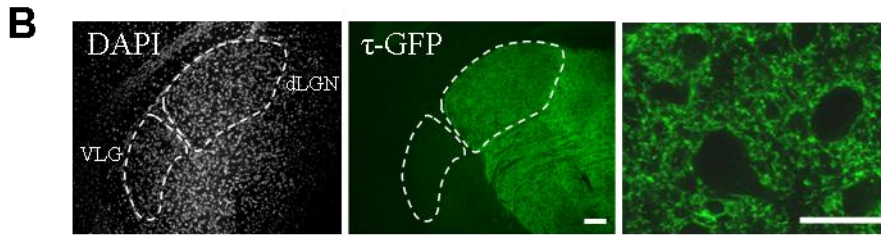
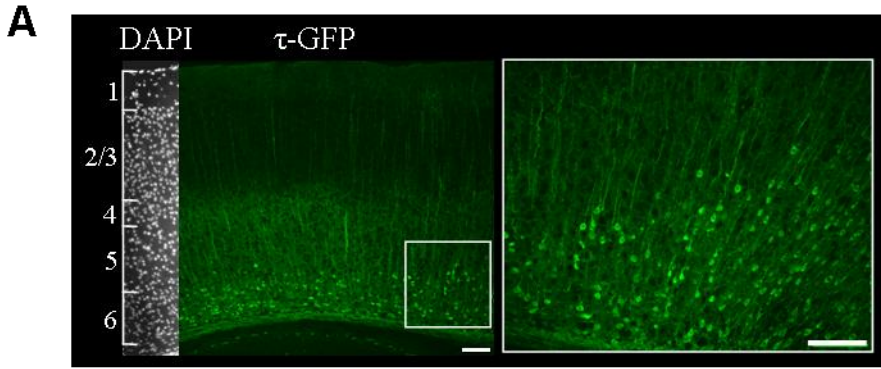


Figure 14

Cortical innervation of thalamus at different postnatal ages.

The pattern of cortical innervation in thalamus is shown in coronal sections from P1, P8, and P14 *golli- τ -GFP* mice. At P1, corticothalamic fibers were seen coursing through the internal capsule and innervating nuclei in ventrolateral thalamus, such as the ventrobasal complex.

Corticothalamic projections continued to innervate thalamus in a ventrolateral to dorsomedial directions. By P8, corticothalamic projections were seen in dLGN. Corticothalamic innervation of thalamus was complete by P14, with dLGN being the last nucleus to be fully innervated. ic, internal capsule; d, dorsal lateral geniculate nucleus; v, ventral lateral geniculate nucleus; VB, ventrobasal complex. Scale bar, 200 μ m.

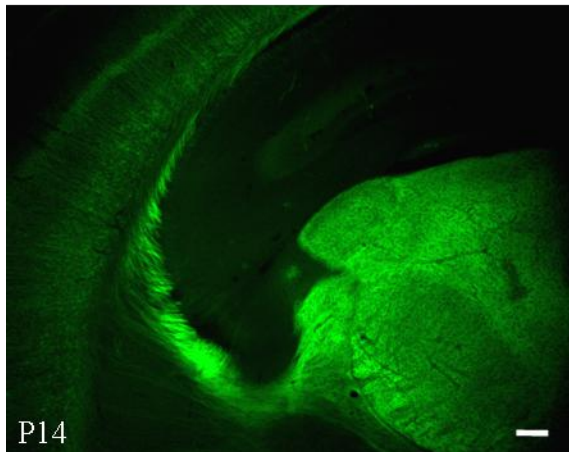
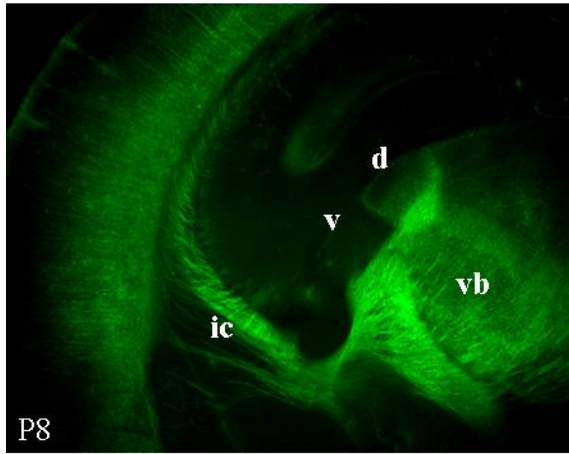
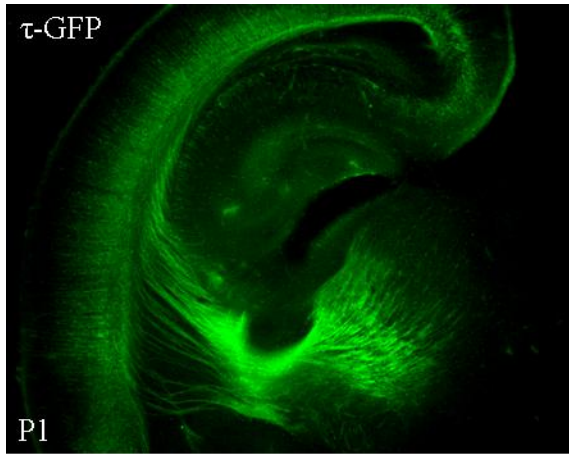


Figure 15

Coordinated innervation of corticogeniculate and retinogeniculate projections in dLGN.

A-B, Coronal sections from *golli- τ -GFP* mice at different postnatal ages. Corticogeniculate projections were visualized with τ -GFP (**A-B**, left panel). Retinogeniculate projections were labeled by making eye injections of CTB conjugated to Alexa Fluor 594 (red) either in both eyes (**A**, middle panel) or one eye (**B**, middle panel). Right panels (**A-B**) show merged images of corticogeniculate (green) and retinogeniculate (red) projections. CG, corticogeniculate projections; RG, retinogeniculate projections. Scale bar, 100 μ m. **C**, Pseudocolor images of τ -GFP are shown to better illustrate the breadth and intensity of corticogeniculate innervation. Bottom far right shows the pseudocolor threshold range. **D**, Summary graph plotting the percent area in dLGN occupied by crossed and uncrossed retinogeniculate projections (red, filled circle), uncrossed retinogeniculate projections (red, open circle) and corticogeniculate projections (green, filled circle) as a function of age. Shown are means and SEMs (CTB, n = 2-6 hemispheres; GFP, n = 2-11). For each hemisphere estimates of spatial extent were based on label from 2-5 successive 70 μ m thick sections through the middle of dLGN and expressed as a percentage of the total area of dLGN.

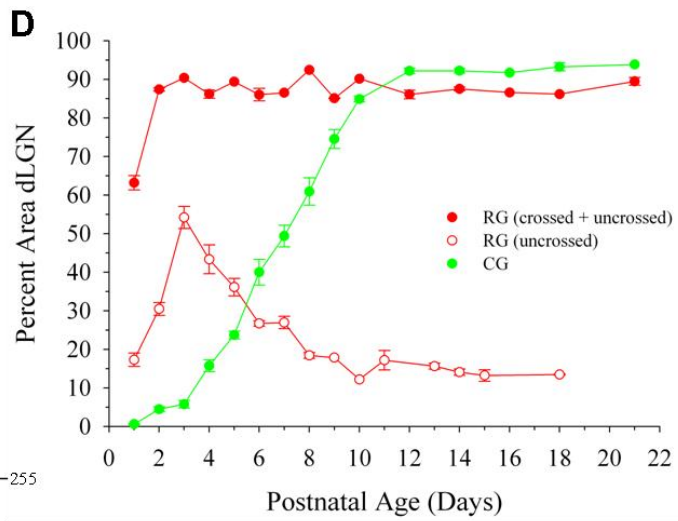
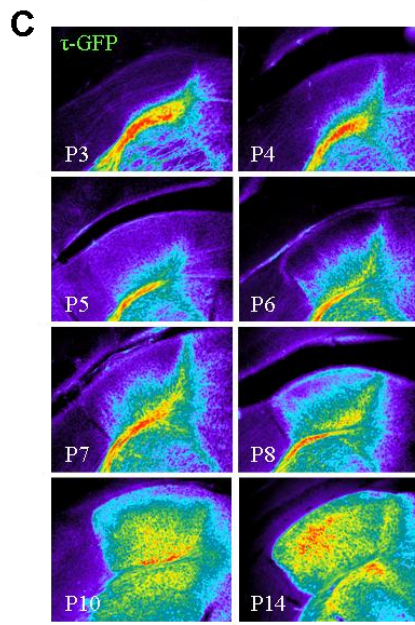
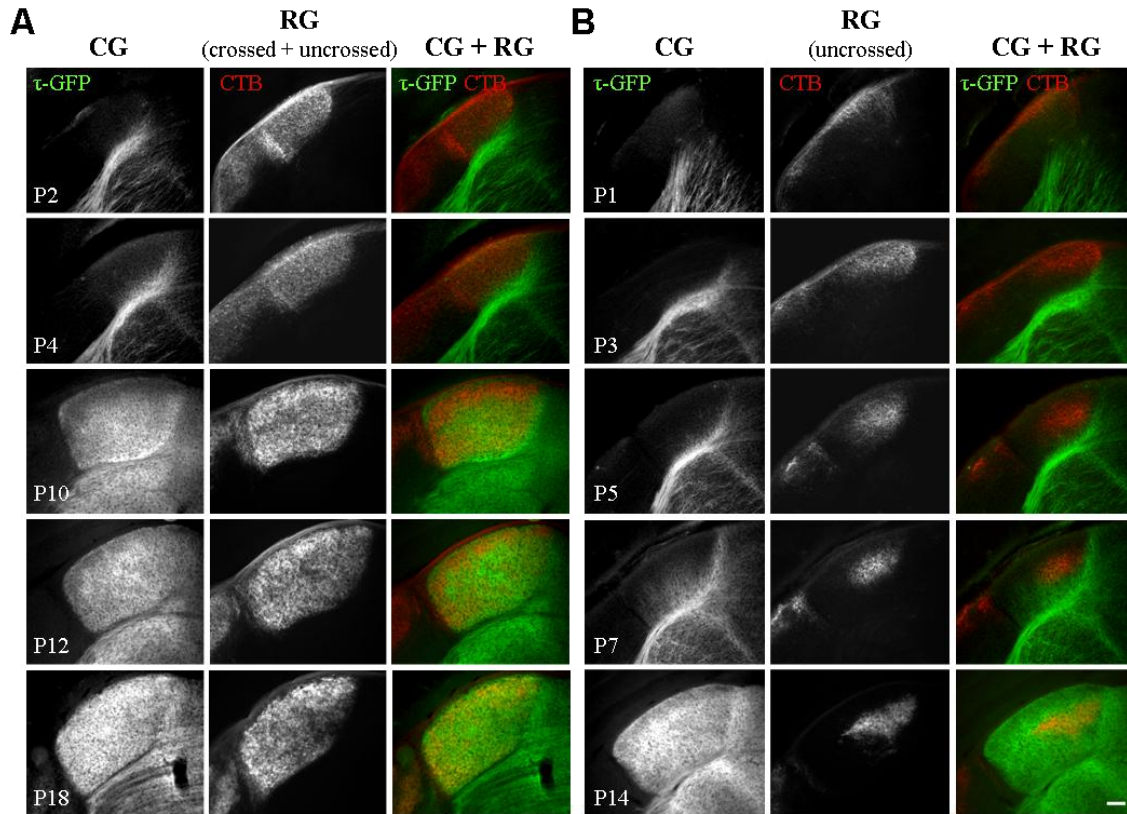


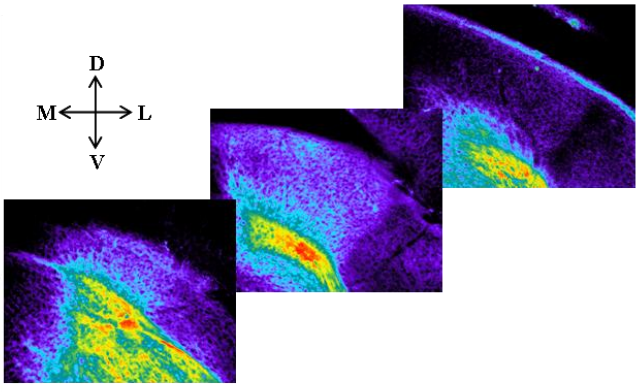
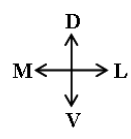
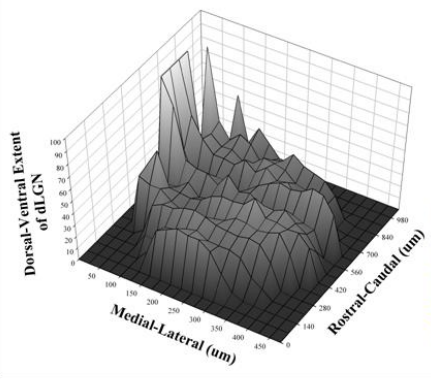
Figure 16

Pattern of corticogeniculate innervation throughout dLGN at P5 and P8.

A-B, 3-D mesh plots showing the dorsal-ventral extent of corticogeniculate projections in dLGN and the medial to lateral and rostral to caudal patterns of corticogeniculate innervation in dLGN at P5 (**A**, left) and P8 (**B**, left). **A**, The mesh plot shows that at P5 the greatest amount of innervation occurred medially in the caudal portion of dLGN. **B**, At P8 innervation was almost complete around the outer edges of dLGN, however in the inner core there was much less innervation as shown in the mesh plot. Mesh plots were based on 12-14 sections that were cut 70 μm thick in the coronal plane through the rostral-caudal extent of dLGN from *golli- τ -GFP* mice. On the right, pseudocolor images of representative rostral, middle, and caudal coronal sections of dLGN are also shown. The pseudocolor threshold range is shown on the far right. D, dorsal; V, ventral; M, medial; L, lateral. Scale bar, 100 μm .

A

P5 golli-tau



B

P8 golli-tau

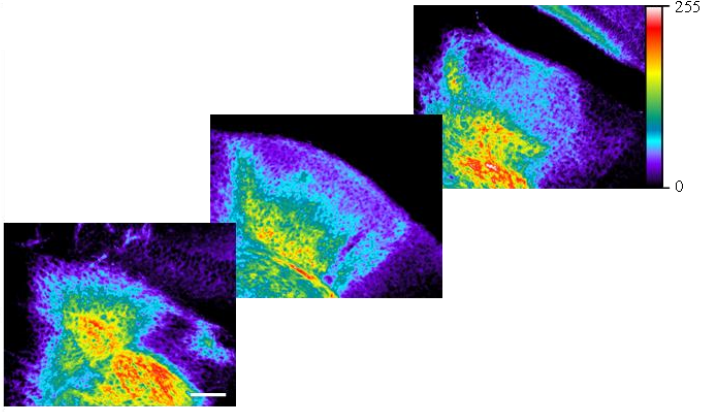
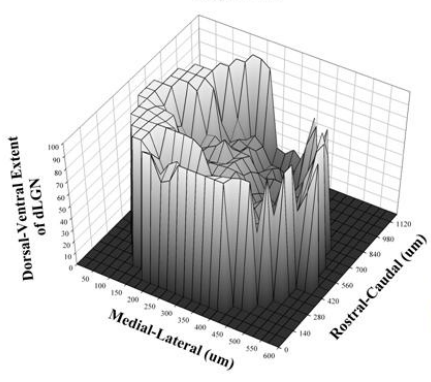


Figure 17

Development of functional corticogeniculate synapses in dLGN.

A, Coronal sections showing VGlut1 staining in dLGN at P7, P9, and P14. Bottom pseudocolor images show VGlut1 for each age. Staining for VGlut1 was very low at P7, but both intensity and spatial extent increased with age. Bottom far right shows the pseudocolor threshold range. Scale bar, 100 μm . **B**, On the left is an example of a CTB-filled, 300 μm thick parasagittal slice of dLGN from a *golli- τ -GFP* mouse. Images are from the same section that was post-fixed overnight after *in vitro* recording and show corticogeniculate projections expressing τ -GFP (green) and retinogeniculate projections labeled with CTB (red). To the right, a schematic of the slice preparation is provided. D, dorsal; A, anterior; dLGN, dorsal lateral geniculate nucleus; TRN, thalamic reticular nucleus; OT, optic tract; VLG, ventral lateral geniculate nucleus; M, medial geniculate nucleus. Recording electrode (white) in dLGN and bipolar stimulating electrode (black) placed in TRN, where corticothalamic axons pass before innervating dLGN, are also shown. Scale bar, 100 μm . **C**, Examples of excitatory postsynaptic potentials (EPSPs) evoked by paired electrical pulses delivered to corticothalamic fibers from three different age groups. Plots showing the mean paired pulse ratio (PPR = EPSP₂/EPSP₁) at different interstimulus intervals (ISI) for P7 (n = 10), P15-P16 (n = 10), and P21-P45 (n = 15) cells. Error bars represent SEM. **D**, Summary plot showing the average paired pulse ratio seen with an ISI of 100 msec during the first few postnatal weeks. The degree of facilitation was significantly higher at the second and third postnatal weeks compared to the first postnatal week (* $p < 0.01$). Error bars represent SEM.

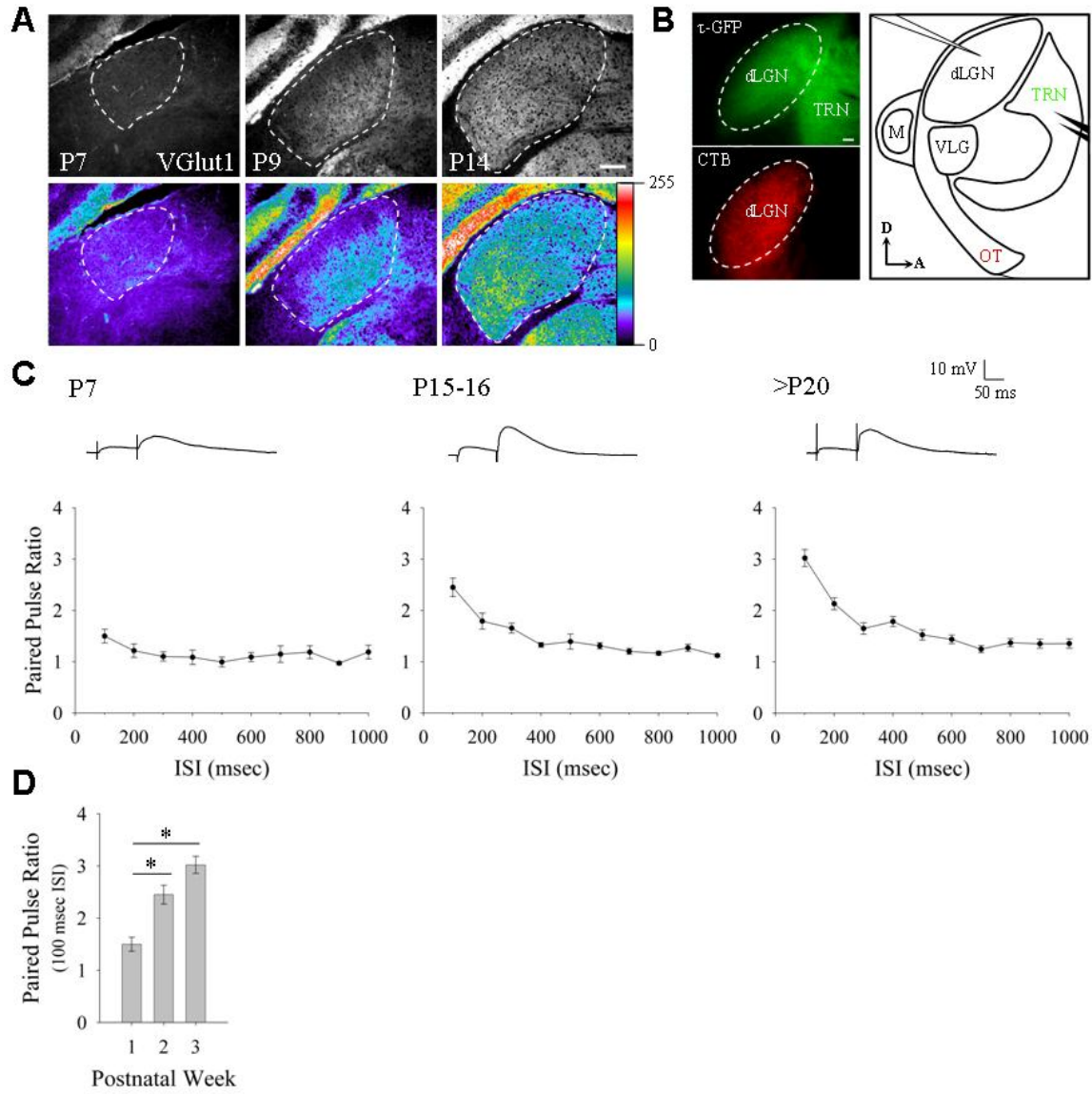


Figure 18

The timing of corticogeniculate innervation in dLGN relies on retinogeniculate innervation.

A, Coronal sections of dLGN showing corticogeniculate (τ -GFP, green) innervation at P3 (top) and P7 (bottom) in controls, mice binocularly enucleated (BE) at birth, and genetically deafferented mice (*math5*^{-/-}). Pseudocolor images of τ -GFP are also shown to illustrate the breadth and intensity of corticogeniculate projections. Bottom far right shows the pseudocolor threshold range. Scale bars, 100 μ m. **B**, Summary graph plotting the mean percent area in dLGN occupied by corticogeniculate projections as a function of age in control (green), binocularly enucleated mice (magenta), genetically deafferented mice (black). Shown are means and SEMs (control, n = 4-11 hemispheres; binocular enucleation, n = 4-12; genetic deafferentation, n = 2-6). For each hemisphere estimates of spatial extent were based on label from 2-5 successive 70 μ m thick sections through the middle of dLGN and expressed as a percentage of the total area of dLGN. Loss of retinal input accelerated corticogeniculate innervation so that between P3-P9 corticogeniculate projections occupied a significantly higher percent area of dLGN in binocularly enucleated and genetically deafferented mice compared to controls.

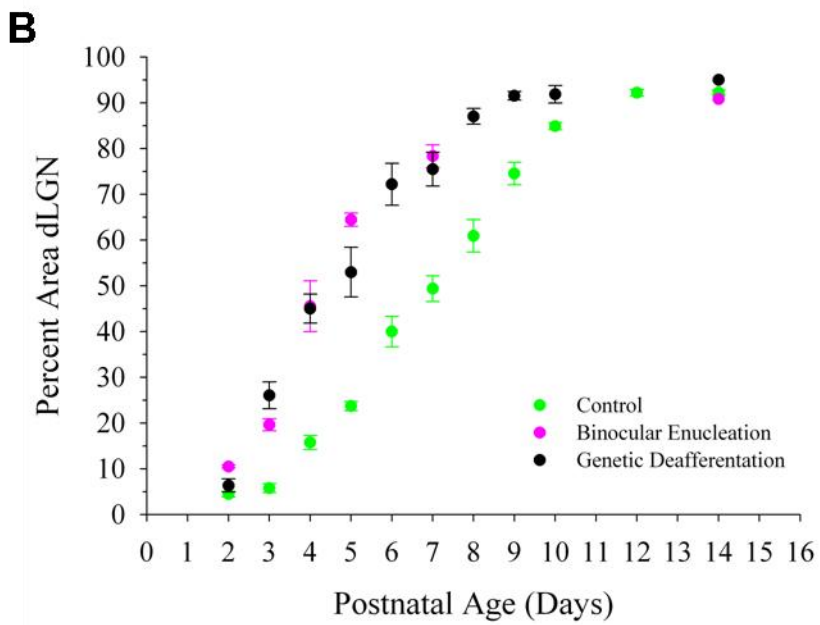
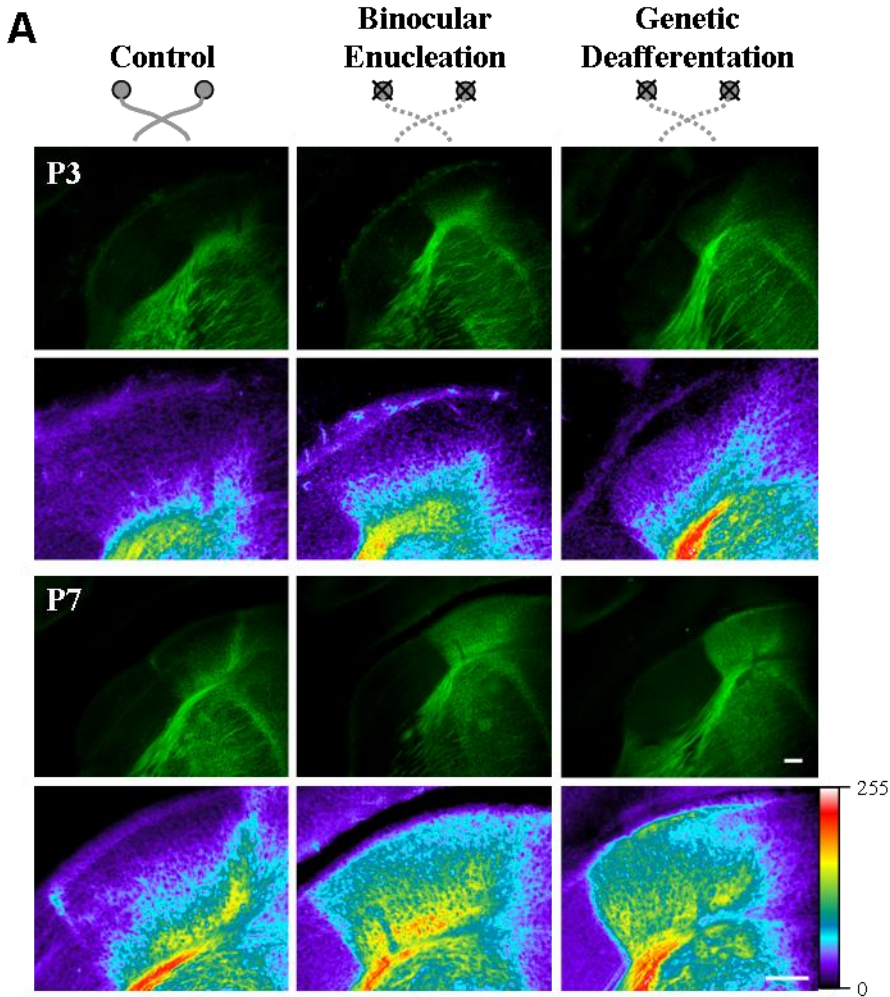


Figure 19

The pattern of corticogeniculate innervation is disrupted in the absence of retinal input.

3-D mesh plot showing the dorsal-ventral extent of corticogeniculate projections in dLGN and the lack of medial-lateral or rostral-caudal patterns of innervation in a P5 *golli- τ -GFP/math5-/-* mouse. Plot shows that corticogeniculate innervation was more uniform in the absence of retinal input. Mesh plot was based on 11 sections that were cut 70 μm thick in the coronal plane through the rostral-caudal extent of dLGN. Pseudocolor images of representative rostral, middle, and caudal coronal sections of dLGN are also shown (right). The pseudocolor threshold range is shown on the far right. D, dorsal; V, ventral; M, medial; L, lateral. Scale bar, 100 μm .

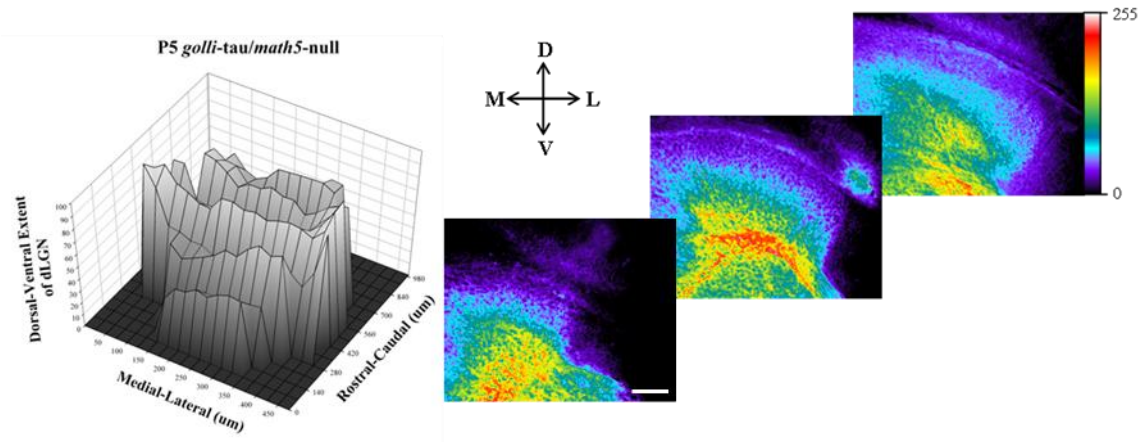
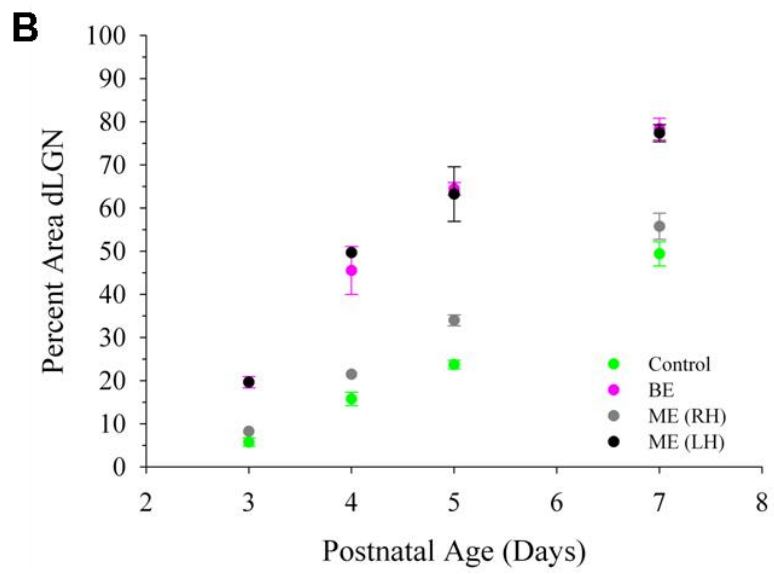
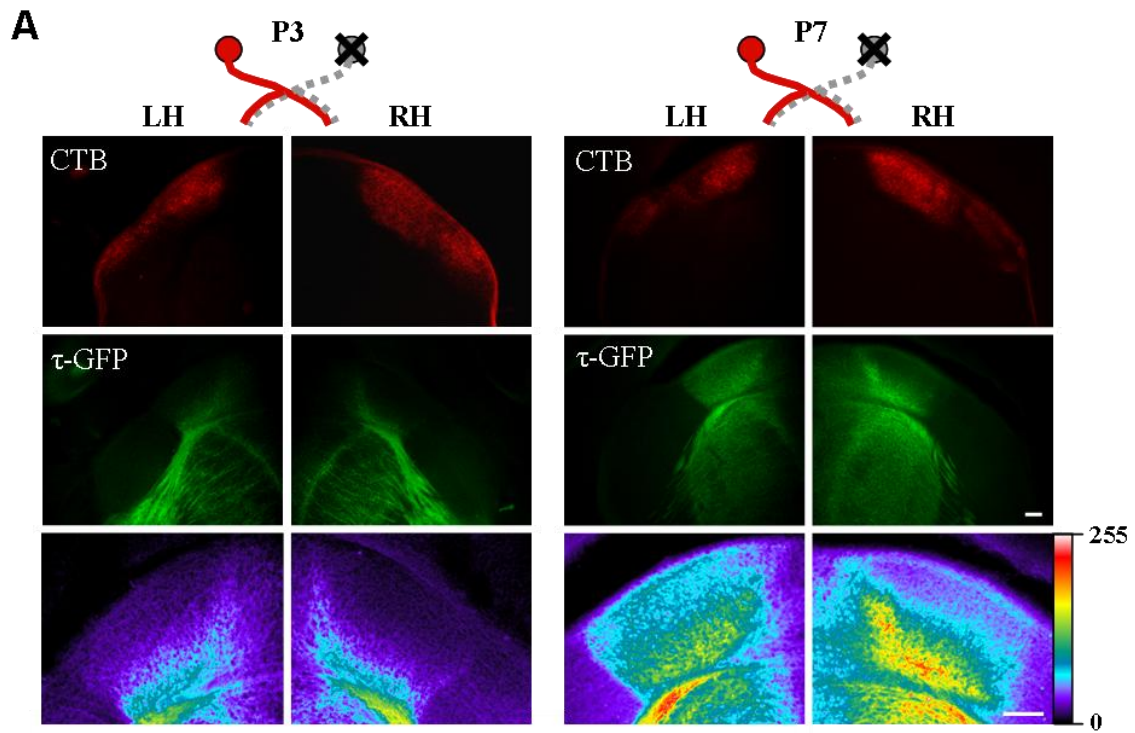


Figure 20

Monocular enucleation only affects the timing of corticogeniculate innervation in dLGN contralateral to the enucleated eye.

A, Coronal sections showing both hemispheres from P3 (left) and P7 (right) mice that were monocularly enucleated at birth. One eye was removed and the spared eye was injected with CTB. The schematic above the panels depicts which eye was removed in relation to crossed and uncrossed projections of left (LH) and right (RH) hemispheres. CTB labeled retinogeniculate projections from the remaining eye (red) are shown in the top panel. Middle panel shows corticogeniculate projections (τ -GFP, green) for the same sections. Pseudocolor images of τ -GFP are shown in the bottom panel. Bottom far right shows the pseudocolor threshold range. Scale bars, 100 μ m. **B**, Summary graph plotting the mean percent area in dLGN occupied by corticogeniculate projections as a function of age in control (green), binocularly enucleated (BE, magenta (see also Fig. 2.6), and monocularly enucleated mice. dLGN contralateral to the enucleated eye (ME, LH, black) and dLGN contralateral to the spared eye (ME, RH, gray). Shown are means and SEMs (control, n = 5-8 hemispheres; BE, n = 4-12; ME, n = 2-5). For each hemisphere estimates of spatial extent were based on label from 2-5 successive 70 μ m thick sections through the middle of dLGN and expressed as a percentage of the total area of dLGN. Accelerated corticogeniculate innervation was evident in the RH, contralateral to the enucleated eye, where only uncrossed retinogeniculate projections were spared.



Discussion

Using the *golli- τ -GFP* mouse we studied the development of the corticogeniculate pathway in detail and in the context of retinogeniculate innervation and remodeling. Our results demonstrate that innervation of dLGN by corticogeniculate and retinogeniculate projections occurs in a coordinated manner. Retinogeniculate projections were the first to innervate dLGN and were followed by corticogeniculate projections only after retinogeniculate innervation was complete. The bulk of corticogeniculate innervation occurred during the time of eye-specific segregation. Once projections from the two eyes were well segregated and formed eye-specific domains in dLGN, corticogeniculate innervation was complete.

The correct formation of connections in the visual system depends on precisely timed interactions between axons and their targets (Blakemore, 1991), so perhaps there is a developmental plan in which the retinogeniculate pathway must be established prior to the formation of nonretinal connections. This is also supported by a recent study examining the ultrastructure of retinal and nonretinal synapses in mouse dLGN during early postnatal development (Bickford et al., 2010). Synapses were found at P7, but appeared immature and lacked the characteristics needed for identification. However, it was suggested that the synaptic terminals present were primarily of retinal origin. By the second postnatal week, both retinal and nonretinal synapses were readily identifiable and the synaptic organization resembled that of the adult. Retinal inputs provide the primary excitatory drive to relay cells and transmit the message that is processed by cortex (Sherman, 2005), so it might be the case that the retinogeniculate

pathway must become firmly established before nonretinal input that will modulate the transmission of visual information can innervate dLGN.

During the period of corticogeniculate innervation, functional synapses between the neurons in layer VI of cortex and relay cells exist. At P7 we observed little VGlut1 staining, however our *in vitro* recording studies showed that in areas of dLGN rich in corticogeniculate innervation, responses were readily evoked by corticothalamic stimulation. We also found that compared to older ages the amount of paired pulse facilitation was significantly lower at P7, suggesting that these corticogeniculate synapses may not become fully mature until after the first postnatal week.

Paired pulse facilitation is a form of short-term synaptic plasticity that is presynaptic in origin and both synaptic vesicle availability and release probability play an important role (Zucker and Regehr, 2002). For example, if a synapse has a low initial probability of neurotransmitter release it prevents vesicle depletion with the initial stimulus. The maturation of facilitation at the corticogeniculate synapse could possibly be explained by the developmental increase in VGlut1 that we observed. In addition to filling synaptic vesicles with glutamate, VGluts have also been found to be important for glutamate release from synapses (Wojcik et al., 2004; Fremeau et al., 2004; Moechars et al., 2006). VGlut1 and VGlut2 mRNA transcripts exhibit distinct, generally nonoverlapping patterns of expression and this differential expression appears to be correlated with probability of release (Fremeau et al., 2001). Recently, VGlut1 has been shown to lower probability of release by inhibiting endophilin, a protein that has been implicated in endocytosis and vesicle cycling (Weston et al., 2011). At hippocampal CA1 synapses the probability of transmitter release appears to decline during early postnatal development (Bolshakov and Siegelbaum, 1995) while at the same time VGlut1 expression is

dramatically upregulated (Ni et al., 1995). Similar events seem to be occurring at the corticogeniculate synapse in dLGN so that over development the increase in VGlut1 may result in a more regulated release of glutamate and an increase in the degree of paired pulse facilitation.

The coordinated innervation of retinal and cortical projections that we observed in dLGN suggests that the retina could be playing a role in regulating corticogeniculate innervation.

Indeed that was the case since our enucleation and genetic deafferentation studies showed that in the absence of all or most retinal input, corticogeniculate projections innervated dLGN at an accelerated rate. With our monocular enucleation paradigm, the timing of corticogeniculate innervation was affected differently depending on whether dLGN was contralateral or ipsilateral to the enucleated eye. This could be due either to the overall amount of retinal projections lost or the lack of a specific set of projections (crossed or uncrossed). For example, the dLGN contralateral to the enucleated eye is lacking the majority of its retinal projections compared to dLGN in the opposite hemisphere, but it is also lacking only crossed projections. Crossed and uncrossed projections originate from different areas of retina that express distinct molecules (Petros et al., 2008). In our experiments it was difficult to separate out these two factors.

The loss of retinal input did not seem to disrupt inter-areal targeting of corticogeniculate projections since projections from layer VI continued to target dLGN and avoid VLG. This is in agreement with results from anophthalmic or eyeless mice, in which neurons in layer VI have been shown to project to their normal targets (Kaiserman-Abramof et al., 1975). However, there is a possibility that targeting of layer VI neurons to their appropriate dorsal thalamic nuclei could be disrupted. Although we did not test this, previous work has shown that dLGN in congenitally blind and binocularly enucleated mice receive aberrant somatosensory afferent axons (Asanuma and Stanfield, 1990).

When we examined the pattern of corticogeniculate innervation in dLGN in control mice we found that it occurred in a ventral to dorsal fashion. Cortical projections began to innervate along the entire ventral border of dLGN, however, a greater amount of innervation took place along the medial edge, which was also higher towards the caudal end of dLGN. This pattern of corticogeniculate innervation is complementary to the pattern of ephrin-A expression that has been previously shown in dLGN (Feldheim et al., 1998). Axons expressing high levels of EphA receptors can be repelled by ephrin-A ligands and this has been shown to be important for the formation of topographic maps in the visual system (Frisen et al., 1998; Feldheim et al., 1998). Gradients of ephrin-As and EphA receptors also exist in cortex and are essential for controlling the establishment of corticothalamic topography in dorsal thalamus (Torii and Levitt, 2005). Perhaps they are also responsible for the early pattern of corticogeniculate innervation. At P8 innervation is more progressed around the outer edges compared to the inner core of dLGN. By this time Ephrin-A expression is downregulated in dLGN (Feldheim et al., 1998; Huberman et al., 2005), so it most likely does not play a role in the pattern of innervation at this stage. Since the normal pattern of innervation was no longer evident in the P5 *math5*^{-/-} mouse, intra-areal targeting appears to be disrupted in the absence of retinal input. This could be due to a disruption in the Eph/ephrin gradient since bilateral enucleation in mice has been shown to reduce the expression of ephrin-A5 in dLGN (Dye et al., 2012).

Our findings point to a role for the retina in regulating the timing of corticogeniculate innervation in dLGN. Retinal projections may be preventing corticogeniculate projections from entering dLGN until the retinogeniculate pathway is established. This could be through a repulsive cue that is mediated either directly by retinal axons or indirectly through interactions involving relay cells, glia, or elements within the neuropil intrinsic to dLGN (Fig. 21A). Once

retinogeniculate innervation is complete the repulsive signal may be downregulated allowing corticogeniculate projections to enter dLGN. If retinogeniculate axons never reach dLGN or are removed early on the molecule repelling corticogeniculate projections may not be expressed or diminished prematurely so that the timing of corticogeniculate innervation is accelerated (Fig. 21B).

In the visual system, several examples of axon-glia interactions involved in guidance and targeting exist. For example, Netrin-1 is expressed in glial cells at the optic disc and RGCs express its receptor DCC (deleted in colorectal cancer) and these have been shown to play a role in mediating the exit of RGC axons from the retina (Deiner et al., 1997). At the optic chiasm, radial glia express ephrinB2 and are important for retinal axon divergence at the midline (Williams et al., 2004). EphrinB2 is selectively inhibitory to retinal axons arising from the ventrotemporal region of retina, which exclusively expresses EphB1, so they are repelled at the chiasm and form the uncrossed pathway. Extracellular matrix molecules such as chondroitin sulfate proteoglycans (CSPGs) and reelin have also been shown to be important for visual system development (Chung et al., 2000; Su et al., 2011). Enzymatic removal of CSPGs with chondroitinase ABC can result in stalling growth cones and misrouting axons of RGCs at the chiasm (Chung et al., 2000) and reelin is important for targeting of intrinsically photosensitive RGCs (ipRGCs) to VLG and the intrageniculate nucleus (Su et al., 2011).

Candidate molecules involved in regulating the timing of corticogeniculate innervation are currently being identified through the use of microarray and immunohistochemical screens. Results from ongoing studies show that aggrecan, a CSPG capable of repelling growing axons, is highly expressed in dLGN at birth and that degradation of aggrecan by ADAMTS (a disintegrin and metalloproteinase with thrombospondin motifs), a family of extracellular proteases,

coincides with corticogeniculate innervation of dLGN (Brooks et al., 2011). *In vitro* assays demonstrate that aggrecan can repel corticogeniculate axons. Moreover, injections of chondroitinase ABC near dLGN, which similar to ADAMTS in that it can cleave the glycosaminoglycan chains of aggrecan blocking its functional ability, result in an increase in the degree of corticogeniculate innervation *in vivo*. This suggests that aggrecan could be the *stop* signal preventing premature innervation of dLGN by corticogeniculate axons.

Innervation of dLGN by the retina and cortex is coordinated and input from the retina is essential for regulating the timing of corticogeniculate innervation. Whether this regulation is activity-dependent or -independent still needs to be tested. Nevertheless, it seems as though the driver input from the retina needs to be established before corticogeniculate projections, which can modulate the transmission of sensory information through dLGN, can begin to innervate. By the onset of vision both structural and functional corticogeniculate innervation is complete.

Figure 21

Corticogeniculate innervation in the presence and absence of retinal input.

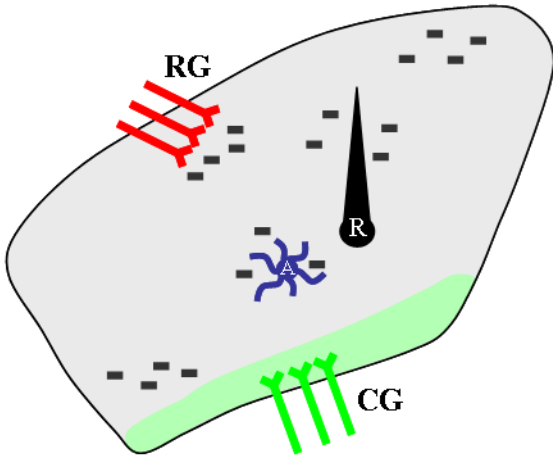
A, Diagram showing how corticogeniculate projections could be prevented from entering dLGN through a repulsive signal that is mediated either directly by retinogeniculate axons or indirectly through interactions involving relay cells, glia, or elements within the neuropil intrinsic to

dLGN. **B**, If retinogeniculate input is no longer present the *stop* signal repelling corticogeniculate axons may be removed allowing them to innervate dLGN at an accelerated rate.

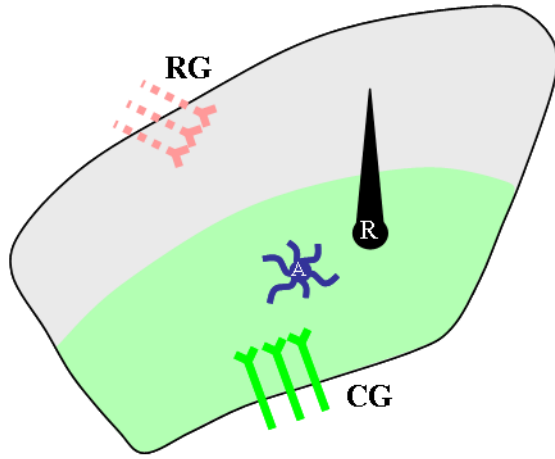
corticogeniculate projections (CG); retinogeniculate projections (RG); relay cell (R); astrocyte

(A).

A



B



Conclusions

Here we made use of different transgenic strains to help examine some unaddressed issues of circuit development in the dLGN of the mouse. In Figure 22, a summary of the timing of structural (*A*) and functional (*B*) innervation occurring within dLGN during early postnatal development is shown. Retinal and nonretinal innervation happens in a coordinated manner (Fig. 22A). For example, retinal innervation occurs perinatally, with crossed and uncrossed retinogeniculate projections entering dLGN at different times. Crossed projections arrive earlier (~E16) than uncrossed ones (~P0) and during early postnatal development both sets of projections undergo a coarse-scale remodeling in dLGN (Godement et al., 1984; Jaubert-Miazza et al., 2005). Initially, uncrossed projections are diffuse and share a substantial amount of terminal space with crossed projections. Around P8 uncrossed projections have receded and projections from the two eyes begin to form non-overlapping eye-specific domains and by the end of the second postnatal week segregation is complete.

In contrast, nonretinal projections enter dLGN at postnatal ages. Previous electron microscopy studies alluded to this, since nonretinal synapses were not apparent in dLGN until the second postnatal week (Bickford et al., 2010). The dLGN receives a massive amount of input from various nonretinal sources and these projections comprise around 90% of the terminals within dLGN (Sherman and Guillery, 2002; Bickford et al., 2010). Even though these nonretinal inputs play a major role in controlling the flow of sensory information through the dLGN not much is known about the early formation of these connections in dLGN. For our study on

nonretinal innervation we focused on the corticogeniculate pathway, since cortical layer VI neurons are one of the largest sources of nonretinal input and have an extensive influence in the dLGN. Using the *golli- τ -GFP* mouse, we found that corticogeniculate innervation was delayed in comparison to retinogeniculate innervation. Cortical projections arrived in thalamus around E18 (Jacobs et al., 2007), but did not begin to innervate dLGN until P4. Most of corticogeniculate innervation occurred around the time of eye-specific segregation and was not complete until eye opening. We also found that the retina plays a role in regulating the timing of corticogeniculate innervation in dLGN, since enucleation and genetic deafferentation accelerated corticogeniculate innervation.

The delayed innervation we saw for corticogeniculate projections might be a conserved process for other types of nonretinal projections, so to examine this we have begun preliminary experiments using other transgenic mouse strains. In both cat and mouse, cholinergic innervation from the parabrachial region of brainstem has been shown to start near the end of the first postnatal week (Carden et al., 2000; Ballesteros et al., 2005). However, these studies used immunohistochemical staining for choline acetyltransferase (ChAT) to label the fibers from brainstem and were not comprehensive enough to determine the exact time course of cholinergic innervation in dLGN. We are now using ChAT-cre knock-in mice (Lowell et al., 2006) crossed with ROSA-tdTomato mice (Madisen et al., 2010) in order to visualize and examine the timing of cholinergic innervation from brainstem in dLGN more closely. Figure 23A shows coronal sections of brainstem nuclei that send projections to dLGN from a ChAT-cre-tdTomato mouse. Cells expressing tdTomato were seen in the laterodorsal tegmental nucleus (LDT), parabigeminal nucleus (PBG), and pedunculopontine tegmental nucleus (PPT). Cholinergic projections to dLGN at P5 and P36 are shown in Figure 23B. Using ChAT immunohistochemistry cholinergic

fibers were first observed at P5 and were very sparse (Ballesteros et al., 2005). However, at P5 we saw many more cholinergic fibers that were often concentrated in the anteromedial portion of dLGN (Fig. 23B). To study innervation from GABAergic cells in the thalamic reticular nucleus (TRN) we used a GAD65-GFP mouse (Erdelyi et al., 2002; Lopez-Bendito et al., 2004; Fig. 24A). TRN innervation is also delayed but begins slightly earlier (~P2) than cortical or brainstem innervation in dLGN and appears to be complete by P9 (Fig. 24B).

To see if the retina is also important for regulating the innervation of these other forms of nonretinal projections we can examine whether cholinergic and TRN innervation is disrupted by a loss of retinal input. This can be achieved by doing either enucleations in the ChAT-cre-tdTomato and GAD65-GFP mice or by crossing these strains with *math5*^{-/-} mice. We have started to do enucleations in these two strains and it seems as though the timing of their innervation is also affected by the absence of retinal input (data not shown). Taken together, this supports the idea that driver or retinal input must be established before modulatory nonretinal inputs can innervate dLGN and that retina may be playing a large role in regulating the timing of nonretinal innervation.

The potential mechanism behind this coordinated innervation may involve a repulsive molecule. Current work is being done to examine the role of aggrecan and ADAMTS in the timing of corticogeniculate innervation (Brooks et al., 2011). Thus far, aggrecan appears to be a good candidate for the molecular brake that regulates when corticogeniculate projections can enter dLGN. It would be really fascinating to see if aggrecan also plays a role in regulating the innervation of other nonretinal projections. However, whether this is the case or if they rely on some other molecular cue remains to be examined.

Our enucleation and genetic deafferentation experiments also demonstrate that the retina

somehow regulates the expression of the molecule controlling the timing of corticogeniculate innervation. Retinal innervation has been shown to control gene expression in chick optic tectum (Herzog et al., 1994). As retinal innervation of tectum increases there is a concurrent increase in BDNF mRNA. These levels are reduced if innervation is prevented by optic stalk transection or if activity is blocked. From our study we were not able to determine if the role of retina in regulating the timing of corticogeniculate innervation is activity-independent or -dependent. Typically activity seems to play a role in the remodeling and refinement of projections. For example, if spontaneous retinal waves are disrupted retinal axon arbors in dLGN remain diffuse and fail to segregate properly into eye-specific domains (Torborg and Feller, 2005). In addition, normal strengthening and pruning of retinal inputs onto relay cells is disrupted if spontaneous activity is blocked (Hooks and Chen, 2006). However, diminished sensory activity through unilateral naris occlusion has been shown to affect cholinergic innervation in the olfactory bulb of the mouse (Salcedo et al., 2011). Also experiments in *Islet2-EphA3* knock-in mice have demonstrated that the retina plays an instructive role in the mapping and alignment of cortical projections to superior colliculus and in the absence of spontaneous retinal activity, corticocollicular projections in these mice are misaligned with the retinocollicular map (Triplett et al., 2009).

To study activity-dependent mechanisms in the visual system, early spontaneous retinal activity is usually blocked with tetrodotoxin (TTX) or disrupted with either epibatidine or through use of a mouse lacking the $\beta 2$ -subunits of neuronal nicotinic acetyl choline receptors ($\beta 2nAChR^{-/-}$; Penn et al., 1998; Herzog et al., 1994; Cook et al., 1999; Rossi et al., 2001; Huberman et al., 2002; Muir-Robinson et al., 2002; Hooks and Chen, 2006; Triplett et al., 2009). We can use similar experimental approaches to help determine whether regulation of

corticogeniculate innervation is activity-dependent. TTX would help us to verify whether retinal activity in general is essential for regulating the timing of corticogeniculate innervation. If activity is involved it would likely be through the stage-II waves driven by cholinergic starburst amacrine cells in the retina, since the timing of these waves is coincident with corticogeniculate innervation. The use of epibatidine or the $\beta 2nAChR^{-/-}$ mouse would allow us to selectively disrupt this activity and assess its possible involvement.

In the absence of retinal input we also saw that the pattern of corticogeniculate innervation was disrupted, so that projections innervated dLGN in a uniform manner. Connections within the visual system are organized to convey information about the position of stimuli in the visual field (Huberman et al., 2008a). The overall layout of these retinotopic maps is organized by gradients of ephrins and their Eph receptors found in the retina and its central visual targets (Feldheim et al., 1998, 2000, 2004; Frisen et al., 1998; McLaughlin and O'Leary, 2005; Flanagan et al., 2006; Pfeiffenberger et al., 2006). EphA7-mediated signaling on cortical axons has also been shown to be important for generating the topographic organization of corticothalamic projections in thalamus (Torii and Levitt, 2005). The ephrin-A gradient in dLGN has been found to be diminished in enucleated mice (Dye et al., 2012). Taken together, this suggests that the topography of corticogeniculate projections in dLGN might also be perturbed by the loss of retinal input but further examination is still needed.

In addition to examining the structural innervation of retinal and nonretinal projections we also looked at when these projections form functional connections within dLGN. We found that functional innervation mirrors the coordinated structural innervation that we observed in that the establishment of functional retinal synapses with relay cells and interneurons precedes the formation of nonretinal synapses (Fig. 22B). It seems to be the case that projections quickly form

functional synapses after they arrive in dLGN. From previous work we know that functional retinal connections with relay cells are present at very early postnatal ages (Mooney et al., 1996; Chen and Regehr, 2000; Ziburkus et al., 2003; Jaubert-Miazza et al., 2005; Bickford et al., 2010). It also appears that the retina forms functional connections with interneurons in dLGN at these early ages, since we were able to record these responses during the first postnatal week. Thus, retinal connections are the first to form in dLGN and then seem to be followed by the formation of nonretinal connections.

Functional innervation of nonretinal projections in dLGN is delayed in comparison to those from the retina and we know of at least two types of connections between nonretinal cells and relay cells that form later during postnatal development. By the end of the first postnatal week we found that corticogeniculate projections form functional connections with relay cells in dLGN. These synapses do not fully mature until sometime after the following week. During the first postnatal week synaptic responses recorded in relay cells are primarily excitatory (Bickford et al., 2010). This along with evidence that there is a lack of GAD67-positive inhibitory nerve terminals at early postnatal ages (Singh et al., 2012) suggests that synapses between intrinsic interneurons and relay cells have not yet developed. These connections are responsible for feedforward inhibition onto relay cells and are not formed until around the second postnatal week (Bickford et al., 2010). It is still not clear when projections from brainstem and TRN form functional connections in dLGN. To examine this it may require the use of optogenetic approaches since it might not be possible to study these connections using electrical stimulation.

It is interesting to look at the timing of nonretinal connections with respect to a number of developmental events including: coarse-scale retinogeniculate remodeling, fine-scale refinement of retinal inputs onto relay cells, timing of spontaneous retinal activity and patterned vision, and

dendritic organization and maturation. Nonretinal innervation is occurring around the periods of coarse-scale remodeling and fine-scale refinement. Functional nonretinal connections are present about the time that spontaneous retinal waves are beginning to be replaced by patterned visual activity. During this time, synapses at the ultrastructural level are mature and reflect the adult profile. In the adult, there is a dendritic organization of retinal and nonretinal contacts on relay cells in dLGN (Guillery, 1969; Wilson et al., 1984; Erisir et al., 1997a). Retinal afferents make synapses on proximal regions of relay cell dendrites close to the cell body. Those from brainstem are also found primarily proximally, adjacent to retinal inputs. Whereas inputs from layer VI of cortex make synapses primarily onto distal dendrites and those from GABAergic sources make contacts with all parts of the dendritic arbor. The time in which functional synapses form might somehow be linked to their position on dendrites.

There is a possibility that retinal inputs may need to undergo pruning and establish their position on proximal regions on relay cell dendrites before nonretinal connections can be made. Different adhesion cues expressed at different sites along a dendritic arbor have been shown to be important for segregating synaptic inputs arising from various sources (Ango et al., 2004; Di Cristo et al., 2004). It would be interesting to see whether the distribution of nonretinal contacts on the dendrites of relay cells is disorganized in the absence of retinal input. There is some evidence of disruption in the normal ultrastructure of dLGN in mice lacking retinal input. In enucleated as well as *math5*^{-/-}, anophthalmic, and microphthalmic strains of mice, terminals consisting of round vesicles, large profile, and dark mitochondria (RLD) were found (Cullen and Kaiserman-Abramof, 1976; Kaiserman-Abramof, 1983; Winkelmann et al., 1985; El-Danaf, 2011). These RLD terminals are not normally present in dLGN. Their origin has not yet been determined, but it is suggested that they are the result of compensatory response arising from the

cortex or brainstem (Kaiserman-Abramof, 1983).

The scaffolding for nonretinal connections is established early on, since around the time that nonretinal inputs are forming functional connections, the relay cells in dLGN are remarkably complex. Both cell class specificity (Krahe et al., 2011) and complexity (El-Danaf, 2008, 2011) are established by the end of the first postnatal week. Relay cells in the dLGN of the mouse do undergo two growth spurts during early postnatal development (El-Danaf, 2008, 2011) similar to what occurs in the rat (Parnavelas et al., 1977). The first growth spurt occurs very early and the second one just comprises of a gradual increase in dendritic field and length.

We did not examine the morphological properties of interneurons quantitatively but it would be interesting to know if their morphology changes during early postnatal development. In rat, during the first few postnatal weeks the dendrites of interneurons expand and their dendritic trees becomes much more complex due to increases in branching (Perreault et al., 2003). These changes in morphology were also accompanied by changes in various types of feedforward inhibition, such as long-range GABA_A-mediated inhibition and long-duration GABA_B-mediated inhibition. In mouse there is also a delay in the development of GABA-mediated inhibition so perhaps it is related to changes in the dendritic trees of interneurons.

The visual system has been used extensively as a model for studying the formation and refinement of synaptic circuits and much of what we know about thalamic function has come from studies in the dLGN. Relay cells transmit visual information from retina to primary visual cortex but the interneurons as well as the numerous nonretinal projections in dLGN have an extensive influence on the way in which that information is relayed to cortex. Therefore is important to have an understanding of how and when these connections form and change throughout development in the dLGN. In summary, we showed that nonretinal innervation is

delayed and that the retina may regulate the temporal and spatial properties of their innervation. We also revealed that the pattern of retinal convergence onto interneurons and the distribution of retinal contacts on these cells is very different from that of relay cells and may reflect their functional role in dLGN. These studies also add to a growing list of evidence that supports the mouse as an experimental platform for studying thalamic circuit development. The cell types and synaptic organization in dLGN seems to be highly conserved throughout different species. One advantage to using mice is the availability of genetic tools that allow for labeling, monitoring, and manipulating defined cell types and neural circuits. The studies described here provide a set of transgenic mice that can be used in future experiments to dissect out the different components of the complex circuitry within dLGN.

Figure 22

Summary of circuit development in the dLGN of the mouse.

A, Timeline of structural innervation of retinal and nonretinal projections in dLGN. Retinal innervation of dLGN occurs at perinatal ages and these projections undergo a period of eye-specific. Nonretinal innervation from cortex, brainstem, and TRN are delayed in comparison to retinal innervation. Connections between relay cells and intrinsic interneurons form around P7-P9, but the full complement of feedforward inhibition is not apparent until the end of the second postnatal week. **B**, Timeline of functional innervation of retinal and nonretinal projections in dLGN. Functional retinal connections with relay cells and interneurons in dLGN form at very early postnatal ages. Disynaptic feedforward inhibition involving intrinsic interneurons and functional connections between neurons in layer VI of cortex and relay cells appear around the end of the first postnatal week. In addition to eye-specific remodeling, individual relay cells undergo a period of refinement. Relay cells initially receive around a dozen retinal inputs but by maturity only 1-3 inputs remain. Interneurons do not undergo refinement and have a high degree of retinal convergence even at late postnatal ages. TRN, thalamic reticular nucleus; R, relay cell; I, interneuron; C, cortex.

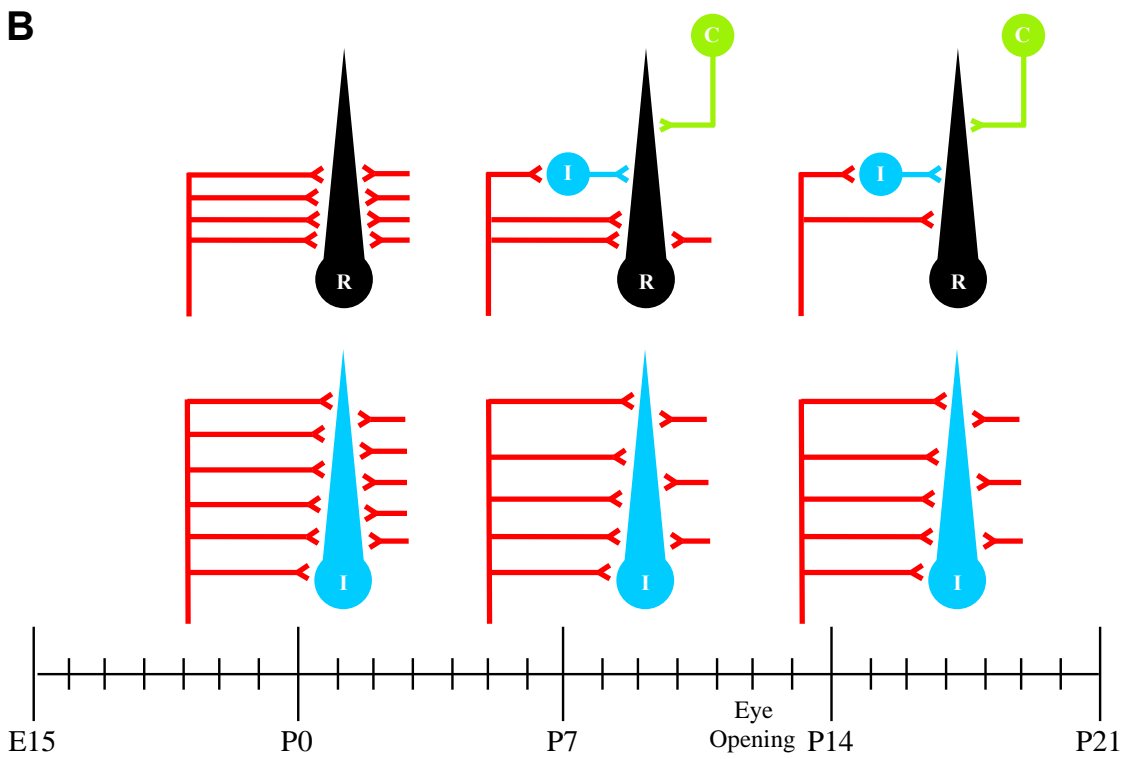
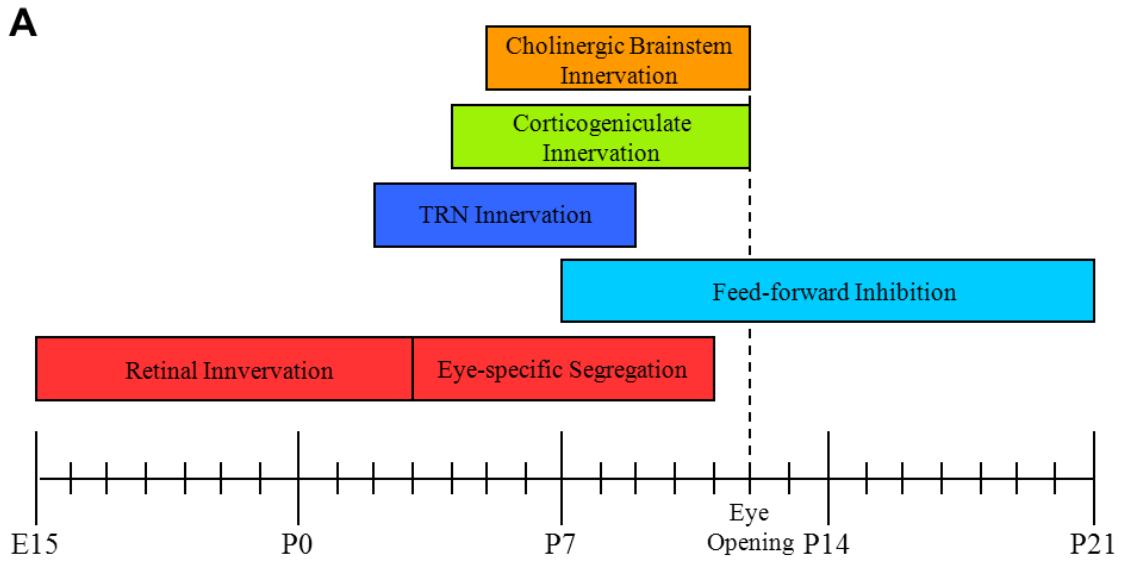


Figure 23

Cholinergic brainstem innervation is delayed in dLGN.

A, Coronal sections of brainstem in a P5 ChAT-cre-tdTomato mouse showing cells expressing tdTomato in the cholinergic nuclei, which project to dLGN. LDT, laterodorsal tegmental nucleus; PBG, parabigeminal nucleus; PPT, pedunculopontine tegmental nucleus. Scale bar, 200 μm . **B**, Cholinergic projections in coronal sections of dLGN at P5 and P36. Scale bar, 100 μm .

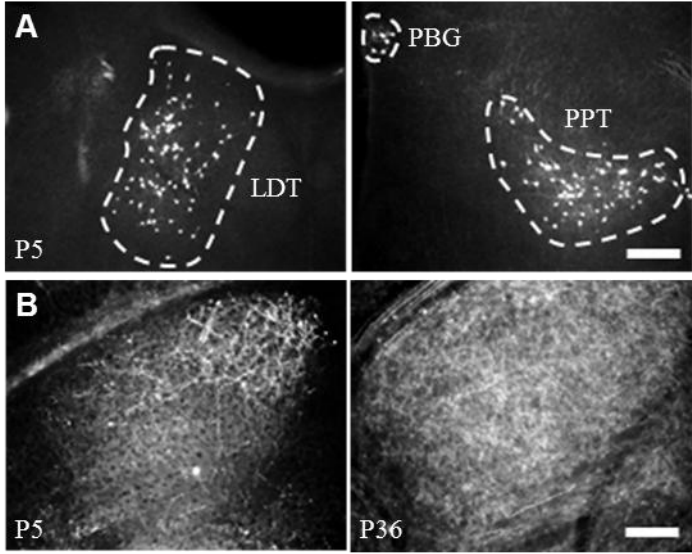
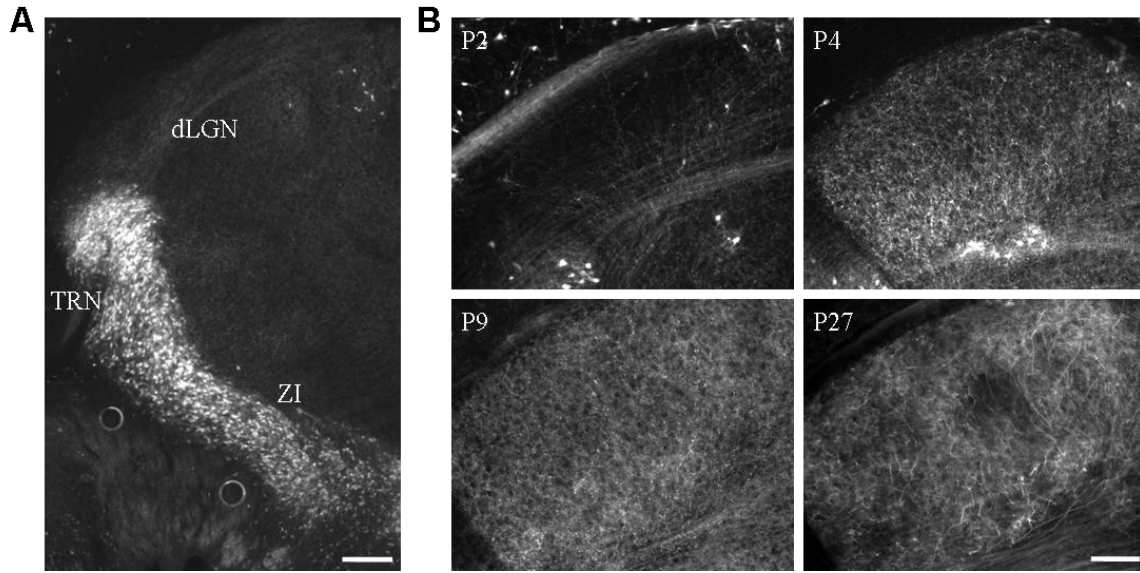


Figure 24

Innervation by the thalamic reticular nucleus is delayed in dLGN.

A, Coronal section showing the GFP-expressing cells in the thalamic reticular nucleus of a P4 GAD65-GFP mouse. dLGN, dorsal lateral geniculate nucleus; TRN, thalamic reticular nucleus; ZI, zona incerta. Scale bar, 200 μm . **B**, Projections from TRN in coronal sections of dLGN at P2, P4, P9, and P27. Scale bar, 100 μm .



Literature Cited

Literature Cited

- Acuna-Goycolea C, Brenowitz SD, Regehr WG (2008) Active dendritic conductances dynamically regulate GABA release from thalamic interneurons. *Neuron* 57:420-431.
- Airaksinen MS, Panula P (1988) The histaminergic system in the guinea pig central nervous system: An immunocytochemical mapping study using an antiserum against histamine. *J Comp Neurol* 273:163-186.
- Alexander GM, Godwin DW (2005) Presynaptic inhibition of corticothalamic feedback by metabotropic glutamate receptors. *J Neurophysiol* 94:163-175.
- Ango F, di Cristo G, Higashiyama H, Bennett V, Wu P, Huang ZJ (2004) Ankyrin-based subcellular gradient of neurofascin, an immunoglobulin family protein, directs GABAergic innervation at purkinje axon initial segment. *Cell* 119:257-272.
- Antal M, Acuna-Goycolea C, Pressler RT, Blitz DM, Regehr WG (2010) Cholinergic activation of M2 receptors leads to context-dependent modulation of feedforward inhibition in the visual thalamus. *PLoS Biol* 8:e1000348.
- Arcelli P, Frassoni C, Regondi MC, De Biasi S, Spreafico R (1997) GABAergic neurons in mammalian thalamus: A marker of thalamic complexity? *Brain Res Bull* 42:27-37.
- Asanuma C, Stanfield BB (1990) Induction of somatic sensory inputs to the lateral geniculate nucleus in congenitally blind mice and in phenotypically normal mice. *Neurosci* 39:533-545.
- Augustinaite S, Yanagawa Y, Heggelund P (2011) Cortical feedback regulation of input to visual cortex: role of intrageniculate interneurons. *J Physiol* 589:2963-2977.
- Ballesteros JM, VAN DER List DA, Chalupa LM (2005) Formation of eye-specific retinogeniculate projections occurs prior to the innervation of the dorsal lateral geniculate nucleus by cholinergic fibers. *Thalamus Relat Syst* 3:157-163.
- Bellocchio EE, Reimer RJ, Fremeau RT Jr, Edwards RH (2000) Uptake of glutamate into synaptic vesicles by an inorganic phosphate transporter. *Science* 289:957-960.
- Bickford ME, Slusarczyk A, Dilger EK, Krahe TE, Kucuk C, Guido W (2010) Synaptic development of the mouse dorsal lateral geniculate nucleus. *J Comp Neurol* 518:622-635.

Blakemore C (1991) Sensitive and vulnerable periods in the development of the visual system. *Ciba Found Symp* 156:129-147.

Blitz DM, Regehr, WG (2005) Timing and specificity of feed-forward inhibition within the LGN. *Neuron*, 45:917-928.

Bloomfield SA, Hamos JE, Sherman SM (1987) Passive cable properties and morphological correlates of neurones in the lateral geniculate nucleus of the cat. *The J Physiol* 383:653-692.

Bloomfield SA, Sherman SM (1989) Dendritic current flow in relay cells and interneurons of the cat's lateral geniculate nucleus. *Pro Natl Acad of Sci* 86:3911-3914.

Bolshakov VY, Siegelbaum SA (1995) Regulation of hippocampal transmitter release during development and long-term potentiation. *Science* 269:1730-1734.

Bourassa J, Deschenes M (1995) Corticothalamic projections from the primary visual cortex in rats: a single fiber study using biocytin as an anterograde tracer. *Neuroscience* 66:253-263.

Briggs F, Usrey WM (2008) Emerging views of corticothalamic function. *Curr Opin Neurobiol* 18:403-407

Brooks J, Su J, Fox MA (2011) Dual roles for aggrecan in cell-type specific axonal targeting of the dorsal lateral geniculate nucleus. *CVCSN Abstract*.

Brown NL, Kanekar S, Vetter ML, Tucker PK, Gemza DL (1998) Math5 encodes a murine basic helix-loop-helix transcription factor expressed during early stages of retinal neurogenesis. *Development*, 125:4821-4833.

Brown NL, Patel S, Brzezinski J, Glaser T (2001) Math5 is required for retinal ganglion cell and optic nerve formation. *Development* 128:2497-2508

Brunso-Bechtold JK, Florence, SL, Casagrande VA (1983) The role of retinogeniculate afferents in the development of connections between visual cortex and the dorsal lateral geniculate nucleus. *Brain Res* 312:33-39.

Brzezinski JA 4th, Brown NL, Tanikawa A, Bush RA, Sieving PA, Vitaterna MH Takahashi JS, Glaser T (2005) Loss of Circadian Photoentrainment and abnormal retinal electrophysiology in Math5 mutant mice. *Invest Ophthalmol Vis Sci* 46:2540-2551.

Carden WB, Datskovskaia A, Guido W, Godwin DW, Bickford ME (2000) Development of the cholinergic, nitrenergic, and GABAergic innervation of the cat dorsal lateral geniculate nucleus. *J Comp Neurol* 418:65-80.

Casagrande VA, Norton TT (1991) Lateral geniculate nucleus: A review of physiology and function. In: *The neural basis of vision function* (Leventhal AG, ed), pp41-84. Hampshire, UK: Macmillan Press.

- Casale AE, McCormick DA (2011) Active action potential propagation but not initiation in thalamic interneuron dendrites. *J Neurosci* 31:18289-18302.
- Chattopadhyaya B, Di Cristo G, Higashiyama H, Knott GW, Kuhlman SJ, Welker E, Huang XJ (2004) Experience and activity-dependent maturation of perisomatic GABAergic innervation in primary visual cortex during a postnatal critical period. *J Neurosci* 24:9598-9611.
- Chen C, Regehr WG (2000) Developmental remodeling of the retinogeniculate synapse. *Neuron* 28:955-966.
- Chung KY, Taylor JS, Shum DK, Chan SO (2000) Axon routing at the optic chiasm after enzymatic removal of chondroitin sulfate in mouse embryos. *Development* 127:2673-2683.
- Clasca F, Angelucci A, Sur M (1995) Layer-specific programs of development in neocortical projection neurons. *Proc Natl Acad Sci* 92:11145-11149.
- Cleland BG, Dubin MW, Levick WR (1971) Sustained and transient neurones in the cat's retina and lateral geniculate nucleus. *J Physiol* 217:473-496.
- Coleman JE, Law K, Bear MF (2009) Anatomical origins of ocular dominance in mouse primary visual cortex. *Neuroscience* 161:561-751.
- Conn PJ, Pin JP (1997) Pharmacology and functions of metabotropic glutamate receptors. *Annu Rev Pharmacol Toxicol* 37:205-237.
- Cook PM, Prusky G, Ramoa AS (1999) The role of spontaneous retinal activity before eye opening in the maturation of form and function in the retinogeniculate pathway of the ferret. *Vis Neurosci* 16:491-501.
- Cosenza RM, Moore RY (1984) Afferent connections of the ventral lateral geniculate nucleus in the rat: an HRP study. *Brain Res* 310:367-370.
- Cox CL, Zhou Q, Sherman SM (1998) Glutamate locally activates dendritic outputs of thalamic interneurons. *Nature* 394:478-482.
- Crandall SR, Cox CL (2012) Local dendrodendritic inhibition regulates fast synaptic transmission in visual thalamus. *J Neurosci* 32:2513-2522.
- Crunelli V, Haby M, Jassik-Gerschenfeld D, Leresche N, Pirchio M (1988) Cl^- - and K^+ - dependent inhibitory postsynaptic potentials evoked by interneurons of the rat lateral geniculate nucleus. *J Physiol* 399:153-176.
- Crunelli V, Lightowler S, Pollard CE (1989) A T-type Ca^{2+} current underlies low-threshold Ca^{2+} potentials in cells of the cat and rat lateral geniculate nucleus. *J Physiol* 413:543-561.

- Cullen MJ, Kaiserman-Abramof IR (1976) Cytological organization of the dorsal lateral geniculate nuclei in mutant anophthalmic and postnatally enucleated mice. *J Neurocytol* 5:407-424.
- Deiner MS, Kennedy TE, Fazeli A, Serafini T, Tessier-Lavigne M, Sretavan DW (1997) Netrin-1 and DCC mediate axon guidance locally at the optic disc: loss of function leads to optic nerve hypoplasia. *Neuron* 19:575-589.
- de Lima AD, Singer W (1987a) The serotonergic fibers in the dorsal lateral geniculate nucleus of the cat: Distribution and synaptic connections demonstrated with immunocytochemistry. *J Comp Neurol* 258:339-351.
- de Lima AD, Singer W (1987b) The brainstem projection to the lateral geniculate nucleus in the cat: Identification of cholinergic and monoaminergic elements. *J Comp Neurol* 259:92-121.
- Demas J, Eglen SJ, Wong RO (2003) Developmental loss of synchronous spontaneous activity in the mouse retina is independent of visual experience. *J Neurosci* 23:2851-2860.
- Deschenes M, Paradis M, Roy JP, Steriade M (1984) Electrophysiology of neurons of lateral thalamic nuclei in cat: Resting properties and burst discharges. *J Neurophysiol* 51:1196-1219.
- Di Cristo G, Wu C, Chattopadhyaya B, Ango F, Knott G, Welker E, Svoboda K, Huang ZJ (2004) Subcellular domain-restricted GABAergic innervation in primary visual cortex in the absence of sensory and thalamic inputs. *Nat Neurosci* 7:1184-1186.
- Dilger EK, Shin HS, Guido W (2011) Requirements for synaptically evoked plateau potentials in relay cells of the dorsal lateral geniculate nucleus of the mouse. *J Physiol* 589:919-937.
- Dilger EK, Krahe TE, Morhardt D, Shin HS, Guido W (submitted) Absence of plateau potentials in dLGN cells leads to a breakdown in retinogeniculate refinement.
- Dolmetsch RE, Pajvani U, Fife K, Spotts JM, Greenberg ME (2001) Signaling to the nucleus by an L-type calcium channel-calmodulin complex through the MAP kinase pathway. *Science* 294:333-339.
- Dubin MW, Cleland BG (1977) Organization of visual inputs to interneurons of lateral geniculate nucleus of the cat. *J Neurophysiol* 40:410-427.
- Dye CA, Abbott CW, Huffman KJ (2012) Bilateral enucleation alters gene expression and intraneocortical connections in the mouse. *Neural Dev* 7:5.
- Ecker JL, Dumitrescu ON, Wong KY, Alam NM, Chen SK, LeGates T, Renna JM, Prusky GT, Berson DM, Hattar S (2010) Melanopsin-expressing retinal ganglion-cell photoreceptors: Cellular diversity and role in pattern vision. *Neuron* 67:49-60.

- El-Danaf RN (2008) Developmental remodeling of relay cells in the dorsal lateral geniculate nucleus of the mouse. Virginia Commonwealth University Thesis.
- El-Danaf RN (2011) Developmental remodeling of relay cells in the dorsal lateral geniculate nucleus (dLGN) of the mouse and the role of retinal innervation. Virginia Commonwealth University Dissertation.
- Erdelyi F, Sekerkova G, Katarova Z, Hajos N, Palhalmi J, Freund TF, Mugnaini E, Szabo G (2002) GAD65-GFP transgenic mice expressing GFP in the GABAergic nervous system. FENS Abstract.
- Erisir A, Van Horn SC, Bickford ME, Sherman SM (1997a) Immunocytochemistry and distribution of parabrachial terminals in the lateral geniculate nucleus of the cat: A comparison with corticogeniculate terminals. *J Comp Neurol* 377:535-549.
- Erisir A, Van Horn SC, Sherman SM (1997b) Relative numbers of cortical and brainstem inputs to the lateral geniculate nucleus. *Pro Natl Acad of Sci* 94:1517-1520.
- Erisir A, Van Horn SC, Sherman SM (1998) Distribution of synapses in the lateral geniculate nucleus of the cat: Differences between laminae A and A1 and between relay cells and interneurons. *J Comp Neurol* 390:247-255.
- Eysel UT, Pape HC, Van Schayck R (1986) Excitatory and differential disinhibitory actions of acetylcholine in the lateral geniculate nucleus of the cat. *J Physiol* 70:233-254.
- Famiglietti EV Jr, Peters A (1972) The synaptic glomerulus and the intrinsic neuron in the dorsal lateral geniculate nucleus of the cat. *J Comp Neurol* 144:285-334.
- Feldheim DA, Vanderhaeghen P, Hansen MJ, Frisen J, Lu Q, Barbacid M, Flanagan JG (1998) Topographic guidance labels in a sensory projection to the forebrain. *Neuron* 21:1303-1313.
- Feldheim DA, Kim YI, Bergemann AD, Frisen J, Barbacid M, Flanagan JG (2000) Genetic analysis of ephrin-A2 and ephrin-A5 shows their requirement in multiple aspects of retinocollicular mapping. *Neuron* 25:563-574.
- Feldheim DA, Nakamoto M, Osterfield M, Gale NW, DeChiara TM, Rohatgi R, Yancopoulos GD, Flanagan JG (2004) Loss-of-function analysis of EphA receptors in retinotectal mapping. *J Neurosci* 24:2542-2550.
- Flanagan JG (2006) Neural map specification by gradients. *Curr Opin Neurobiol* 16:59-66.
- Freneau RT, Troyer MD, Pahner I, Nygaard GO, Tran CH, Reimer RJ, Bellocchio EE, Fortin D, Storm-Mathisen J, Edwards RH (2001) The expression of vesicular glutamate transporters defines two classes of excitatory synapse. *Neuron* 31:247-260.

Freneau RT, Voglmaier S, Seal RP, Edwards RH (2004) VGLUTs define subsets of excitatory neurons and suggest novel roles for glutamate. *Trends Neurosci* 27:98-103.

Friedlander MJ, Lin CS, Stanford LR, Sherman SM (1981) Morphology of functionally identified neurons in lateral geniculate nucleus of the cat. *J Neurophysiol* 46:80-129.

Frisen J, Yates PA, McLaughlin T, Friedman GC, O'Leary DD, Barbacid M (1998) Ephrin-A5 (AL-1/RAGS) is essential for proper retinal axon guidance and topographic mapping in the mammalian visual system. *Neuron* 20:235-243.

Gabbott PL, Somogyi J, Stewart MG, Hamori J (1986) A quantitative investigation of the neuronal composition of the rat dorsal lateral geniculate nucleus using GABA-immunocytochemistry. *Neuroscience* 19:101-111.

Garey LJ, Dreher B, Robinson SR (1991) The organization of the visual thalamus. In: *Neuroanatomy of the visual pathways and their development* (Dreher B, Robinson SR, eds), pp176-234. Hampshire, UK: Macmillan Press.

Gilbert CD (1977) Laminar differences in receptive field properties of cells in cat primary visual cortex. *J Physiol* 268:391-421.

Godement P, Salaun J, Imbert M (1984) Prenatal and postnatal development of retinogeniculate and retinocollicular projections in the mouse. *J Comp Neurol* 230:552-575.

Godwin DW, Vaughan JW, Sherman SM (1996) Metabotropic glutamate receptors switch visual response mode of lateral geniculate nucleus cells from burst to tonic. *J Neurophysiol* 76:1800-1816.

Govindaiah, Cox CL (2004) Synaptic activation of metabotropic glutamate receptors regulates dendritic outputs of thalamic interneurons. *Neuron* 41:611-623.

Govindaiah G, Cox CL (2006) Metabotropic glutamate receptors differentially regulate GABAergic inhibition in thalamus. *J Neurosci* 26:13443-13453.

Granseth B, Ahlstrand E, Lindstrom S (2002) Paired pulse facilitation of corticogeniculate EPSCs in the dorsal lateral geniculate nucleus of the rat investigated in vitro. *J Physiol* 544:477-486.

Granseth B, Lindstrom S (2003) Unitary EPSCs of corticogeniculate fibers in the rat dorsal lateral geniculate nucleus in vitro. *J Neurophysiol* 89:2952-2960.

Grossman A, Lieberman AR, Webster KE (1973) A golgi study of the rat dorsal lateral geniculate nucleus. *J Comp Neurol* 150:441-66.

Grubb MS, Thompson ID (2003) Quantitative characterization of visual response properties in the mouse dorsal lateral geniculate nucleus. *J Neurophysiol* 90:3594-3607.

- Guido W (2008) Refinement of the retinogeniculate pathway. *J Physiol* 586:4357-4362.
- Guillery RW (1969) The organization of synaptic interconnections in the laminae of the dorsal lateral geniculate nucleus of the cat. *Z Zellforsch Mikrosk Anat* 96:1-38.
- Hamos JE, Van Horn SC, Raczkowski D, Uhlrich DJ, Sherman SM (1985) Synaptic connectivity of a local circuit neurone in lateral geniculate nucleus of the cat. *Nature* 317:618-621.
- Hamos JE, Van Horn SC, Raczkowski D, Sherman SM (1987) Synaptic circuits involving an individual retinogeniculate axon in the cat. *J Comp Neurol* 259:165-192.
- Herzog KH, Bailey K, Barde YA (1994) Expression of the BDNF gene in the developing visual system of the chick. *Development* 120:1643-1649.
- Hooks BM, Chen C (2006) Distinct roles for spontaneous and visual activity in remodeling of the retinogeniculate synapse. *Neuron* 52:281-291.
- Hubel DH, Wiesel TN (1961) Integrative action in the cat's lateral geniculate body. *J Physiol* 155:385-398.
- Huberman AD, Stellwagen D, Chapman B (2002) Decoupling eye-specific segregation from lamination in the lateral geniculate nucleus. *J Neurosci* 22:9419-9429.
- Huberman AD, Murray KD, Warland DK, Feldheim DA, Chapman B (2005) Ephrin-A5 mediate targeting of eye-specific projections to the lateral geniculate nucleus. *Nat Neurosci* 8:1013-1021.
- Huberman AD, Feller MB, Chapman B (2008a) Mechanisms underlying development of visual maps and receptive fields. *Annu Rev Neurosci* 31:479-509.
- Huberman AD, Manu M, Koch SM, Susman MW, Lutz AB, Ullian EM, Baccus SA, Barres BA (2008b) Architecture and activity-mediated refinement of axonal projections from a mosaic of genetically identified retinal ganglion cells. *Neuron* 59:425-438.
- Huberman AD, Wei W, Elstrott J, Stafford BK, Feller MB, Barres BA (2009) Genetic identification of an On-Off direction-selective retinal ganglion cell subtype reveals a layer-specific subcortical map of posterior motion. *Neuron* 62:327-334.
- Humphrey AL, Weller RE (1988) Structural correlates of functionally distinct X-cells in the lateral geniculate nucleus of the cat. *J Comp Neurol* 268:448-468.
- Irvin GE, Norton TT, Sesma MA, Casagrande VA (1986) W-like response properties of interlaminar zone cells in the lateral geniculate nucleus of a primate (*Galago crassicaudatus*). *Brain Res* 362:254-270.

Jacobs EC, Campagnoni C, Kampf K, Reyes SD, Kalra V, Handley V, Xie YY, Hong-Hu Y, Spreur V, Fisher RS, Campagnoni AT (2007) Visualization of corticofugal projections during early cortical development in a tau-GFP-transgenic mouse. *Eur J Neurosci* 25:17-30.

Jaubert-Miazza L, Green E, Lo FS, Bui K, Mills J, Guido W (2005) Structural and functional composition of the developing retinogeniculate pathway in the mouse. *Vis Neurosci* 22:661-676.

Kaas JH, Huerta MF, Weber JT, Harting JK (1978) Patterns of retinal terminations and laminar organization of the lateral geniculate nucleus of primates. *J Comp Neurol* 182:517-553.

Kaiserman-Abramof IR, Graybiel AM, Nauta WJH (1975) Neural connections of area 17 in an anophthalmic mouse strain. *Soc Neurosci Abstract*.

Kaiserman-Abramof IR (1983) Intrauterine enucleation of normal mice mimics a structural compensatory response in the geniculate of eyeless mutant mice. *Brain Res* 270:149-153.

Kay JN, De la Huerta I, Kim IJ, Zhang Y, Yamagata M, Chu MW, Meister M, Sanes JR (2011) Retinal ganglion cells with distinct directional preferences differ in molecular identity, structure, and central projections. *J Neurosci* 31:7753-7762

Kielland A, Erisir A, Walaas SI, Heggelund P (2006) Synapsin utilization differs among functional classes of synapses on thalamocortical cells. *J Neurosci* 26:5786-5793.

Kim IJ, Zhang Y, Yamagata M, Meister M, Sanes JR (2008) Molecular identification of a retinal cell type that responds to upward motion. *Nature* 452:478-482.

Krahe TE, El-Danaf RN, Dilger EK, Henderson SC, Guido W (2011) Morphologically distinct classes of relay cells exhibit regional preferences in the dorsal lateral geniculate nucleus of the mouse. *J Neurosci* 31:17437-17448.

Landry CF, Pribyl TM, Ellison JA, Givogri MI, Kampf K, Campagnoni CW, Campagnoni AT (1998) Embryonic expression of the myelin basic protein gene: Identification of a promoter region that targets transgene expression to pioneer neurons. *J Neurosci* 18:7315-7327.

Lennie P (1980) Parallel visual pathways: a review. *Vision Res* 20:561-594.

Li J, Wang S, Bickford ME (2003) Comparison of the ultrastructure of cortical and retinal terminals in the rat dorsal lateral geniculate and lateral posterior nuclei. *J Comp Neurol* 460:394-409.

Lo FS, Lu SM, Sherman SM (1991) Intracellular and extracellular in vivo recording of different response modes for relay cells of the cat's lateral geniculate nucleus. *Exp Brain Res* 83:317-328.

Lo FS, Ziburkus J, Guido W (2002) Synaptic mechanisms regulating the activation of a Ca²⁺-mediated plateau potential in developing relay cells of the LGN. *J Neurophysiol* 87:1175-1185.

Lonze BE, Ginty DD (2002) Function and regulation of CREB family transcription factors in the nervous system. *Neuron* 35:605-623.

Lopez-Bendito G, Sturgess K, Erdelyi F, Szabo G, Molnar Z, Paulsen O (2004) Preferential origin and layer destination of GAD65-GFP cortical interneurons. *Cereb Cortex* 14:1122-1133.

Lowell BB, Olson D, Yu J (2006) Development and phenotype of ChAT-IRES-Cre mice MGI Direct Data Submission J:114556.

Lu SM, Guido W, Sherman SM (1993) The brain-stem parabrachial region controls mode of response to visual stimulation of neurons in the cat's lateral geniculate nucleus. *Vis Neurosci* 10:631-642.

Lund RD, Cunningham TJ, Lund JS (1973) Modified optic projections after unilateral eye removal in young rats. *Brain Behav Evol* 8:51-72.

MacLeod N, Turner C, Edgar J (1997) Properties of developing lateral geniculate neurones in the mouse. *Int J Dev Neurosci* 15:205-224.

Madisen L, Zwingman TA, Sunkin SM, Oh SW, Zariwala HA, Gu H, Ng LL, Palmiter RD, Hawrylycz MJ, Jones AR, Lein ES, Zeng H (2010) A robust and high-throughput Cre reporting and characterization system for the whole mouse brain. *Nat Neurosci* 13:133-140.

Manford M, Campbell G, Lieberman AR (1984) Postnatal development of ipsilateral retino-geniculate projections in normal albino rats and the effects of removal of one eye at birth. *Anat Embryol* 170:71-78.

Mastrorarde DN (1987) Two classes of single-input X-cells in cat lateral geniculate nucleus. II. Retinal inputs and the generation of receptive-field properties. *J Neurophysiol* 57:381-413.

McCormick DA, Feeser HR (1990) Functional implications of burst firing and single spike activity in lateral geniculate relay neurons. *Neuroscience* 39:103-113.

McCormick DA, von Krosigk M (1992) Corticothalamic activation modulates thalamic firing through glutamate "metabotropic" receptors. *Proc Natl Acad Sci* 89:2774-2778.

McLaughlin T, O'Leary DD (2005) Molecular gradients and development of retinotopic maps. *Annu Rev Neurosci* 28:327-355.

Meister M, Wong RO, Baylor DA, Shatz CJ (1991) Synchronous bursts of action potentials in ganglion cells of the developing mammalian retina. *Science* 252:939-943.

Mermelstein PG, Bito H, Deisseroth K, Tsien RW (2000) Critical dependence of cAMP response element-binding protein phosphorylation on L-type calcium channels supports a selective response to EPSPs in preference to action potentials. *J Neurosci* 20:266-273.

Meulders M, Godfraind JM (1969) Influence of arousal on the size of the visual receptive fields of suprageniculate and geniculate neurons in the intact alert cat and in the "cerveau isole" cat. *Exp Brain Res* 9:201-220.

Moechars D, Weston MC, Leo S, Callaerts-Vegh Z, Goris I, Daneels G, Buist A, Cik M, van der Spek P, Kass S, Meert T, D'Hooge R, Rosenmund C, Hampson RM (2006) Vesicular glutamate transporter VGLUT2 expression levels control quantal size and neuropathic pain. *J Neurosci* 26:12055-12066.

Montero VM (1986) Localization of gamma-aminobutyric acid (GABA) in type 3 cells and demonstration of their source to F2 terminals in the cat lateral geniculate nucleus: A golgi-electron-microscopic GABA-immunocytochemical study. *J Comp Neurol* 254:228-245.

Montero VM (1991) A quantitative study of synaptic contacts on interneurons and relay cells of the cat lateral geniculate nucleus. *Exp Brain Res* 86:257-270.

Mooney R, Penn AA, Gallego R, Shatz CJ (1996) Thalamic relay of spontaneous retinal activity prior to vision. *Neuron* 17:863-874.

Moshiri A, Gonzalez E, Tagawa K, Maeda H, Wang M, Frishman LJ, Wang SW (2008) Near complete loss of retinal ganglion cells in the *math5/brn3b* double knockout elicits severe reductions of other cell types during retinal development. *Dev Biol* 316:214-227.

Muir-Robinson G, Hwang BJ, Feller MB (2002) Retinogeniculate axons undergo eye-specific segregation in the absence of eye-specific layers. *J Neurosci* 22:5259-5264.

Murphy PC, Duckett SG, Sillito AM (1999) Feedback connections to the lateral geniculate nucleus and cortical response properties. *Science* 286:1552-1554.

Nassi JJ, Callaway EM (2009) Parallel processing strategies of the primate visual system. *Nat Rev Neurosci* 10:360-372.

Ni B, Wu X, Yan GM, Wang J, Paul SM (1995) Regional expression and cellular localization of the Na⁺-dependent inorganic phosphate cotransporter of rat brain. *J Neurosci* 15:5789-5799.

Norton TT, Holdefer RN, Godwin DW (1989) Effects of bicuculline on receptive field center sensitivity of relay cells in the lateral geniculate nucleus. *Brain Res* 1989 488:348-352.

Norton TT, Godwin DW (1992) Inhibitory GABAergic control of visual signals at the lateral geniculate nucleus. *Prog Brain Res* 90:193-217.

Ottersen OP, Storm-Mathisen J (1984) GABA-containing neurons in the thalamus and pretectum of the rodent. An immunocytochemical study. *Anat Embryol* 170:197-207.

Pape HC, Budde T, Mager R, Kisvarday ZF (1994) Prevention of Ca^{2+} -mediated action potentials in GABAergic local circuit neurones of rat thalamus by a transient K^{+} current. *J Physiol* 478:403-422.

Pape HC, McCormick DA (1995) Electrophysiological and pharmacological properties of interneurons in the cat dorsal lateral geniculate nucleus. *Neuroscience* 68:1105-1125.
Parnavelas JG, Mounty EJ, Bradford R, Lieberman AR (1977) The postnatal development of neurons in the dorsal lateral geniculate nucleus of the rat: a Golgi study. *J Comp Neurol* 171:481-499.

Penn AA, Riquelme PA, Feller MB, Shatz CJ (1998) Competition in retinogeniculate patterning driven by spontaneous activity. *Science* 279:2108-2112.

Perreault MC, Qin Y, Heggelund P, Zhu JJ (2003) Postnatal development of GABAergic signalling in the rat lateral geniculate nucleus: presynaptic dendritic mechanisms. *J Physiol* 546:137-148.

Petros TJ, Rebsam A, Mason CA (2008) Retinal axon growth at the optic chiasm: To cross or not to cross. *Annu Rev Neurosci* 31:295-315.

Pfeiffenberger C, Yamada J, Feldheim DA (2006) Ephrin-As and patterned retinal activity act together in the development of topographic maps in the primary visual system. *J Neurosci* 26:12873-12884.

Pham TA, Rubenstein JL, Silva AJ, Storm DR, Stryker MP (2001) The CRE/CREB pathway is transiently expressed in thalamic circuit development and contributes to refinement of retinogeniculate axons. *Neuron* 31:409-420.

Rafols JA, Valverde F (1973) The structure of the dorsal lateral geniculate nucleus in the mouse. A golgi and electron microscopic study. *J Comp Neurol* 150:303-32.

Ralston, HJ (1971) Evidence for presynaptic dendrites and a proposal for their mechanism of action. *Nature* 230:585-587.

Rhoades RW, Mooney RD, Fish SE (1985) Subcortical projections of area 17 in the anophthalmic mouse. *Brain Res* 349:171-181.

Rivlin-Etzion M, Zhou K, Wei W, Elstrott J, Nguyen PL, Barres BA, Huberman AD, Feller MB (2011) Transgenic mice reveal unexpected diversity of on-off direction-selective retinal ganglion cell subtypes and brain structures involved in motion processing. *J Neurosci* 31:8760-8769.

Rossi FM, Pizzorusso T, Porciatti V, Marubio LM, Maffei L, Changeux JP (2001) Requirement of the nicotinic acetylcholine receptor beta 2 subunit for the anatomical and functional development of the visual system. *Proc Natl Acad Sci* 98:6453-6458.

Salcedo E, Tran T, Ly X, Lopez R, Barbica C, Restrepo D, Vijayaraghavan S (2011) Activity-dependent changes in cholinergic innervation of the mouse olfactory bulb. *PLoS One* 6:e25441.

Shatz CJ, Rakic P (1981) The genesis of efferent connections from the visual cortex of the fetal rhesus monkey. *J Comp Neurol* 196:287-307.

Sherman SM (1985) Functional organization of the W-, X-, Y-cell pathways: a review and hypothesis. In: *Progress in psychobiology and physiological psychology* (Sprague JM, Epstein, AN, eds), pp233-314. New York: Academic.

Sherman SM (2001) Tonic and burst firing: Dual modes of thalamocortical relay. *Trends Neurosci* 24:122-126.

Sherman SM (2004) Interneurons and triadic circuitry of the thalamus. *Trends Neurosci* 27:670-675.

Sherman SM (2005) Thalamic relays and cortical functioning. *Prog Brain Res* 149:107-126.

Sherman SM, Guillery RW (1998) On the actions that one nerve cell can have on another: Distinguishing "drivers" from "modulators". *Proc Natl Acad of Sci* 95:7121-7126.

Sherman SM, Guillery RW (2002) The role of the thalamus in the flow of information to the cortex. *Philos Trans R Soc Lond B Biol Sci* 357:1695-1708.

Sherman SM, Spear PD (1982) Organization of visual pathways in normal and visually deprived cats. *Physiol Rev* 62:738-855.

Sillito AM, Kemp JA (1983) The influence of GABAergic inhibitory processes on the receptive field structure of X and Y cells in cat dorsal lateral geniculate nucleus (dLGN). *Brain Res* 277:63-77.

Singh R, Su J, Brooks J, Terauchi A, Umemori H, Fox MA (2012) Fibroblast growth factor 22 contributes to the development of retinal nerve terminals in the dorsal lateral geniculate nucleus. *Front Mol Neurosci* 4:61.

Smith Y, Pare D, Deschenes M, Parent A, Steriade M (1988) Cholinergic and non-cholinergic projections from the upper brainstem core to the visual thalamus in the cat. *Exp Brain Res* 70:166-180.

So KF, Schneider GE, Frost DO (1978) Postnatal development of retinal projections to the lateral geniculate body in Syrian hamsters. *Brain Res* 142:343-352.

Stanford LR, Friedlander MJ, Sherman SM (1981) Morphology of physiologically identified W-cells in the C laminae of the cat's lateral geniculate nucleus. *J Neurosci* 1:578-584.

Stanford LR, Friedlander MJ, Sherman SM (1983) Morphological and physiological properties of geniculate W-cells of the cat: A comparison with X- and Y-cells. *J Neurophysiol* 50:582-608.

Steriade M, McCormick DA, Sejnowski TJ (1993) Thalamocortical oscillations in the sleeping and aroused brain. *Science* 262:679-685.

Stone J (1983) *Parallel processing in the visual system*. New York: Plenum.

Su J, Haner CV, Imbery TE, Brooks JM, Morhardt DR, Gorse K, Guido W, Fox MA (2011) Reelin is required for class-specific retinogeniculate targeting. *J Neurosci* 31:575-586.

Szentagothai J (1963) The structure of the synapse in the lateral geniculate body. *Acta Anat* 55:166-185.

Takamori S, Rhee JS, Rosenmund C, Jahn R (2000) Identification of a vesicular glutamate transporter that defines a glutamatergic phenotype in neurons. *Nature* 407:189-194.

Tamamaki N, Yanagawa Y, Tomioka R, Miyazaki J, Obata K, Kaneko T (2003) Green fluorescent protein expression and colocalization with calretinin, parvalbumin, and somatostatin in the GAD67-GFP knock-in mouse. *J Comp Neurol* 467:60-79.

Tavazoie SF, Reid RC (2000) Diverse receptive fields in the lateral geniculate nucleus during thalamocortical development. *Nat Neurosci* 3:608-616.

Tootle JS, Friedlander MJ (1986) Postnatal development of receptive field surround inhibition in kitten dorsal lateral geniculate nucleus. *J Neurophysiol* 56:523-541.

Torborg CL, Feller MB (2005) Spontaneous patterned retinal activity and the refinement of retinal projections. *Prog Neurobiol* 76:213-235.

Torborg CL, Hansen KA, Feller MB (2005) High frequency, synchronized bursting drives eye-specific segregation of retinogeniculate projections. *Nat Neurosci* 8:72-78.

Torii M, Levitt P (2005) Dissociation of corticothalamic and thalamocortical axon targeting by an EphA7-mediated mechanism. *Neuron* 48:563-575.

Triplett JW, Owens MT, Yamada J, Lemke G, Cang J, Stryker MP, Feldheim DA (2009) Retinal input instructs alignment of visual topographic maps. *Cell* 139:175-185.

Turner JP, Salt TE (1998) Characterization of sensory and corticothalamic excitatory inputs to rat thalamocortical neurones in vitro. *J Physiol* 510:829-843.

Uhlrich DJ, Manning KA, Pienkowski TP (1993) The histaminergic innervation of the lateral geniculate complex in the cat. *Vis Neurosci* 10:225-235.

Usrey WM, Reppas JB, Reid RC (1999) Specificity and strength of retinogeniculate connections. *J Neurophysiol* 82:3527-3540.

Van Horn SC, Erisir A, Sherman SM (1997) Re-evaluation of relative distribution of synaptic terminals in the LGN of cats. *Soc Neurosci Abstract*.

Van Horn SC, Erisir A, Sherman SM (2000) Relative distribution of synapses in the A-laminae of the lateral geniculate nucleus of the cat. *J Comp Neurol* 416:509-520.

Wang SW, Kim BS, Ding K, Wang H, Sun D, Johnson RL, Klein WH, Gan L (2001) Requirement for *math5* in the development of retinal ganglion cells. *Genes Dev* 15:24-29.

Wang X, Vaingankar V, Sanchez CS, Sommer FT, Hirsch JA (2011a) Thalamic interneurons and relay cells use complementary synaptic mechanisms for visual processing. *Nat Neurosci* 14:224-231.

Wang X, Sommer FT, Hirsch JA (2011b) Inhibitory circuits for visual processing in thalamus. *Curr Opin Neurobiol* 21:726-733.

Wee R, Castrucci AM, Provencio I, Gan L, Van Gelder RN (2002) Loss of photic entrainment and altered free-running circadian rhythms in *math5*^{-/-} mice. *J Neurosci* 22:10427-10433.

Weston MC, Nehring RB, Wojcik SM, Rosenmund C (2011) Interplay between VGLUT isoforms and endophilin A1 regulates neurotransmitter release and short-term plasticity. *Neuron* 69:1147-1159.

Williams SE, Mason CA, Herrera E (2004) The optic chiasm as a midline choice point. *Curr Opin Neurobiol* 14:51-60.

Williams SR, Turner JP, Anderson CM, Crunelli V (1996) Electrophysiological and morphological properties of interneurons in the rat dorsal lateral geniculate nucleus in vitro. *J Physiol* 490:129-147.

Wilson JR, Hendrickson AE (1981) Neuronal and synaptic structure of the dorsal lateral geniculate nucleus in normal and monocularly deprived Macaca monkeys. *J Comp Neurol* 197:517-539.

Wilson JR, Friedlander MJ, Sherman SM (1984) Fine structural morphology of identified X- and Y-cells in the cat's lateral geniculate nucleus. *Proc R Soc Lond B Biol Sci* 221:411-436.

Winkelmann E, Garey LJ, Brauer K (1985) Ultrastructural development of the dorsal lateral geniculate nucleus of genetically microphthalmic mice. *Exp Brain Res* 60:527-534.

Wojcik SM, Rhee JS, Herzog E, Sigler A, Jahn R, Takamori S, Brose N, Rosenmund C (2004) An essential role for vesicular glutamate transporter 1 (VGLUT1) in postnatal development and control of quantal size. *Proc Natl Acad Sci* 101:7158-7163.

Wrobel A (1981) Light level induced reorganization of cat's lateral geniculate nucleus receptive fields: A spatiotemporal study. *Acta Neurobiol Exp* 41:447-466.

Xie Y, Skinner E, Landry C, Handley V, Schonmann V, Jacobs E, Fisher R, Campagnoni A (2002) Influence of the embryonic preplate on the organization of the cerebral cortex: A targeted ablation model. *J Neurosci* 22:8981-8991.

Yonehara K, Shintani T, Suzuki R, Sakuta H, Takeuchi Y, Nakamura-Yonehara K, Noda M (2008) Expression of SPIG1 reveals development of a retinal ganglion cell subtype projecting to the medial terminal nucleus in the mouse. *PLoS One* 3:e1533.

Yoshida M, Satoh T, Nakamura KC, Kaneko T, Hata Y (2009) Cortical activity regulates corticothalamic synapses in dorsal lateral geniculate nucleus of rats. *Neurosci Res* 64:118-127.

Young P, Feng G (2004) Labeling neurons in vivo for morphological and functional studies. *Curr Opin Neurobiol* 14:642-646.

Zhan XJ, Cox CL, Rinzel J, Sherman SM (1999) Current clamp and modeling studies of low-threshold calcium spikes in cells of the cat's lateral geniculate nucleus. *J Neurophysiol* 81:2360-2373.

Zhu J, Heggelund P (2001) Muscarinic regulation of dendritic and axonal outputs of rat thalamic interneurons: a new cellular mechanism for uncoupling distal dendrites. *J Neurosci* 21:1148-1159.

Zhu JJ, Uhrich DJ, Lytton WW (1999a) Burst firing in identified rat geniculate interneurons. *Neuroscience* 91:1445-1460.

Zhu JJ, Uhrich DJ, Lytton WW (1999b) Properties of a hyperpolarization-activated cation current in interneurons in the rat lateral geniculate nucleus. *Neuroscience* 92:445-457.

Ziburkus J, Lo FS, Guido W (2003) Nature of inhibitory postsynaptic activity in developing relay cells of the lateral geniculate nucleus. *J Neurophysiol* 290:1063-1070.

Ziburkus J, Guido W (2006) Loss of binocular responses and reduced retinal convergence during the period of retinogeniculate axon segregation. *J Neurophysiol* 96:2775-2784.

Ziburkus J, Dilger EK, Lo FS, Guido W (2009) LTD and LTP at the developing retinogeniculate synapse. *J Neurophysiol* 102:3082-3090.

Zucker RS, Regehr WG (2002) Short-term synaptic plasticity. *Annu Rev Physiol* 64:355-405.

Vita

Tania Alexis Seabrook was born on February 9, 1982, in Voorhees, New Jersey, and is an American citizen. She graduated from John Randolph Tucker High School, Richmond, Virginia in 2000. She received her Bachelor of Science in Biology and Bachelor of Science in Forensic Science with minor in Chemistry from Virginia Commonwealth University, Richmond, Virginia in 2005 and subsequently worked as a Research and Laboratory Specialist for Dr. Kimber White in the Department of Pharmacology and Toxicology at Virginia Commonwealth University for one year. The year before entering graduate school she worked as a Laboratory Specialist for Dr. William Guido in the Department of Anatomy and Neurobiology at Virginia Commonwealth University.

Publications

1. Krahe TE*, **Seabrook TA***, Chen C-KJ, Fox MA, Guido W (2012) Modulation of CREB in the dorsal lateral geniculate nucleus of dark-reared mice. *Neural Plasticity*, vol. 2012, Article ID 426437, 8 pages, 2012. doi:10.1155/2012/426437.

Publications in Preparation

1. **Seabrook TA**, El-Danaf RN, Krahe TE, Fox MA, Guido W. Timing of corticogeniculate innervation in the dorsal lateral geniculate nucleus of the mouse relies on retinogeniculate axon innervation.
2. **Seabrook TA**, Dilger EK, El-Danaf RN, Krahe TE, Guido W. The degree of retinal convergence onto interneurons in the dorsal lateral geniculate nucleus of the mouse is maintained during postnatal development.

Awards

Best Abstract and Poster Presentation, Central Virginia Chapter Society for Neuroscience Annual Symposium and Poster Session: Richmond, VA, 2012

Central Virginia Chapter Society for Neuroscience Travel Award, Society for Neuroscience 41st Annual Meeting: Washington, DC, 2011

Japan Neuroscience Society Travel Award, the 34th Annual Meeting of the Japan Neuroscience Society: Yokohama, Japan, 2011

Best Abstract Award, Central Virginia Chapter Society for Neuroscience Annual Poster Session: Richmond, VA, 2010

Best Abstract Award, Central Virginia Chapter Society for Neuroscience Annual Poster Session: Richmond, VA, 2009